Theoretical Studies of Electronic, Vibrational, and Structural Properties of Solids under Pressure

A doctoral dissertation by

Steven Paul Lewis

B.S. (University of Illinois at Urbana-Champaign) 1988

M.A. (University of California at Berkeley) 1990

Ph.D. (University of California at Berkeley) 1993

REPORT DOCUMENTATION PAGE

Form Approved
OMB No. 0704-0188

1. AGENCY USE ONLY (Leave Blank)	2. REPORT DATE	3. REPORT TYPE AND DATES COVERED
	1993	Final

4. TITLE AND SUBTITLE
Theoretical Studies of Electronic, Vibrational, and Structural Properties of Solids under Pressure

5. FUNDING NUMBERS

6. AUTHORS
Steven Paul Lewis

AFRL-SR-BL-TR-98-

0030

7. PERFORMING ORGANIZATION NAME(S) AND ADDRESS(ES)
University of California at Berkeley

9. SPONSORING/MONITORING AGENCY NAME(S) AND ADDRESS(ES)
AFOSR/NI
110 Duncan Avenue, Room B-115
Bolling Air Force Base, DC 20332-8080

10. SPONSORING/MONITORING AGENCY REPORT NUMBER

11. SUPPLEMENTARY NOTES

12a. DISTRIBUTION AVAILABILITY STATEMENT
Approved for Public Release

12b. DISTRIBUTION CODE

13. ABSTRACT *(Maximum 200 words)*
See attached.

14. SUBJECT TERMS	15. NUMBER OF PAGES
	16. PRICE CODE

17. SECURITY CLASSIFICATION OF REPORT	18. SECURITY CLASSIFICATION OF THIS PAGE	19. SECURITY CLASSIFICATION OF ABSTRACT	20. LIMITATION OF ABSTRACT
Unclassified	Unclassified	Unclassified	UL

Theoretical Studies of Electronic, Vibrational, and

Structural Properties of Solids under Pressure

by

Steven Paul Lewis

B.S. (University of Illinois at Urbana-Champaign) 1988
M.A. (University of California at Berkeley) 1990

A dissertation submitted in partial satisfaction of the

requirements for the degree of

Doctor of Philosophy

in

Physics

in the

GRADUATE DIVISION

of the

UNIVERSITY of CALIFORNIA at BERKELEY

Committee in Charge:

Professor Marvin L. Cohen, Chair

Professor Peter Y. Yu

Professor Eicke R. Weber

1993

The dissertation of Steven Paul Lewis is approved:

Marvin L. Cohen August 16, 1993

Chair Date

Peter Yu 9/7/93

Date

Eric R. Weber 9/1/93

Date

University of California at Berkeley

1993

Abstract

Theoretical Studies of Electronic, Vibrational, and
Structural Properties of Solids under Pressure

by

Steven Paul Lewis

Doctor of Philosophy in Physics

University of California at Berkeley

Professor Marvin L. Cohen, Chair

This dissertation describes first-principles quantum mechanical investigations of several realistic solid-state systems. The main goal of this research has been to understand and predict the electronic, vibrational, and structural properties of materials under pressure. Microscopic information on these properties is obtained within local density functional theory using *ab initio* pseudopotentials. This work focuses on three categories of materials:

- Part I deals with the high-pressure behavior of elemental systems from group IV of the Periodic Table. The pressure-dependences of Raman-active phonon modes of high-pressure, metallic phases of silicon, germanium, and tin are studied within the frozen-phonon approximation. In addition, the structural properties of a recently discovered orthorhombic phase of silicon are calculated. The aim of these two investigations is to understand and explain recent experimental results. A third investigation predicts the existence of an orthorhombic, high-pressure phase of germanium.

- Part II focuses on group V of the Periodic Table. The electronic and vibrational properties of elemental arsenic are studied with the aim of understanding the measured pressure-dependences of the superconducting transition temperature and the normal-state resistance. In addition, several candidate atomic phases of solid nitrogen are studied to determine their structural-stability and

electronic properties.

- Finally, Part III considers the effect of varying the stoichiometry in compound systems. In particular, model calculations are performed to explore the Ga-As system with the goal of motivating experimental studies. The electronic properties of several model Ga-As systems with varying stoichiometry are studied.

Marvin L. Cohen
August 16, 1993

In loving memory of

my grandmother

Dorathe Greenstein

for her pride and encouragement

Contents

List of Figures

List of Tables

Foreword

Over the last two decades significant experimental advances in condensed matter physics and materials science have opened avenues of materials research that were never before accessible. One example is the development and refinement of the diamond anvil cell (DAC) for achieving extremely high pressures [Jay83]. Static pressures as high as ~400 GPa have been reported [Ruo90]. Because of the transparency and high thermal conductivity of diamond, a host of probes can be used to investigate the properties of samples pressurized in the DAC. With the DAC investigators have been able to address a wide variety of subjects including the properties of materials that are only stabilized under pressure [Mig86], the behavior of the Earth far below its surface [Kni91], and long-standing basic questions such as whether or not hydrogen will metallize [Hem88].

Another important advance has been the development of modern high-precision materials synthesis techniques, such as Molecular Beam Epitaxy (MBE), which provide a great deal of control in preparing new materials. By manipulating parameters such as temperature, substrate, and so forth, it is possible to grow substances which do not occur naturally, but which have interesting and useful properties [Her89].

Concurrent with these experimental advances has been the development of powerful theoretical methods for computing the properties of real materials from first principles. Previous first-principles methods were restricted to idealized model systems for investigating general trends. Conversely, highly accurate approaches for studying real materials, such as the empirical pseudopotential method [Coh70, Coh88], relied on experimental information about the solid, and thus were limited in their predictive power. Modern first-principles approaches, however, are able to investigate the structural, electronic, vibrational, bonding, and superconducting properties of solids to a high degree of accuracy using only information

about the constituent atoms as inputs. Because these methods are inherently *ab initio* they are capable of a high level of predictive power. This has made them ideally suited to explore the effect of high pressures and to investigate novel materials, thus complementing the experimental situation described above.

Density functional theory (DFT) [Hoh64, Lun83] provides the theoretical framework of most modern *ab initio* methods for studying solids. In this theory, the total ground-state energy of a system of interacting electrons in the presence of an external field (*e.g.*, the Coulomb fields produced by the constituent atomic nuclei) is shown to be a unique functional of the electron number density. The exact many-body ground state of the system is then given by the density that minimizes the energy functional and the resulting energy. Thus, the problem of solving for the ground-state coordinates of, say, 10^{23} interacting particles is reduced to determining a single function of only three spatial variables. It has been shown that DFT can be recast variationally into a set of self-consistent single-particle equations called the Kohn-Sham equations [Koh65]. Most applications of DFT use this form.

Since DFT is an exact ground-state theory for a system of interacting electrons, it is, in principle, possible to calculate exactly any property that depends only on the ground-state electron density. In practice, however, several approximations must be adopted to make calculations tractable. Despite these approximations, DFT-based methods have enjoyed enormous successes in accurately explaining and predicting the properties of a large class of systems [Coh82, Coh86, Coh89]. The exact nature of the approximations and the details of the computational method are discussed extensively in the literature (see, for example, Ref. [Pic89] and references therein) and, therefore, will not be duplicated here. Only the most salient features follow.

The Kohn-Sham equations are solved assuming that the constituent atomic nuclei are fixed in space relative to the electrons. This is the Born-Oppenheimer approximation [Mad78] and is valid for nuclear masses much larger than the electronic mass. With the nuclear degrees of freedom projected out of the Kohn-Sham

Hamiltonian, the resulting effective potential contains only electron-based terms. In particular, the effective potential is a sum of electron-nucleus interactions and electron-electron interactions.

A common (and very successful) approach for treating the electron-nucleus interaction is the pseudopotential method [Phi59, Coh70]. In this approach the electrons in the constituent atoms are separated into core and valence electrons, and the nucleus and core electrons are then combined into a single inert entity called an ion core. The valence electrons interact with the ion core via a pseudopotential. The justification for this approximation is that solid-state phenomena primarily involve only the valence electrons. Core electrons behave essentially as they would in a free atom, and thus can be considered as "frozen" with respect to the solid-state environment. The value of the pseudopotential concept is that the resulting shallower potential is simpler to characterize in a plane-wave expansion.

In the past pseudopotenials were either based on idealized models or empirical inputs. However, in the late 1970's methods for generating pseudopotentials using only the atomic number as input were developed. These are the non-local, norm-conserving *ab initio* pseudopotentials of Hamann, Schlüter, and Chiang [Ham79] which, by construction, are highly transferrable to a wide variety of chemical environments.

Because the exchange and correlation energies are complicated functionals of the electron density (in fact, the exact form of these terms is not known), it is very difficult to treat the electron-electron interaction without making an approximation. The simplest and most universally used method for describing the exchange and correlation energies is the local-density approximation (LDA). In this approach the exchange-correlation potential in a given volume element of the solid is approximated by that of a uniform electron gas with number density equal to the average density within the volume element. The validity of the LDA relies on a slow spatial variation of the charge density over the given volume element. While this approximation

seems quite strong, the highly successful results obtained within the LDA suggest otherwise.

Once the pseudopotential and local-density approximations have been adopted, it is straightforward to recast the total-energy problem in a momentum-space form [Ihm79, Coh82, Pic89] and use a plane-wave basis for expanding the potential and wavefunctions. Aside from its obvious simplicity, a plane-wave basis offers a number of useful features. First, a plane-wave basis provides a quantitative and systematic way of improving calculations by increasing the size of the basis. The size of the basis is governed by a single parameter: the cutoff energy. All plane waves with "kinetic energy" less than or equal to the cutoff energy are included in the basis. Another advantage of plane waves is that they are not biased by the composition or structure of the system under investigation as atomic-centered bases often are.

This dissertation reports on a collection of first-principles theoretical investigations of solids using the computational method described above (referred to as the *ab initio* pseudopotential plane-wave total energy method). The demonstrated predictive power of this method [Coh82, Coh86, Coh89] encourages not only the study of experimentally realized systems but also the exploration of hypothetical materials with the aim of motivating experimental research. This work contains examples of both of types investigations. Phenomena studied here include structural, electronic, and vibrational properties of elemental systems under pressure, and stoichiometric effects in compounds. In particular, this thesis is organized into three parts:

Part I deals with the high-pressure behavior of elemental systems from group IV of the Periodic Table. Chapter 1 presents a study of the pressure-dependences of Raman-active phonon modes in high-pressure metallic phases of Si, Ge, and Sn, with the aim of understanding recent measurements which found differences between the behavior of Si and Ge. In Chap. 2 the calculated structural properties of a recently discovered orthorhombic phase of Si are reported. This phase, observed for pressures between the transition pressures of the β-Sn and simple hexagonal phases,

is found to transform continously from a β-Sn-like structure at low pressures to the simple hexagonal structure at high pressures. Finally, a third investigation (Chap. 3) predicts the existence of the same orthorhombic structure as a high-pressure phase of Ge.

Part II focuses on group V of the Periodic Table. Chapter 4 contains the theoretical portion of a combined experimental and theoretical investigation of superconductivity in As at high pressures. The experiments observed a peak in the superconducting transition temperature and a kink in the normal-state resistance at a pressure corresponding to the rhombohedral to cubic structural transition. Calculations of the electronic and vibrational properties of As provide a theoretical description consistent with the observations. In Chap. 5 several candidate atomic phases of solid nitrogen are studied to determine their structural-stability and electronic properties. A simple tetragonal phase is singled out as a possible metastable metallic phase at high pressures.

Part III considers the effect of varying stoichiometry on the properties of compound systems. In particular, Chap. 6 describes calculations designed to explore the Ga-As system with the goal of motivating experimental studies. The electronic properties of a family of hypothetical (except GaAs) Ga-As compounds with varying stoichiometry are studied. This family of materials all share the same underlying diamond lattice and range from pure As through zincblende GaAs to pure Ga.

The investigations reported in this dissertation have also been reported in six articles written by the author [Che92, Lew92, Lew93a, Lew93b, Lew93c, Lew93d]. At the present writing, these articles have been published or submitted for publication.

Acknowledgements

I am truly fortunate to have had Professor Marvin Cohen as my thesis advisor. His calm, nurturing manner, his reassuring support and encouragement, and his wise advice have been invaluable to me. Choosing to join Marvin's group is one of the best decisions I have made. I have matured a lot both professionally and personally under his guidance, and I shall miss working with him on a daily basis.

I am deeply grateful to Dr. Amy Liu and Dr. Alberto García for patiently showing me the ropes. They were excellent role-models for a fledgling researcher and remain good friends. I wish also to thank the many other people I have encountered in the Condensed Matter Theory group for making the fifth floor of Birge Hall a friendly and intellectually exciting place to work. I am particularly grateful to Prof. Steven Louie, Dr. Andrew Rappe, Jennifer Corkill, Dr. Eric Shirley, Vincent Crespi, Dr. Troy Barbee, Dr. Angel Rubio, Dr. Xuejun Zhu, Jing Zhu, and Dr. Michael Surh for many interesting and fruitful scientific interactions.

I wish to express my appreciation to Prof. Peter Yu and Prof. Eicke Weber for their suggestions and support. In addition, I am pleased to acknowledge collaborations with Dr. Anthony Chen, Zhenpeng Su, Prof. Peter Yu, and Dr. David Penn.

I am indebted to Anne Takizawa and Ken Miller for cheerfully welcoming me to Berkeley and the Physics Department in August 1988 and for smoothly guiding me through the university and department bureaucracies for the next five years. I shall miss them both.

I gratefully acknowledge the financial support of the National Science Foundation and the U. S. Department of Defense through consecutive graduate fellowships.

Many friends have helped make my life happy over the last five years. I owe them my gratitude for helping to ease the many stresses of graduate school. I am especially grateful to Jen, Tom, Kanwal, Andy, Barri, Chris, Dan, all my UCBD

friends, and, of course, Newton.

Most importantly, my deepest appreciation goes to my family, for in this area I have been truly blessed. Mom, Danny, Bonnie, and Pete, I cannot adequately convey how important your love, support, and friendship have been to me over the past five years and over my whole life. You are my closest friends, and I am proud to call you my family. I love you all.

Finally, it would be my greatest joy to be able to thank my father. Unfortunately, I only knew him for a short $7\frac{1}{2}$ years. I am told by those who knew him and who know me that I am a lot like him in many ways. By all accounts, that is quite a compliment. I hope that those who knew him and loved him will accept my heartfelt gratitude in his stead.

Part I

Group IV Elements Under Pressure

Introduction

There is little doubt that the elements in group IV of the Periodic Table are among the most technologically important solids and are among the most thoroughly investigated. The practical applications of carbon (in both the diamond and graphite forms), silicon, germanium, tin, and lead are manifold. In fact, an entire industry was developed to exploit the uses of Si. In condensed matter physics the group IV elements (particularly C and Si) often serve as prototypical materials and act as "testing grounds" for new theoretical and experimental techniques.

The importance of the group IV elements extends to the study of their behavior at high pressures. While the high-pressure properties of carbon and lead have been investigated [Fah87, Liu91], this Part considers only the properties of Si, Ge, and Sn under pressure. Over the last three decades, the high-pressure behavior of these three group IV elements has been the subject of many experimental [Min62, Wen63, Jay63, Bun63, Jam63a, Kas64, Bat65, Jam65, Bar66, Wit66, Pie75, Wei75, Asa78, Gup80, Oli84a, Oli84b, Hu84, Liu86, Voh86, Hu86, Ers86, Duc87, Des89, Duc90, Oli92] and theoretical [Van71, Van72, Yin80, Yin81a, Yin82, McM83, Cha84, Nee84, Cha85a, Cha85b, Dac85, Coh85, Cha86c, Cha86d, Mar88, Liu88, Zan90, Cor91, Nee91, Che91, Nee93] investigations. In particular, these elements are found to undergo a series of pressure-induced structural phase transitions which are summarized in Fig. 0.1.

The following three chapters and their associated publications [Lew93a, Lew93c, Lew93d] contain new contributions to this vast literature on Si, Ge, and Sn under pressure. Chapter 1 contains a study of the vibrational properties of Si, Ge and Sn in the β-Sn structure and Si in the hcp structure. The main goal of this study is to understand recent measurements [Oli92] which found differences between the behavior of Si and Ge. In Chap. 2 the calculated structural properties of a re-

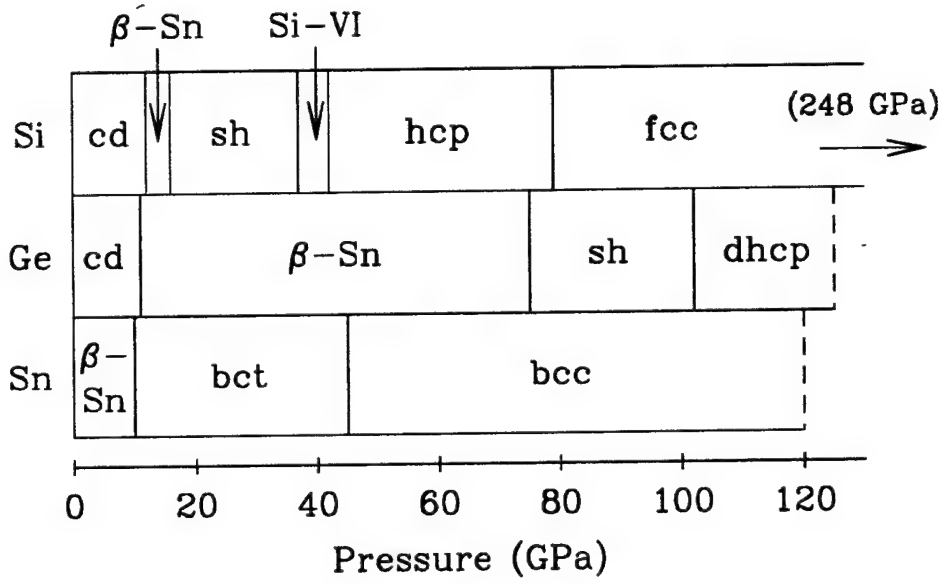

Figure 0.1: A schematic summary of the experimentally observed room temperature structural phases of Si, Ge, and Sn as a function of pressure in GPa. The transition pressures are taken from Ref. [Duc90] for Si, Ref. [Voh86] for Ge, and Ref. [Oli84a] and [Des89] for Sn. The dashed lines correspond to the highest reported pressure for each element; for Si, the highest pressure achieved is 248 GPa and is not shown. The structural abbreviations are defined as follows: cubic diamond (cd), simple hexagonal (sh), hexagonal close-packed (hcp), face-centered cubic (fcc), double-hcp (dhcp), body-centered tetragonal (bct), and body-centered cubic (bcc). The results of Chap. 2 and 3 will slightly modify this diagram.

cently discovered [McM93] orthorhombic phase of Si are reported. Finally, a third investigation, described in Chap. 3, predicts the existence of the same orthorhombic structure as a high-pressure phase of Ge.

Chapter 1

Raman Modes in High-Pressure Phases of Si, Ge, and Sn

1.1 Introduction

A structural phase common to the group IV elements Si, Ge, and Sn is the metallic β-Sn phase (see Fig. 0.1). This is the stable low-pressure structure of Sn at room temperature [1]. Upon compression to 9.5 GPa, Sn transforms to a body-centered tetragonal phase. Both Si and Ge exist in the diamond structure at low pressures and transform to the β-Sn structure at about 10 GPa. They both then transform to the simple hexagonal (sh) structure at about 15 GPa for Si and at 75 GPa for Ge. Upon further compression, Si transforms to an intermediate phase, denoted Si-VI, at about 38 GPa and to the hexagonal-close-packed (hcp) structure at about 42 GPa. No such transitions are observed in Ge.

Recently, Olijnyk [Oli92] has used Raman spectroscopy to study the pressure-dependence of the Raman-active phonon modes of Si, Ge, and Sn in the β-Sn structure and of Si in the Si-VI and hcp structures. For all three elements in the β-Sn phase, the frequency of the doubly-degenerate TO Raman mode [2] is found to increase with pressure over the range of stability, although with slightly decreasing mode-Grüneisen parameter. In contrast, the behavior of the LO Raman mode [2] is found to change in going from Si to Ge to Sn. For Si, the LO mode is found to decrease with pressure, with an increasingly negative Grüneisen parameter, over the range of stability. This is attributed [Oli92] to the onset of the β-Sn $\rightarrow$ sh transition and is addressed more fully below. For Ge, the LO mode is found to increase initially and then level off by 50 GPa. No measurements on Ge are presented for pressures between 50 GPa and the transition to the sh structure at 75 GPa, although

it is speculated [Oli92] that the mode will start to soften near the transition, as is seen for Si. Finally, the LO mode for Sn is found to increase over the whole range of stability, although more gradually than the TO mode, and with a more rapidly decreasing Grüneisen parameter. Two Raman modes are seen for Si-VI, the lower of which becomes the doubly-degenerate TO Raman mode for hcp-Si. This mode is first seen at 33 GPa; it increases linearly with pressure (at least up to 47 GPa); and it is continuous across the Si-VI → hcp transition.

This chapter reports on a first-principles investigation of the pressure-dependence of the Raman modes discussed above. Since the exact structure of Si-VI is not known, it is assumed to be the hcp structure, and the structural transition sequence is assumed to be sh → hcp instead of sh → Si-VI → hcp. These assumptions are acceptable for the purposes of the present study, since the lower frequency Si-VI Raman mode and the TO hcp Raman mode are closely related to each other and are both associated to the distortion back to the sh structure [Oli92]. The higher frequency Si-VI Raman mode is not addressed in this study. The calculated results of phonon frequency vs pressure agree very well with the measurements of Ref. [Oli92]. Discussion will focus primarily on Si and Ge in the β-Sn structure, and the behavior of the LO Raman mode in particular. This feature of the data is the most challenging to understand because of the dissimilarity of the behavior of Si and Ge. An explanation of this dissimilarity based on the presence of d electrons in the Ge core is provided. This chapter is organized as follows. Section 1.2 discusses the methods used in the calculations and provides some computational details. A description of the structures and relevant phonon modes is contained in Sec. 1.3. Section 1.4 presents the computational results. Finally, in Sec. 1.5 the discrepancy between Si and Ge in the pressure-dependence of the β-Sn–structure LO Raman mode is discussed.

1.2 Computational Methods

Calculations are performed using the *ab initio* pseudopotential total energy method [Ihm79, Coh82, Pic89]. Electron-ion interactions are evaluated in this method using nonlocal, norm-conserving pseudopotentials [Ham79]. The Si, Ge, and Sn pseudopotentials used here have reference configurations $3s^{2.0}3p^{0.5}3d^{0.5}$, $4s^{2.0}4p^{0.5}4d^{0.5}$, and $5s^{2.0}5p^{0.5}5d^{0.5}$, respectively. The cutoff radii (in a.u.) for the s-, p-, and d-potentials are equal to (1.12, 1.35, and 1.17), (1.17, 1.35, and 1.77), and (1.20, 1.50, and 2.55) for the three elements respectively. Electronic exchange and correlation energies are calculated within the local-density approximation (LDA) [Lun83] using a standard form for the exchange-correlation potential [Cep80]. The only external inputs to the calculation are the atomic numbers and masses of the constituent atoms and the basic crystal structure. All relaxed structural parameters are calculated from first principles.

Wavefunctions and pseudopotentials are expanded in a plane-wave basis up to an energy cutoff of 35 Ry for Si and Ge and 30 Ry for Sn. The irreducible part of the Brillouin zone is sampled at 148 (279) special points [Cha73, Mon77] for the TO (LO) mode of the β-Sn structure and at 128 special points for the TO mode of the hcp structure. To overcome numerical instabilities associated with filling energy levels over a discretely sampled Brillouin zone, all energy levels are broadened into Gaussians with widths of about 0.7 mRy. Values of the computational parameters are chosen such that the calculated total energies are converged to within 1 mRy.

Phonon frequencies are calculated within the frozen-phonon approximation. In this approach, the total energy is calculated for a crystalline system with a static phonon distortion of given amplitude imposed. Such calculations are done for several phonon amplitudes up to about 2% of the bond length. The total energy vs amplitude data are then fitted, within the harmonic approximation, to a quadratic polynomial, and the phonon frequency is extracted from the coefficient of the leading term.

In these calculations, the unit cell volume is a more natural choice for the independent variable than pressure. Therefore, to make contact with experiments, in which pressure is the more natural choice for the independent variable, an equation of state is required. For each system considered, the equation of state is obtained by first calculating the total energy at several unit cell volumes and fitting these data to the Murnaghan equation of state [Mur44]. A correction to account for the zero-point energy of the ions is then added (see below). Parameters of the fit to the Murnaghan equation are tabulated in Table 1.1 for each of the four systems considered here. For Si, Ge, and Sn in the β-Sn structure, these parameters are in good agreement with the previously calculated values of Ref. [Nee84], [Cha86d], and [Cor91], respectively. The agreement for Si with the calculated equation of state of Ref. [Cha85a] is only fair, due primarily to the smaller Brillouin zone sampling and energy cutoff used in the earlier calculation. Calculations for Ge and Sn in the β-Sn structure and for Si in the hcp structure agree well with experimental equations of state. No experimental equation of state for Si in the β-Sn structure has been published, to our knowledge, probably because the range of stability of this phase is so small. However, the calculations are consistent with the few measurements of volume vs pressure that exist [Oli84b, Hu84].

Since the pressure is obtained as the negative of the derivative of the total energy with respect to volume, at high pressures the pressure is a sensitive function of volume, and the error can be significant. This often represents the largest error in the calculation. For Si in the β-Sn structure, the range of stability ($\sim$4 GPa) is of the same order as the error in the calculated pressure. Therefore, volumes whose pressures are calculated to lie within the range of stability may, in fact, lie outside of it. To account for this, calculations for Si in the β-Sn structure have been performed for a volume range larger than the range of stability.

The present computational method treats the ion cores classically, and the effect of the zero-point motion of the cores on the equation of state is approximated by a

Debye model:

$$E_{ZPM} = \frac{9}{8}\hbar\omega_D = \frac{9}{8}\hbar v_s q_D = \frac{9}{8}\hbar\sqrt{\frac{B}{\rho}}q_D \qquad (1.1)$$

where ω_D is the Debye freqency, v_s is the speed of sound, B is the bulk modulus, ρ is the mass density, and q_D is the Debye wavevector. Volume-dependence of E_{ZPM} is contained in B, ρ, and q_D. The total energy is taken as the sum of the static-core total energy and the approximate zero-point energy correction. Because of the increasing mass, the zero-point energy becomes less important in going from Si to Ge to Sn.

1.3 Structures and Phonon Modes

The β-Sn structure (Fig. 1.1) is made up of two interpenetrating body-centered tetragonal (bct) sublattices displaced from each other by the vector $[0, a/2, c/4]$. The relaxed values of c/a are fairly independent of volume, and are found to be about 0.545, 0.560, and 0.555 for Si, Ge, and Sn, respectively, in good agreement with experiments and previous calculations. The calculated phonon frequencies, however, are not very sensitive to c/a. Each atom in the β-Sn structure has four nearest neighbors by symmetry, but because of the value of c/a, the two second-nearest neighbors at $\pm[0, 0, c]$ are only slightly farther away. Thus, the atoms are effectively six-fold coordinated with a nearest neighbor distance slightly larger than a/2. This represents an increase in coordination number from the four-fold coordination of the diamond structure. Increasing coordination number with pressure is a common feature of structural phase transitions and is attributed to the importance of the ion-ion Coulomb interaction (Ewald interaction) at high pressure (small unit cell volume).

Both the LO and the doubly-degenerate TO phonon modes at the center of the β-Sn Brillouin zone are Raman active. The TO mode corresponds to an opposing motion of the two interpenetrating bct sublattices in any direction perpendicular to the c-axis. The LO mode corresponds to an opposing motion of the sublattices

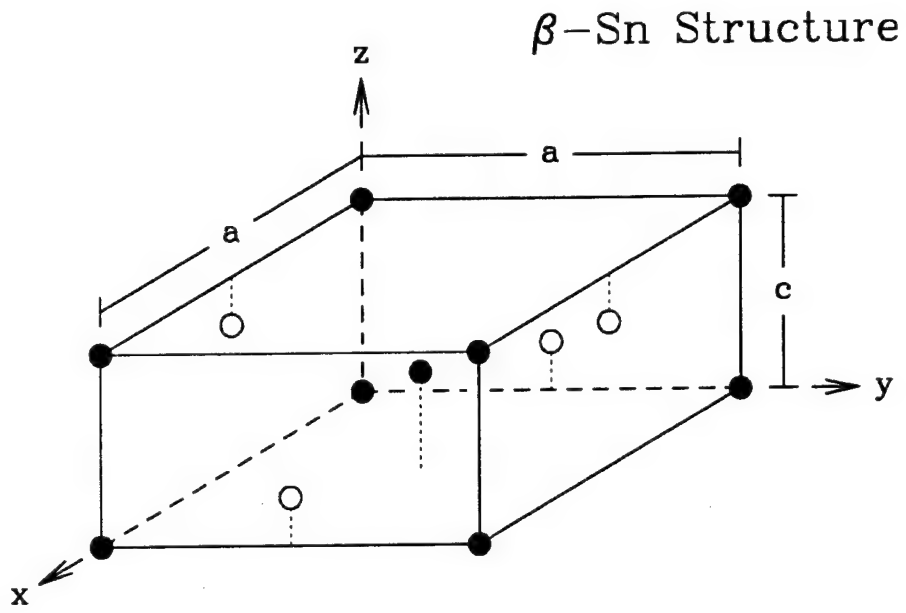

Figure 1.1: A ball-and-stick model of the β-Sn conventional cell. Open circles correspond to one of the bct sublattices, and filled circles correspond to the other. The two sublattices are separated by the vector $[0, a/2, c/4]$. Dotted lines serve only to show atomic positions. The c/a ratio is roughly 0.55 for Si, Ge, and Sn in this structure.

parallel to the c-axis.

For Si in the hcp structure, the relaxed c/a ratio is found to be about 1.68, essentially independent of volume. This value is slightly higher than the ideal hcp c/a ratio (1.633), but is in very good agreement with experiments [Oli84b, Hu86, Duc87, Duc90] and previous calculations [McM83, Cha85a]. The doubly-degenerate TO phonon mode at the center of the hcp Brillouin zone is Raman active. This mode corresponds to an opposing motion of adjacent hexagonal planes in a direction perpendicular to the c-axis.

Two of the Raman modes under consideration are associated with structural phase transitions. The β-Sn LO mode is related to the β-Sn $\rightarrow$ sh phase transition in that an LO-type displacement of the β-Sn lattice of amplitude c/8, accompanied by slight modifications of axial ratios, yields the sh lattice. The c-axis for the sh structure is parallel to the a-axis for the β-Sn structure. Similarly, the hcp TO mode is related to the sh $\rightarrow$ hcp transition. A distortion with amplitude $a/\sqrt{6}$ will bring the hexagonal layers into registry, and then a slight expansion of c/a brings about the stable sh structure.

1.4 Results

Figures 1.2–1.4 show calculated frequency vs pressure of the phonon modes described above for Si, Ge, and Sn, respectively. These theoretical results are compared to the experimental results of Ref. [Oli92], and are shown to be in very good agreement. In particular, the observed change in the pressure-dependence of the β-Sn LO mode in going from Si to Ge to Sn is also exhibited by the calculations. Moreover, the speculation in Ref. [Oli92] that the Ge LO mode will start to decrease with pressure beyond 50 GPa is not born out by the calculations which show that this mode merely plateaus up to 80 GPa.

It is known that a displacive first-order structural phase transition is often accompanied by a softening of an associated phonon mode (see, for example, [Bei90]

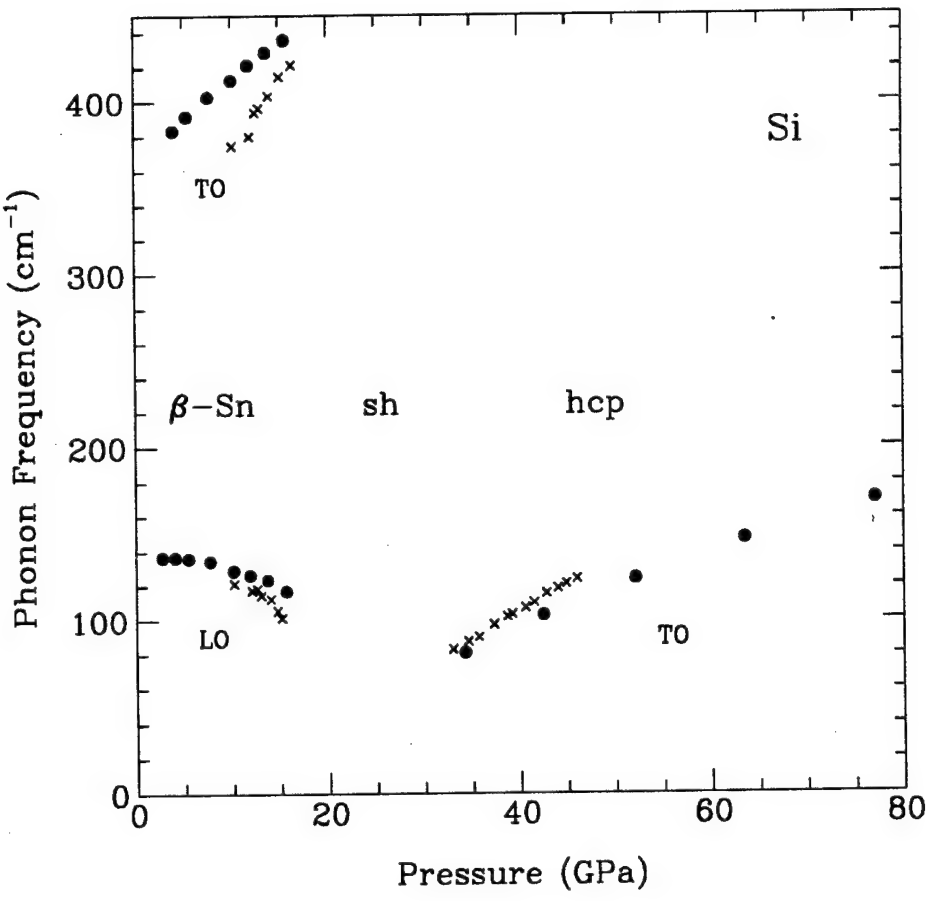

Figure 1.2: Phonon frequency vs pressure for the LO and TO Raman modes of Si in the β-Sn structure, and for the TO Raman mode of Si in the hcp structure. The black dots are the calculated results of the present study. The crosses are the experimental results of Ref. [Oli92].

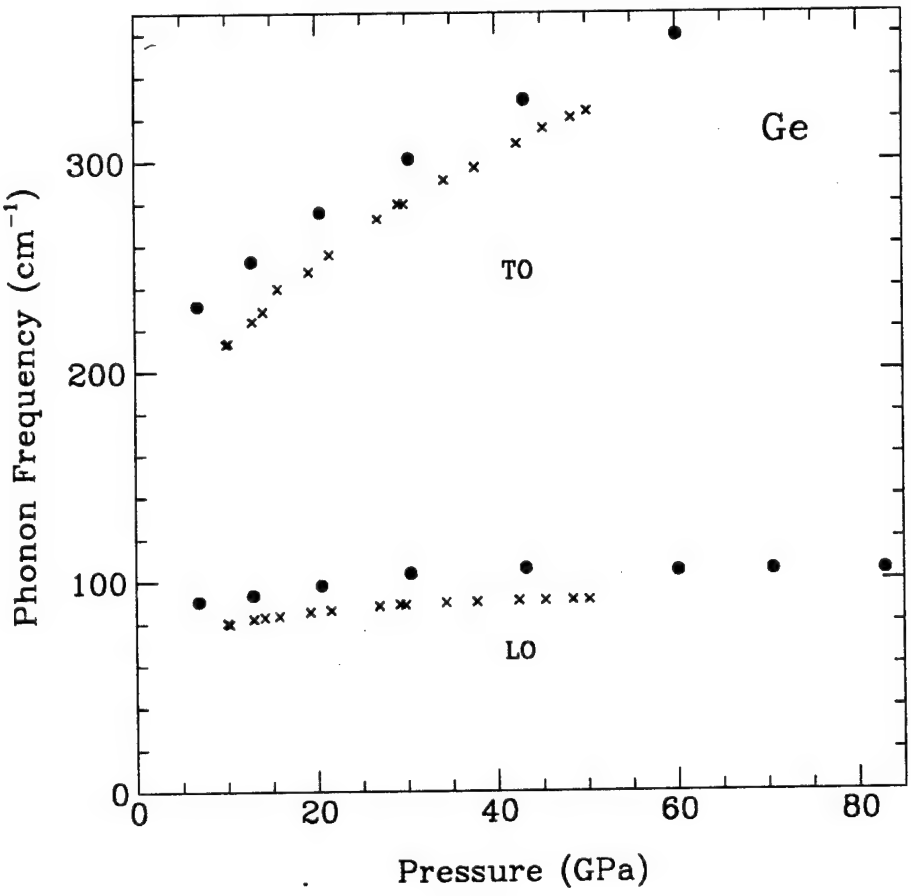

Figure 1.3: Phonon frequency vs pressure for the LO and TO Raman modes of Ge in the β-Sn structure. The black dots are the calculated results of the present study. The crosses are the experimental results of Ref. [Oli92].

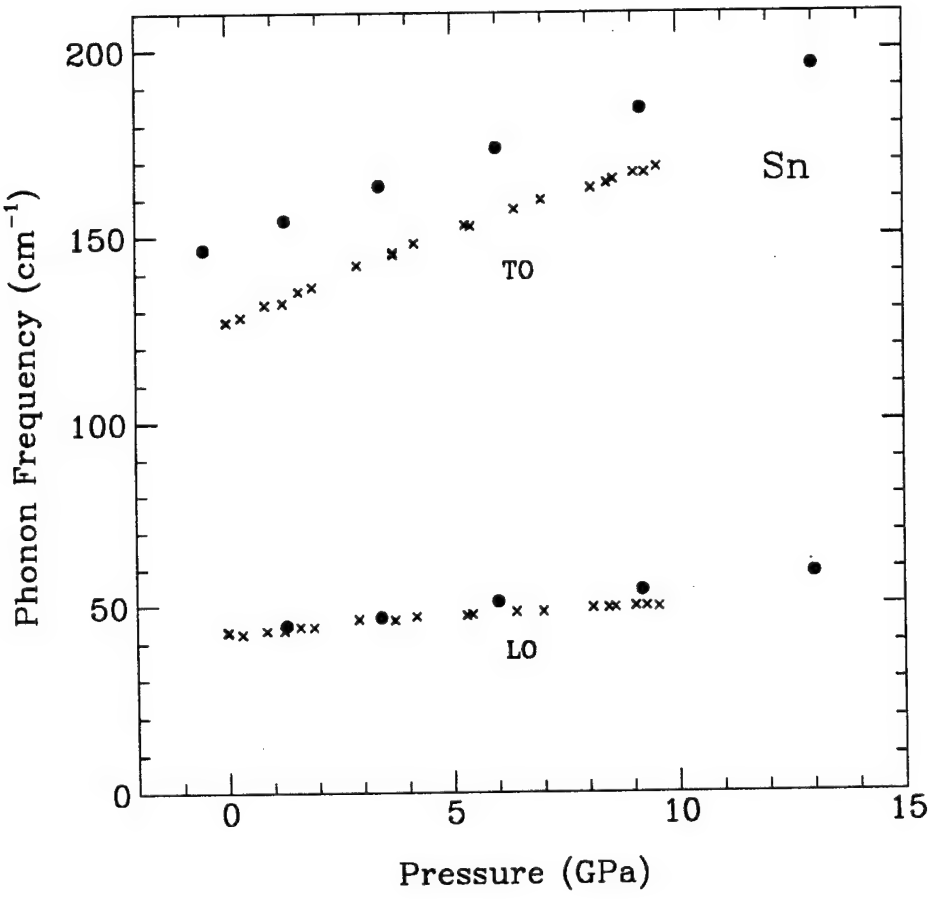

Figure 1.4: Phonon frequency vs pressure for the LO and TO Raman modes of β-Sn. The black dots are the calculated results of the present study. The crosses are the experimental results of Ref. [Oli92].

or [Che92]), although the frequency of this mode need not vanish [Kru92]. The β-Sn $\rightarrow$ sh and sh $\rightarrow$ hcp transitions are both displacive transitions of this kind, and they are associated with the β-Sn LO mode and the hcp TO mode, respectively, as mentioned in Sec. 1.3. For Si, these modes both soften approaching their respective transition to the sh structure, as expected. However, for Ge, which also undergoes a β-Sn $\rightarrow$ sh transformation, the β-Sn LO mode does not soften near the transition pressure. In fact, the frequency increases initially with pressure and only levels off near the transition. This discrepancy is discussed in the next section.

The phonon frequency for a given mode is found to be highest in Si, next highest in Ge, and lowest in Sn (see Figs. 1.2–1.4). This ordering is anticipated since, in the harmonic approximation, phonon frequencies scale inversely as the square root of the mass. Furthermore, for the β-Sn structure TO mode the frequencies at a given pressure obey this scaling law almost exactly. This behavior is only approximated for the LO mode, since the pressure-dependence of this mode is different for the three elements.

In the β-Sn structure, the TO modes lie at higher frequencies than the LO modes because of the geometry of the structure. The bonds between the two bct sublattices are nearly perpendicular (angle $\sim 75°$) to the c-axis. Therefore, for a given amplitude, the TO mode distorts the bonds more than the LO mode, resulting in a stiffer bond for the TO mode.

Figure 1.5 exhibits the calculated charge density contours in the (100) plane for Ge in the β-Sn structure at 13 GPa (Fig. 1.5(a)) and 60 GPa (Fig. 1.5(b)). The region of the plane shown contains the two atoms of the basis plus two adjacent atoms along the c-axis. The analogous contour plots for Si and Sn are qualitatively very similar to these, and thus have not been included. While the charge density is clearly highest between the two atoms of the basis, there is also a lot of charge between the two adjacent atoms along the c-axis, indicating a secondary bond. This is not surprising considering that the interatomic distance along the c-axis is only

slightly larger than the nearest-neighbor distance.

The binding in the β-Sn phase is mainly metallic over the whole pressure range. This can be seen in the degree of uniformity of the charge density. Even at low pressure, the lowest value of the interstitial charge density in the (100) plane is about 5 electrons/cell, not much less than the average value of 8 electrons/cell. However, the peaking of the charge density in the bond region clearly indicates that there is still covalent character to the binding. Upon compression, the system becomes more metallic. This is seen in Fig. 1.5(b) by the transfer of charge from the bond regions to the interstitial region. The peak in the charge density decreases from 14.5 electrons/cell at 13 GPa to 14.0 electrons/cell at 60 GPa. Similarly, the charge density minimum in the interstitial region increases from 5.0 electrons/cell at 13 GPa to 5.6 electrons/cell at 60 GPa.

The decrease in bond charge with increasing pressure (decreasing volume) for Si, Ge, and Sn in the β-Sn structure is summarized in Fig. 1.6, which shows the calculated bond charge as a function of unit cell volume for the three elements. For the purpose of this study, the bond charge is defined as the amount of charge, in excess of a uniform background, contained in a symmetric ellipsoid whose major axis extends from one atom of the basis to the other, and whose minor axis is chosen to be half of the major axis. This definition is scale independent, and therefore, the choice of aspect ratio is somewhat arbitrary. The value used here was chosen to include in the ellipsoid all closed charge density level surfaces. For each element, the bond charge is found to vary linearly with volume. The curves for Si and Ge have approximately the same slope ($\sim$ 0.0084 electrons/cell), whereas the slope of the curve for Sn is about a third smaller. At a given cell volume, the bond charge is largest in Si and smallest in Sn, which is consistent with an increase in metallic character in going from Si to Ge to Sn. This trend is also seen for these elements in the diamond structure, and is attributed to the more effective screening of the nucleus by the core electrons with increasing atomic number [Coh88].

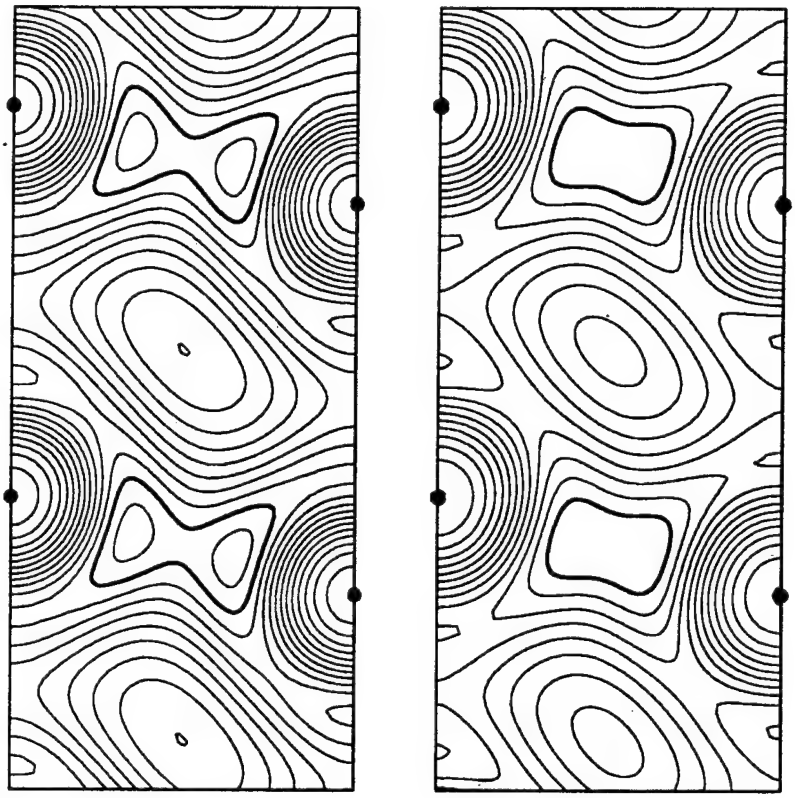

Figure 1.5: Charge density contours in the (100) plane of the β-Sn structure for Ge at (a) 13 GPa and (b) 60 GPa. The maximum and minimum contours are (a) 14 and 2 electrons/cell, and (b) 13 and 1 electrons/cell, respectively, and the spacing between contours is 1 electron/cell. Black dots represent the locations of the atoms, and heavy solid lines denote the 13 electrons/cell contours for reference. The charge density peak goes from 14.5 electrons/cell in (a) to 14.0 electrons/cell in (b). The minimum in the interstitial region goes from 5.0 electrons/cell to 5.6 electrons/cell.

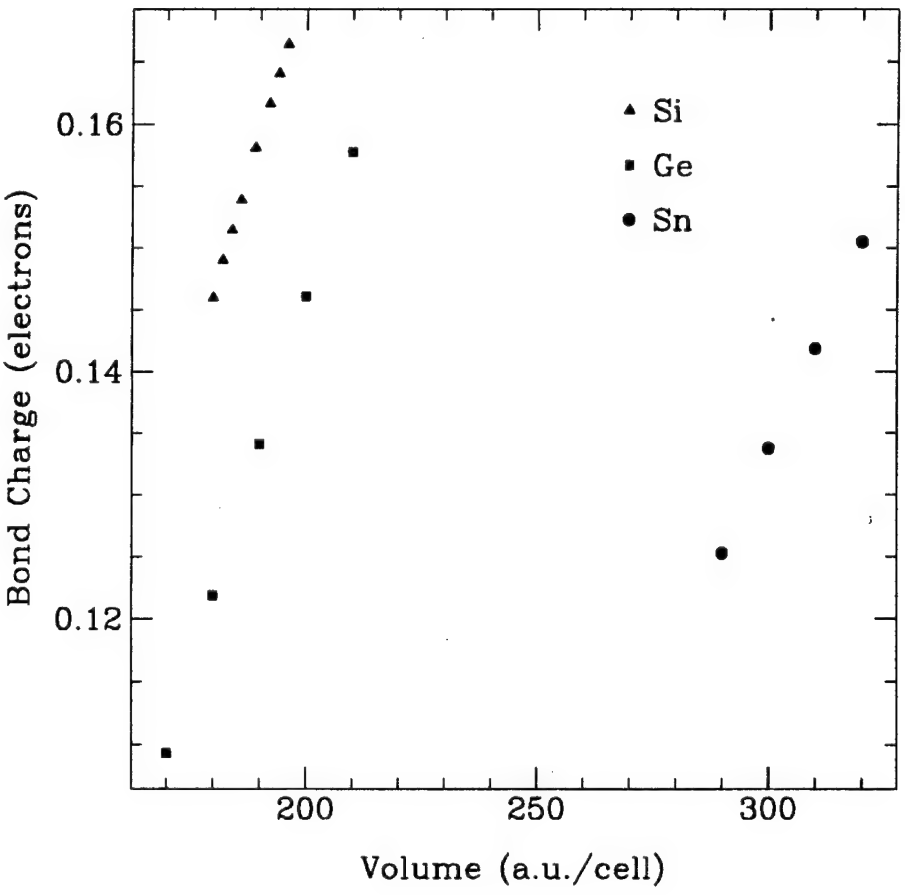

Figure 1.6: Bond charge vs cell volume for Si, Ge, and Sn in the β-Sn structure. The bond charge is defined as the amount of charge in excess of a uniform background contained in an ellipsoid. See text for details.

1.5 Discussion

This section discusses the difference in the pressure-dependence of the LO mode for Si and Ge in the β-Sn structure, as described in Sec. 1.4. To understand this anomaly, it is useful to see how the different terms in the total energy contribute. The total energy can be written as [Pic89]

$$E_{tot} = E_{Ewald} + E_{1-el} + E_{Hartree} + E_{xc} + E_{\alpha} \tag{1.2}$$

where E_{Ewald} is the ion-ion Coulomb energy, E_{1-el} is the energy associated with single-electron effects such as kinetic energy and the electron-ion interaction, $E_{Hartree}$ is the electron-electron Coulomb energy, E_{xc} is the sum of the exchange and correlation energies, and E_{α} is a term to account for the difference between the pseudopotential and a Coulomb potential. This last term depends only on volume and therefore does not contribute to the phonon frequency.

If each term in the total energy is fitted to a quadratic polynomial in the phonon amplitude u, then a component phonon frequency ω_i can be defined as follows

$$E_i = A_i u^2 + B_i = \frac{1}{2} M \omega_i^2 u^2 + E_{0i} \tag{1.3}$$

where A_i, B_i, and E_{0i} are constants, and M is the atomic mass. The term linear in phonon amplitude vanishes rigorously for each component of the total energy because the crystal is symmetric about u=0 for this phonon mode. The total phonon frequency ω can be decomposed into the component phonon frequencies in the following way:

$$\omega^2 = \sum_i \omega_i^2. \tag{1.4}$$

In Figs. 1.7 and 1.8 we present the decomposition of ω^2 as a function of pressure for the LO mode of Si and Ge, respectively, in the β-Sn structure. For both Si and Ge, the pressure-dependence of the phonon frequency comes mainly from the one-electron term since the other terms are fairly independent of pressure. Thus, the discrepancy between Si and Ge should arise from single-particle effects. The

primary difference between Si and Ge is that Ge has *d* electrons in its ion core. Therefore, the *d*-component of the Ge pseudopotential is more repulsive than the Si *d* potential. This difference has been used effectively to explain why Ge is stable in the β-Sn structure over a much larger pressure range than Si [Cha86d].

In Ref. [Cha86d] the *d*-component of the valence electronic wavefunction is found to increase in going from the β-Sn structure to the sh structure. Furthermore, this component is found to increase with pressure for both phases. Since the sh structure is essentially the β-Sn structure with a large amplitude LO phonon distortion, the *d*-component of the wavefunction for a smaller amplitude distortion should have a value somewhere between these two extremes. Thus, it is expected that an LO phonon distortion of the β-Sn structure produces an increase in the *d*-character of the wavefunction.

This same conclusion is reached by examining the effect on the charge density produced by a small LO distortion. Figure 1.9 shows contours in the (100) plane of the *difference* in charge density between the distorted and undistorted crystal. Solid (dashed) lines represent positive (negative) contours and correspond to an increase (decrease) in charge density upon distortion. Heavy solid lines represent zero change in the charge density, and black dots denote atomic positions for the undistorted system. Contours shown range from -0.50 to 0.35 electrons/cell. The two lobes (one positive, one negative) surrounding each atom are primarily caused by a rigid shift of the charge density with the distortion and are not particularly relevant. The most physically relevant feature of Fig. 1.9 is the shift of charge density from the bond region (negative contours) to the interstitial region (positive contours). This is analogous to the effect of increasing pressure (see Fig. 1.5), and, since the *d*-component increases with pressure [Cha86d], it is consistent with the notion that the *d*-character of the wavefunction increases with an LO distortion.

This behavior can be used to explain the initial increase with pressure (decreasing volume) of the β-Sn-structure LO mode of Ge. At smaller volumes the ion cores

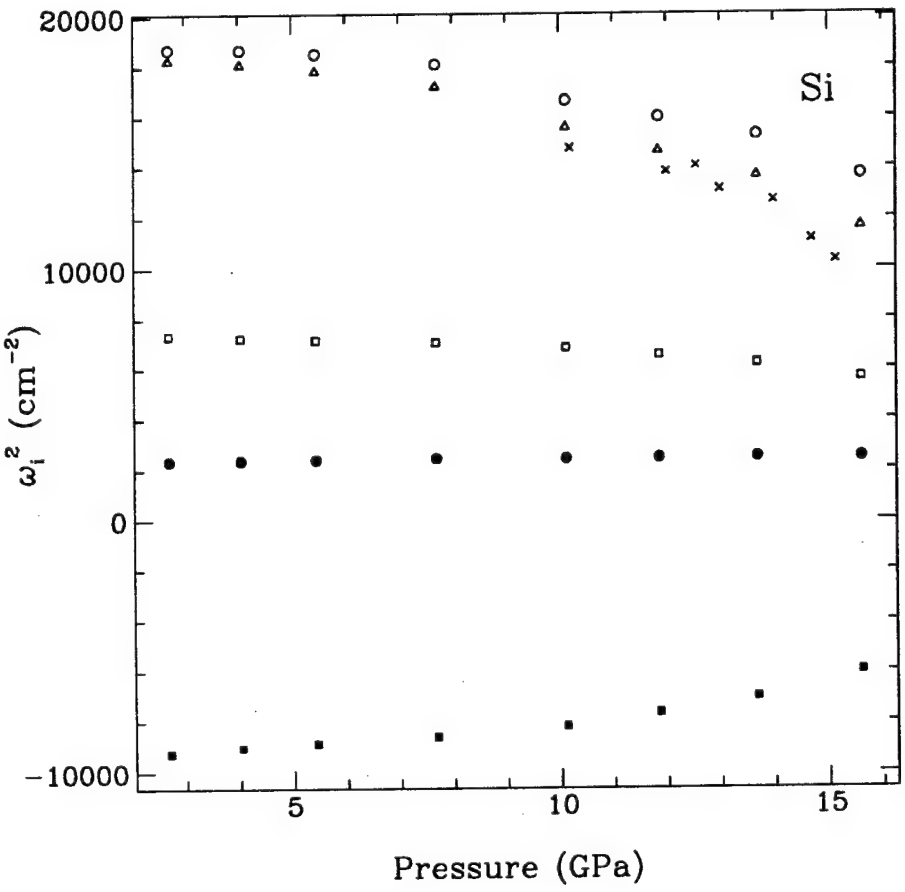

Figure 1.7: Components of ω^2 vs pressure for the LO mode of Si in the β-Sn structure. The total ω^2 is given by an open circle, the one-electron component is given by an open triangle, the Hartree component is given by a filled square, the exchange and correlation component is given by an open square, the Ewald component is given by a filled circle, and the experimental results of Ref. [Oli92] are given by crosses.

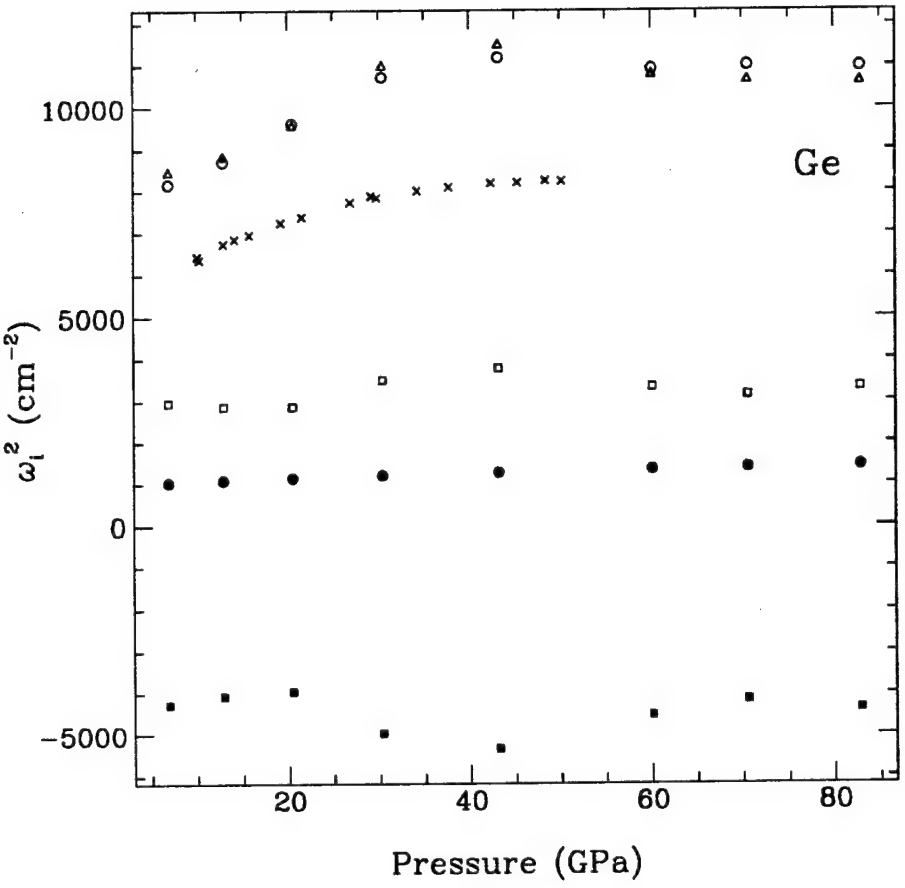

Figure 1.8: Components of ω^2 vs pressure for the LO mode of Ge in the β-Sn structure. The total ω^2 is given by an open circle, the one-electron component is given by an open triangle, the Hartree component is given by a filled square, the exchange and correlation component is given by an open square, the Ewald component is given by a filled circle, and the experimental results of Ref. [Oli92] are given by crosses.

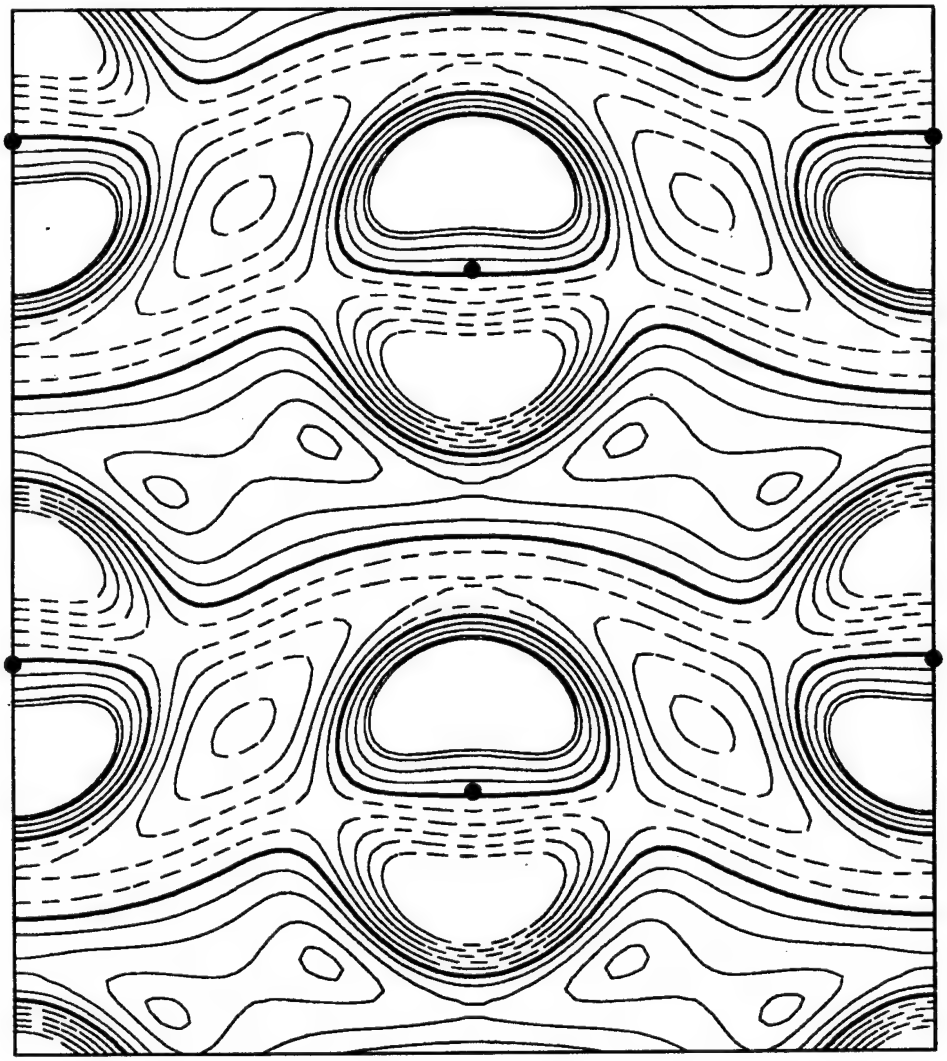

Figure 1.9: The difference in charge density (in the (100) plane) between β-Sn–Ge at 60 GPa with and without a static LO distortion of amplitude 0.08 a.u. Solid (dashed) lines denote positive (negative) contours; heavy solid lines denote zero change in charge density. The maximum (minimum) contour shown is 0.35 (-0.50) electrons/cell. Black dots correspond to atomic positions of the undistorted system.

make up a larger fraction of the unit cell volume. Since Ge has core *d* electrons, its pseudopotential is relatively repulsive to *d*-symmetry valence electrons, which are, therefore, effectively blocked from the core region. Thus, as pressure increases, the valence *d* electrons in Ge are confined to a decreasing fraction of the volume, and are thus increasingly energetic. Since an LO phonon distortion of the β-Sn structure produces an increase in the *d*-component of the wavefunction, the energy of the distorted system for Ge should increase with pressure more rapidly than that of the undistorted system. Therefore, the curvature of the energy of Ge with respect to LO phonon amplitude increases as a function of pressure due to this "decreasing-volume-fraction" effect. In other words, the LO phonon frequency for Ge in the β-Sn structure should increase with pressure. Since Si has no *d* electrons in its core, this effect is less pronounced in Si.

It is also found in Ref. [Cha86d] that the increase in the *d*-component of the wavefunction with pressure is slightly more rapid for the sh phase than for the β-Sn phase. Therefore, by similar reasoning as above, it is expected that, for an LO distortion of the β-Sn structure, the accompanying increase in the *d*-character of the wavefunction will increase slightly with pressure. Further evidence of this is obtained by examining contour plots like Fig. 1.9 for several different pressures. The shift in charge from the bond region to the interstitial region upon distortion, which was shown to signal an increase in *d* character, is found to be somewhat more pronounced at higher pressures. This is consistent with the above assertion that the distortion-induced increase in the *d*-component of the wavefunction increases with pressure. Such behavior serves to enhance the "decreasing-volume-fraction" effect described in the preceding paragraph, and, therefore, also has a positive effect on increasing the phonon frequency with pressure.

The plateauing of the Ge LO mode near the transition pressure is caused by the competing effect of phonon mode softening due to the onset of a displacive structural transition.

NOTES

[1] At atmospheric pressure, β-Sn becomes more stable than α-Sn (cubic diamond structure) above 13°C. At absolute zero, the α-Sn $\rightarrow$ β-Sn transition is estimated to occur at about 0.5 GPa.

[2] The Raman modes are designated either TO or LO in the manner of Ref. [Oli92].

System	V_0 (a.u./atom)	B_0 (GPa)	B_0'
β-Sn			
Si	98.9	119	4.00
Ge	116.8	91	4.04
Sn	167.1	59	5.08
hcp			
Si	92.4	102	3.72

Table 1.1: Best-fit parameters to the Murnaghan equation of state [Mur44] for Si, Ge, and Sn in the β-Sn structure and for Si in the hcp structure. The parameters are the equilibrium volume V_0 and the bulk modulus B_0 and its pressure derivative B_0' at this volume.

Chapter 2

High-Pressure Orthorhombic Silicon

2.1 Introduction

A recent angle-dispersive x-ray diffraction study by McMahon and Nelmes [McM93] of Si at high pressure reports a new intermediate structural phase at pressures between the transition pressures for the β-Sn and simple hexagonal (sh) phases. Although the high-pressure properties of Si have been widely investigated both theoretically and experimentally (see Ref. [Lew93a] and references therein), until now Si was thought to transform directly from the β-Sn structure to the sh structure at about 16 GPa. In particular, a previous x-ray diffraction study [Hu84] interpreted the diffraction pattern between 13.2 and 16.4 GPa as resulting from a mixture of the β-Sn and sh phases, with the transformation completed by 16.4 GPa. However, McMahon and Nelmes [McM93] are unable to fit their data to any such mixture. Instead, they index the diffraction pattern to a body-centered orthorhombic lattice with space group Imma which is a generalization of both the β-Sn and sh structures. This structure (denoted Imma) is the monatomic equivalent of the proposed structure for high-pressure compound phases of InSb II [Nel93] and GaAs III [Wei89].

Previous theoretical studies have considered the possibility of an intermediate orthorhombic phase between the β-Sn and sh phases [Nee84, Cha85a], although not in detail. In Ref. [Nee84], the total energy was calculated for five structures along a linear, Imma-based path from β-Sn to the sh structure. It was found that within the resolution of their calculation ($\sim$0.7 mRy/atom) the continuum of structures along this path were viable candidates for stable phases. The authors of Ref.

[Cha85a] suggested that an accurate calculation of the energy barrier between β-Sn and sh phases would involve varying several structural parameters. Their suggested structural variations are equivalent to exploring the Imma structure.

This chapter reports on a first-principles investigation of the structural properties of the proposed orthorhombic phase of Si and its relative stability compared to both the β-Sn and sh structures. The energy of the new phase is found to be lower than or equal to the energy of both the β-Sn and sh phases for all unit cell volumes. For small (large) volumes the Imma and sh (β-Sn) structures are comparable in energy, whereas for intermediate volumes the energies of all three structures are distinct. Similar behavior is found in the volume-dependence of the optimal structural parameters (*i.e.*, axial ratios and internal parameters) of the Imma phase. For very large volumes, the Imma structural parameters approach the values that give the β-Sn structure. As volume decreases, the optimal Imma structure gradually deviates from the β-Sn-like structure and approaches the sh structure. At very small volumes (high pressure), the Imma and sh structures are nearly identical. This calculated trend in the Imma structure from a β-Sn-like phase to a sh-like phase accounts for the changes seen in the x-ray diffraction pattern [McM93] upon compression.

The overall agreement between the calculations and the measurements of Ref. [McM93] is excellent. In particular, calculated structural parameters for the three phases agree with reported experimental values to within 0.5% (and in some cases much better) for axial ratios and a few percent for internal parameters. For the reference volume (13.6 Å^3) at which the diffraction pattern for the Imma phase was indexed, calculations show that the Imma structure is distinct from and lower in energy than both the β-Sn and sh phases. This is consistent with the observed x-ray data.

Section 2.2 contains a description of the Imma structure and its relationship to the β-Sn and sh structures, followed by an account of the computational method.

Next, the calculated structural properties of the Imma, β-Sn, and sh phases of Si are presented and compared in detail in Sec. 2.3. This is followed in Sec. 2.4 by a discussion of the calculated structural trends and some comments on previous work in light of the present results.

2.2 Computations

Figure 2.1 shows schematically the structure of the Imma phase, with open and filled circles referring, respectively, to the two Si atoms of the basis. As mentioned above, this structure has a body-centered orthorhombic Bravais lattice with space group Imma. Its two-atom primitive cell is defined by lattice vectors

$$\begin{aligned} \mathbf{a}_1 &= \frac{1}{2}(a, b, -c) \\ \mathbf{a}_2 &= \frac{1}{2}(-a, b, c) \\ \mathbf{a}_3 &= \frac{1}{2}(a, -b, c)\,, \end{aligned} \tag{2.1}$$

and atomic postions

$$\tau_{\pm} = \pm[\frac{1}{4}\mathbf{a}_1 + (\frac{1}{4} + u)\mathbf{a}_2 + u\mathbf{a}_3]\,, \tag{2.2}$$

where u is an internal parameter (varying from $\frac{1}{4}$ to $\frac{1}{8}$) which determines the relative z coordinate of the two atom in the basis. The three parameters b/a, c/a, and u specify the structure for a given cell volume. In practice, b/a is slightly less than or equal to unity, and c/a is slightly larger than $\frac{1}{2}$.

The Imma structure is a generalization of the β-Sn and sh structures in that they both can be described by the Imma unit cell with specific restrictions on the structural parameters. In particular, the two parameters u and b/a are restricted by symmetry for both the β-Sn and sh structures, leaving only c/a as a free variable. The β-Sn structure is body-centered tetragonal with a two atom basis, and is given by the Imma structure with $b/a = 1$ and $u = \frac{1}{8}$. The simple hexagonal structure is obtained from Imma by setting $u = \frac{1}{4}$ and $b/a = \sqrt{3}\,c/a$. The resulting sh cell

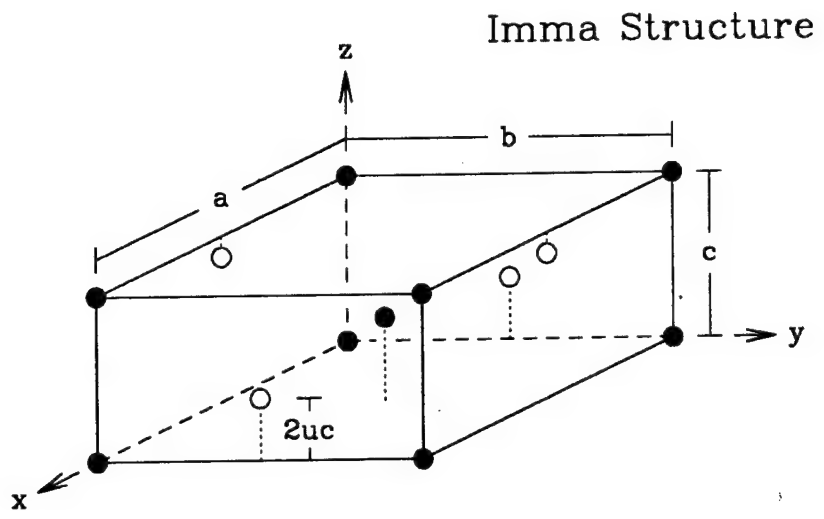

Figure 2.1: Schematic representation of the body-centered orthorhombic Imma structure. Open and filled circles correspond to the two Si atoms of the basis. The parameters that define this structure for a given volume are b/a, c/a, and u which describes the difference in the z component of the two atoms in the basis. Dotted lines serve only to show atomic positions. See the text for a thorough description of the Imma structure.

is not the conventional primitive cell but is related to it in the following way: if primed letters denote axes of the conventional sh cell and unprimed letters denote Imma axes, then $c' = \frac{1}{2}a$ and $a' = c$. Thus, the Imma cell is rotated with respect to the conventional sh cell and is twice the size. The axial ratios of the two cells are related by $(c/a) \times (c'/a') = \frac{1}{2}$.

Calculations are performed using the *ab initio* pseudopotential total energy method in a plane wave basis [Ihm79, Coh82, Pic89]. In this method, electron-ion interactions are evaluated using a semi-local, norm-conserving pseudopotential [Ham79]; electronic exchange and correlation energies are calculated within the local-density approximation (LDA) [Lun83] using a standard form for the exchange-correlation potential [Cep80]; and the temperature is assumed to be zero.

Because the three metallic structures are very close in energy, it is necessary to calculate total energy differences very accurately. To accomplish this, a large Fourier expansion cutoff energy (30 Ry) is used, and the irreducible part of the Brillouin zone is sampled at a large number (550) of points. These values were chosen to produce relative energies that are converged to within 0.05 mRy/atom. Typically, this degree of precision is not achievable when comparing different structures since systematic errors are usually larger. However, because the systems involved are so similar, errors tend to be correlated and therefore cancel in energy differences.

All structural parameters for the three phases are optimized at each unit cell volume, with the degree of optimization governed by the desired precision in relative energies. Energy minimization is carried out for a given structure and volume by stepping along the gradient of the energy with respect to structural parameters until the magnitude of the gradient is smaller than a specified threshold. The gradient of the total energy with respect to structural parameters is calculated using *ab initio* determined quantum mechanical forces [Ihm79] and stresses [Nie85].

2.3 Results

The calculated volume-dependence of the optimal structural parameters of the three phases is presented in Fig. 2.2. Points with dashed lines through them represent parameters that are constant by definition. For clarity, error bars have been omitted for data points for which errors are comparable to or smaller than the size of the dots that denote them. The computed structural parameters are consistent with structural data from previous less-converged calculations and less resolved measurements (see Ref. [Lew93a] and references therein), and are in excellent agreement with reported experimental values of Ref. [McM93] as is shown in Table 2.1.

At large volumes, the optimal Imma structure is close to β-Sn structure. However as this phase is compressed, its structural parameters are found to diverge from the β-Sn values and approach the sh values. By a volume of 86 a.u./atom, the sh and Imma structures are nearly indistinguishable, whereas for intermediate volumes all three structures are clearly distinct. The rate at which the Imma phase changes with volume can also be seen in Fig. 2.2. As it is compressed, the Imma phase deviates slowly from β-Sn structure, but by 95 a.u./atom it starts rapidly changing into the sh structure.

Calculated equations of state for the three phases of Si are shown in Fig. 2.3, where solid lines are fits of computed data points (solid dots) for each structure to the Birch equation of state [Bir78]. The fits for the β-Sn and sh structures are in good agreement with previous calculations [Lew93a, Nee84, Cha85a].

The total energy for the optimal Imma structure is calculated to be lower than that of β-Sn structure for all volumes considered. However, at large volumes (low and negative pressures) where the two structures are quite similar, the difference in energies of the two phases is within the systematic uncertainty of the calculation. At relatively low pressures experiments observe only the β-Sn phase even though the calculations show that the Imma structure is competitive if not lower in energy than the β-Sn structure. Since the two structures are so similar in this pressure

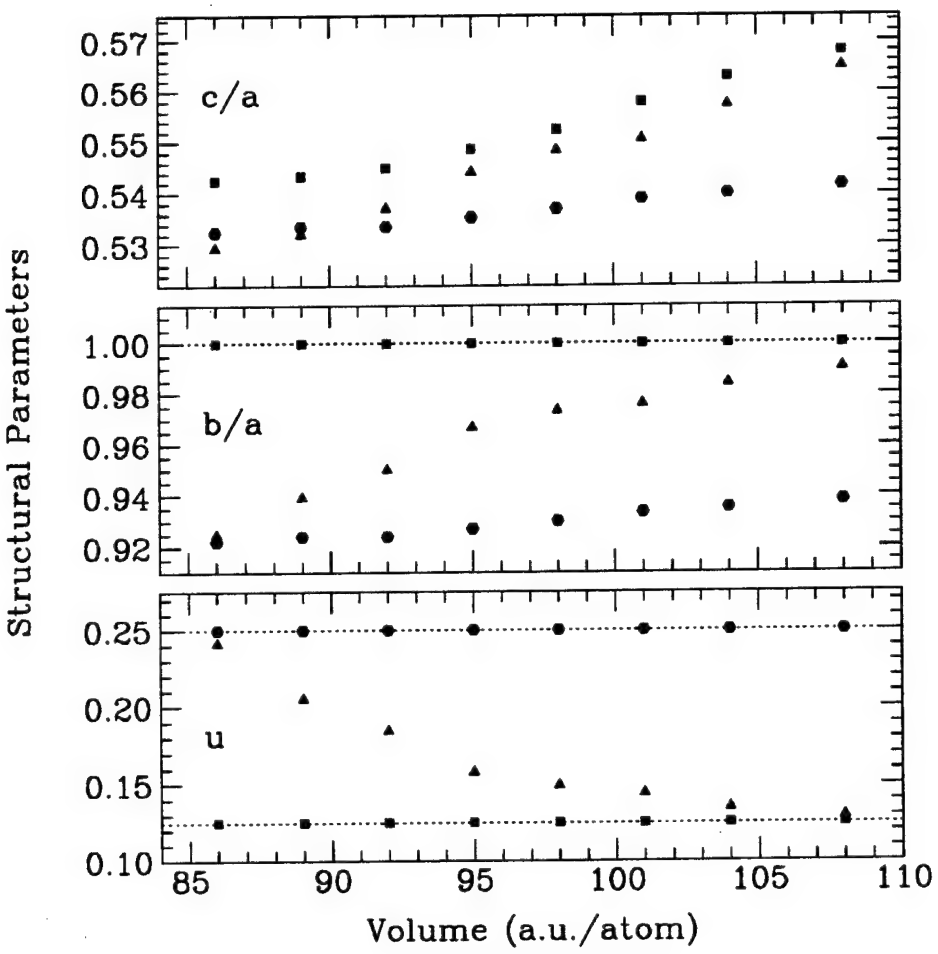

Figure 2.2: Calculated volume-dependence of the optimal structural parameters of the Imma (triangles), β-Sn (squares), and sh (hexagons) structures. Points with dashed lines through them represent parameters that are constant by definition. For the sh structure, the value of b/a is related to c/a by $b/a = \sqrt{3}\,c/a$. Errors in the parameter values are comparable to or smaller than the size of the dots.

Structure	Volume (a.u./atom)	Theory (present work)	Experiment (from Ref. [McM93])
sh	89	c/a=0.534	0.533
Imma	92	c/a=0.537	0.538
		b/a=0.950	0.950
		u=0.185	0.193
β-Sn	95	c/a=0.549	0.551

Table 2.1: Comparison between calculated structural parameters for the β-Sn, Imma, and sh phases and reported measurements from Ref. [McM93].

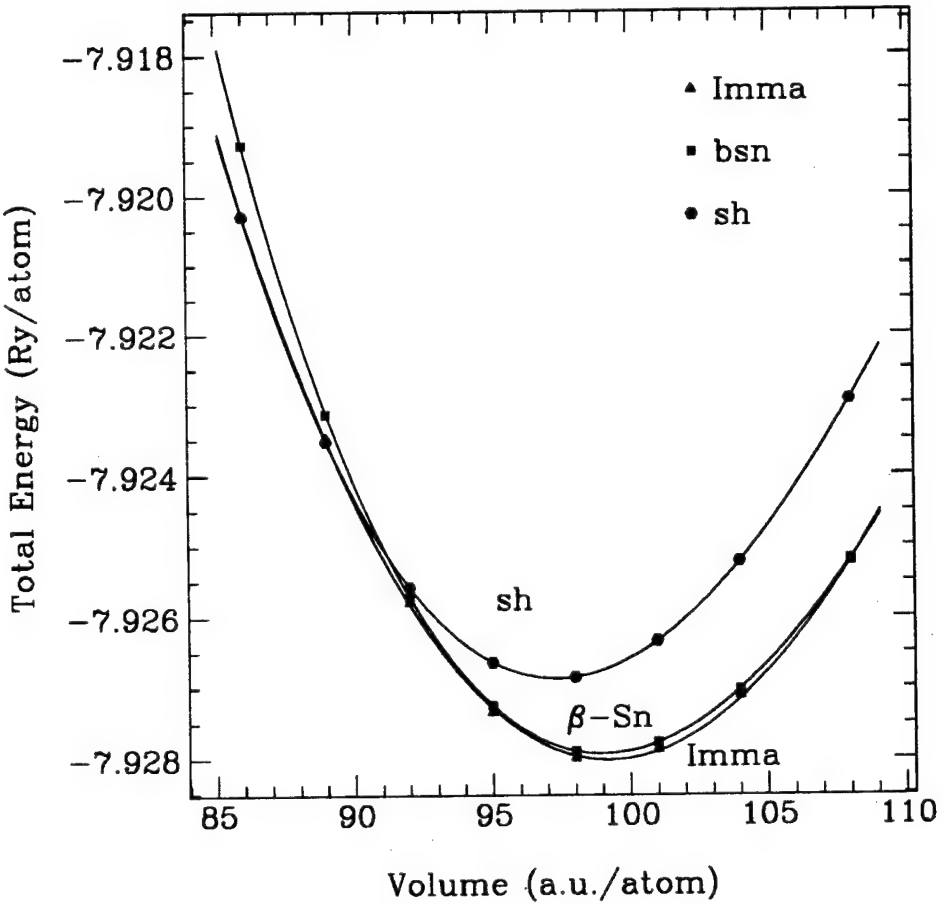

Figure 2.3: Calculated total energy versus volume, fitted to the Birch equation of state [Bir78], for Si in the Imma, β-Sn, and sh structures. Structural parameters have been optimized at each volume for all three phases.

region, perhaps they are indiscernable at finite temperatures, which could explain the discrepancy between theory and experiment.

The Imma phase is also found to be lower in energy than the sh phase for all but the smallest volumes, where, within the resolution of the calculation, the two equations of state merge. It is interesting to note that the merging of the total energies (at ~90 a.u./atom) occurs while the two structures are still distinct (see Fig. 2.2). This point is discussed below.

2.4 Discussion

Transformation of the Imma phase from the β-Sn-like to the sh-like structure results from relative changes in the various terms of the total energy as a function of cell volume. The total energy can be viewed as the sum of five terms:

$$E_{tot} = E_{1-el} + E_{Hartree} + E_{xc} + E_{Ewald} + E_{\alpha} \tag{2.3}$$

where E_{1-el}, also called the band energy, is associated with single-electron effects such as kinetic energy and the electron-ion interaction; $E_{Hartree}$ is the direct electron-electron Coulomb energy (Hartree energy); E_{xc} is the sum of the exchange and correlation energies; E_{Ewald} is the ion-ion Coulomb energy (Ewald energy); and E_{α} is a term to account for the difference between the pseudopotential and a Coulomb potential. Figure 2.4 shows the volume-dependences of the first four terms of Eq. 2.3 for the β-Sn and sh phases relative to the Imma phase. The E_{α} term is essentially the same for all three phases.

Because electrons and ions are more uniformly distributed in the more closely packed sh structure, the repulsive Coulomb-based terms, $E_{Hartree}$ and E_{Ewald}, tend to favor this phase over the β-Sn structure. Conversely, the band and exchange and correlation energies tend to favor the β-Sn structure. For E_{1-el} this trend is due to greater band dispersion in the more highly coordinated sh phase; whereas for E_{xc} the trend is due to the attractive nature of the exchange interaction which favors

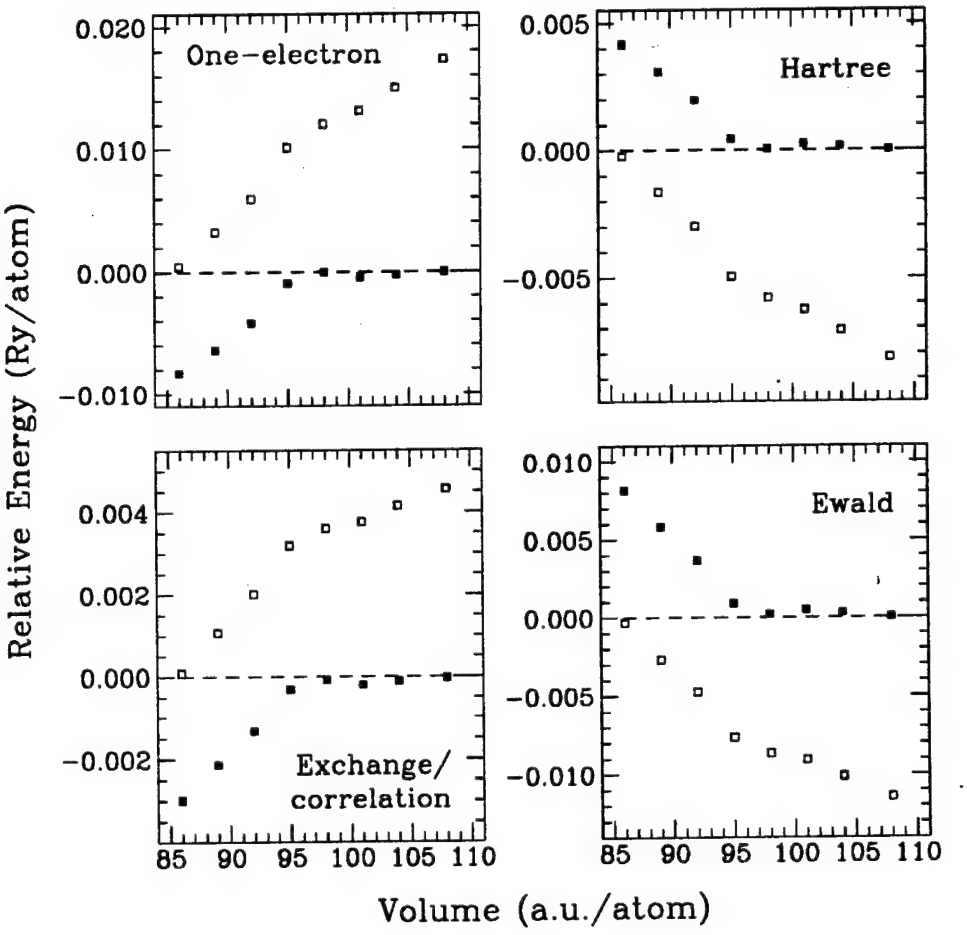

Figure 2.4: Volume-dependence of the one-electron, Hartree, exchange and correlation, and Ewald terms of the total energy for Si in the β-Sn (filled squares) and sh (open squares) structures. Energies are measured relative to the values for the Imma structure, so that the dashed line through zero on each panel corresponds to the Imma phase.

less uniform electron distributions.

At large volumes the band and exchange and correlation terms dominate the relative total energies, so that the lowest energy structure is β-Sn-like. However, as volume decreases the repulsive Coulomb-based terms become more dominant, and the lowest energy structure becomes more sh-like. It is interesting to note that the Imma structure is not favored by any individual term of the total energy, but that the terms cancel in such a way as to make it lowest in energy. Figure 2.4 also explains the merging of the Imma and sh equations of state while the structures are still different (see above). Individual total-energy components for the two phases remain distinct as long as the structures do. However the terms combine to produce comparable total energies even before the structures have merged.

Previous studies have attributed the pressure-induced β-Sn $\rightarrow$ sh structural transition to a softening of the zone-center LO phonon of the β-Sn phase. Described in terms of Imma structural parameters, this mode corresponds to a variation of u about $u = \frac{1}{8}$, and hence lies along the coordinate of the largest component of the structural transformation. Recent experimental [Oli92] and theoretical [Lew93a] (see Chapter 1) investigations of the pressure-dependence of this mode have found that it does indeed soften under pressure. However, in light of the discovery of the Imma phase, we now re-examine these experimental and theoretical results.

Raman measurements of Ref. [Oli92] can be reconciled with the present results by reassigning the crystal structure of the observed phonon mode from β-Sn to the more general Imma structure. The observed phonon softening can still be viewed as related to a structural transition even though technically the structure remains Imma throughout. Since the Imma crystal structure is symmetric in u about $u = \frac{1}{4}$ (the sh value), the total energy is always an extremum in u for this value. Thus, as the optimal Imma structure approaches sh under pressure, the topology of the total energy surface must adjust itself to accomodate this symmetry. Since the curvature in u of the total energy surface at its minimum defines the phonon frequency, this

adjustment in topology is likely to result in a softening of the phonon mode.

The theoretical results of Ref. [Lew93a] can be understood in similar terms. Since that calculation only considered the β-Sn structure, the value of b/a was fixed at unity. For this value of b/a, however, the Imma crystal structure is symmetric in u about the β-Sn value of $u = \frac{1}{8}$, and therefore, the β-Sn structure is an extremum in u of the total energy. Calculations show it to be a minimum, thus giving a real-valued LO phonon frequency. Since varying b/a from unity removes the constraint, the optimal value of u is free to deviate from its β-Sn value when $b/a \neq 1$. However, it is likely that the structural minimum for $b/a = 1$ behaves similarly to $b/a \neq 1$ minimum. In particular, the calculations of Ref. [Lew93a] show that the curvatures in u of the two minima (*i.e.*, their phonon frequencies) have the same pressure-dependence. Despite the agreement with the measured pressure-dependence of the phonon frequency, the calculation gave values of the frequency that were systematically somewhat larger than the experimental values. This discrepancy may be due to the structural differences that are now known to have existed.

The authors of Ref. [McM93] speculate that a transition from the β-Sn to the Imma structure might account for the discontinuous jump observed in the superconducting transition temperature (T_c) in the same pressure region [Mig86]. However, the present calculation of a continuous Imma-based transformation to the sh structure would seem to contradict this hypothesis. A calculation of electron-lattice coupling and T_c of Si in the Imma structure is beyond the scope of this study, however two possible explanations of the discontinuity observed in T_c are offered. One possiblity is tied to an increase in the rate of change of the Imma structure for volumes < 95 a.u./atom (see above). If this effect were to manifested itself in analogous changes in the phonon frequencies or density of states at the Fermi level, then a shift in T_c that appears discontinuous might occur. We have calculated the volume-dependence of the density of states at the Fermi level and have found no rapid change near 95 a.u./atom. Another explanation is the possibility of slight pres-

sure inhomogeneities in the T_c versus pressure measurements causing discontinuous structural transformations.

Theoretical and experimental results on the Imma-mediated β-Sn $\rightarrow$ sh structural transition in Si suggest a similar mechanism for Ge which undergoes the same pressure-induced β-Sn $\rightarrow$ sh transformation [Voh86]. This hypothesis is considered in the next chapter.

Chapter 3

Prediction of an Orthorhombic Phase of Germanium

3.1 Introduction

From their many studies of highly condensed Si and Ge (see Ref. [Lew93a] and references therein), high-pressure investigators have come to agree that the first three structures of both elements are the diamond, β-Sn, and simple hexagonal (sh) structures, respectively. The phase transitions occur at about 12 and 16 GPa, respectively, for Si and about 11 and 75 GPa, respectively, for Ge. However, as was stated in Chap. 2, a recent x-ray diffraction study by McMahon and Nelmes [McM93] on Si up to $\sim$18 GPa has called this picture into question. These investigators discovered a new orthorhombic phase (denoted Imma after its space group) for pressures between the transition pressures of the β-Sn and sh phases, suggesting the structural sequence: diamond $\rightarrow$ β-Sn $\rightarrow$ Imma $\rightarrow$ sh.

In the last chapter, we presented results of an *ab initio* investigation of the structural properties of the β-Sn, Imma, and sh phases of Si that were in excellent agreement with the experimental results of Ref. [McM93]. It was further shown for Si, however, that the energy of the Imma structure is lower than or equal to that of the β-Sn and sh structures for all unit cell volumes. The optimal structural parameters (*i.e.*, axial ratios and internal parameters) that define Imma-Si were found to vary continuously with cell volume from values at large volumes that give the β-Sn structure to values at small volumes that give the sh structure. At intermediate volumes the three structures were clearly distinct. In this region the Imma phase was noticeably lower in energy than either the β-Sn or sh phase. Thus the picture that emerges for the structural sequence of Si consists of the diamond phase trans-

forming into the Imma phase, with the β-Sn-like and sh structures being limiting cases of the latter. Since Ge has also been observed to transform from the β-Sn to the sh structure [Voh86], the results on the Imma phase of Si strongly suggest the possibility of an Imma phase for Ge.

This chapter reports the results of a first-principles investigation of Ge in the Imma structure. The stability properties and structural trends of Imma-Ge are found to be analogous to those of Imma-Si. In particular, the energy of the Imma phase is calculated to be lower than or equal to the energy of both the β-Sn and sh structures for all unit cell volumes. Furthermore the optimal Imma structure for Ge is found to transform continuously under pressure from a β-Sn-like structure to the sh structure as it does for Si. Vohra, *et al.* [Voh86] found that the β-Sn $\rightarrow$ sh transformation was isovoluminal within the resolution of their measurements. The prediction here of a continuous, Imma-based transformation to the sh structure is consistent with that observation.

3.2 Computations

Chapter 2 contains a detailed picture (Fig. 2.1) and description of the Imma structure, only the most salient features of which are reviewed here. The Imma structure has a body-centered orthorhombic Bravais lattice with a two-atom basis. Its lattice vectors and atomic positions are given by $\mathbf{a}_1 = \frac{1}{2}(a, b, -c)$, $\mathbf{a}_2 = \frac{1}{2}(-a, b, c)$, and $\mathbf{a}_3 = \frac{1}{2}(a, -b, c)$, and $\tau_\pm = \pm[\frac{1}{4}\mathbf{a}_1 + (\frac{1}{4} + u)\mathbf{a}_2 + u\mathbf{a}_3]$, respectively. For a given cell volume, the three parameters c/a, b/a, and u specify the structure. If b/a and u are set equal to unity and $\frac{1}{8}$, respectively, then the β-Sn structure is obtained. Likewise, the sh structure is obtained for $b/a = \sqrt{3}\, c/a$ and $u = \frac{1}{4}$.

Total energies for the three Ge systems are calculated within the the local-density approximation (LDA) [Lun83] using *ab initio* norm-conserving pseudopotentials [Ham79] and the momentum-space formalism [Ihm79, Coh82, Pic89]. In order to resolve the very small energy differences between the three metallic struc-

tures under investigation, it is necessary to truncate the Fourier expansion at a large cutoff energy (30 Ry) and to sample the Brillouin zone at a large number (550) of irreducible k-points. These values produce highly converged relative energies (within ~0.05 mRy/atom). While this degree of precision cannot ordinarily be achieved when comparing different structures, the structures being studied are so similar that systematic errors tend to be correlated and therefore cancel in energy differences. All structural parameters for the three phases are optimized at each unit cell volume, with the degree of optimization governed by the desired precision in relative energies.

3.3 Results

The calculated volume-dependences of the optimal structural parameters for Ge in the Imma, β-Sn, and sh structures are displayed in Fig. 3.1. This figure is to be compared with the analogous figure for Si (Fig. 2.2). Points with dashed lines through them indicate parameters that are defined as constant. The computed c/a ratios for the β-Sn and sh [1] structures lie entirely within the experimental error bars of the measurements of Ref. [Voh86].

At large volume (low pressure), the optimal structural parameters are found to be close to the β-Sn values. Upon compression the Imma structure stays β-Sn-like until a volume of about 100 a.u./atom where the parameters start to shift toward the sh values. By 75 a.u./atom, the Imma and sh structures are nearly indistinguishable. For intermediate volumes, the three structures are clearly distinct. This volume-dependence of the Imma structure for Ge is very similar to that of Si, except that the β-Sn-like optimal Imma structure persists for a larger volume range in Ge than in Si.

Figure 3.2 shows the calculated equations of state for the three phases of Ge. Computed data points (dots) are fitted for each structure to the Birch functional form of the equation of state [Bir78], with parameters of the fits tabulated in Table

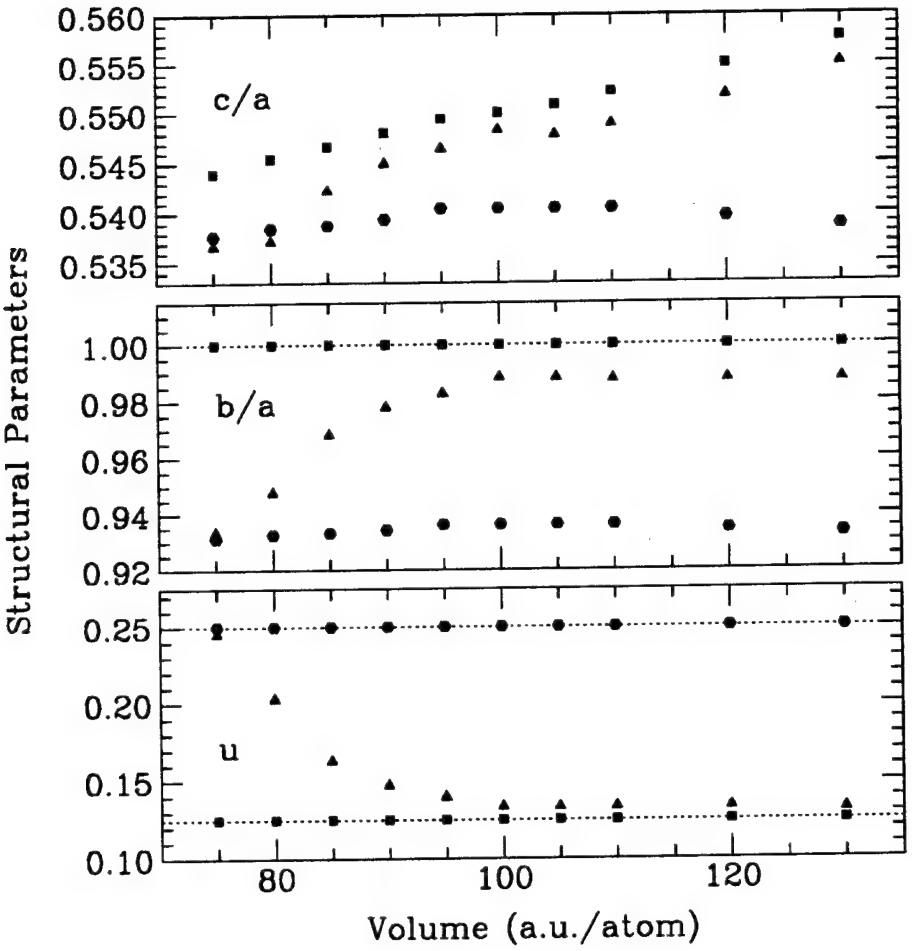

Figure 3.1: Calculated volume-dependence of the optimal structural parameters of the Imma (triangles), β-Sn (squares), and sh (hexagons) structures for Ge. Points with dashed lines through them represent parameters that are constant by definition. For the sh structure, the value of b/a is related to c/a by $b/a = \sqrt{3}\,c/a$. Errors in the parameter values are comparable to or smaller than the size of the dots.

3.1. The fit for the β-Sn structure is in good agreement with previous calculations [Cha86d, Lew93a]. Because of the large energy scale of Fig. 3.2, the energy of the Imma structure cannot be distinctly resolved at any volume. To overcome this difficulty, the total energies of the β-Sn and sh structures are plotted in Fig. 3.3 relative to the Imma total energy at each volume.

The energy of the Imma structure is seen to be equal, within the precision of the calculation, to the sh (β-Sn) energy for volumes < 80 (> 90) a.u./atom. For intermediate volumes, the Imma phase is distinctly lower in energy than the other two phases. This is also the range of volumes where the Imma structure is the most different from the other two structures (see Fig. 3.1).

3.4 Discussion

The stability of the Imma phase for Si and its continuous transformation from a β-Sn-like structure to the sh structure was shown in Chapter 2 to be caused by a competition between various terms of the total energy. Terms which favor the relatively compact sh structure (*i.e.*, the Ewald and Hartree energies) compete with terms that favor the less uniform distribution of the β-Sn structure (*i.e.*, the band and exchange and correlation energies). The Imma structure is a compromise between these conflicting tendencies. At low pressure the latter terms dominate, and so the optimal Imma structure is β-Sn-like. Whereas with increasing pressure the former terms become more dominant, and the optimal Imma structure deforms toward its sh limit.

This explanation is found to be equally valid for Ge. In fact, the most significant difference between Si and Ge in the behavior of the Imma structure is the much larger volume (and pressure) range over which the structure of the Imma phase is β-Sn-like for Ge than for Si. The experiments observe this as the much larger range of pressures for which Ge is stable in the β-Sn phase compared to Si. An explanation of this phenomenon based on the presence of d electrons in the ion core of Ge but

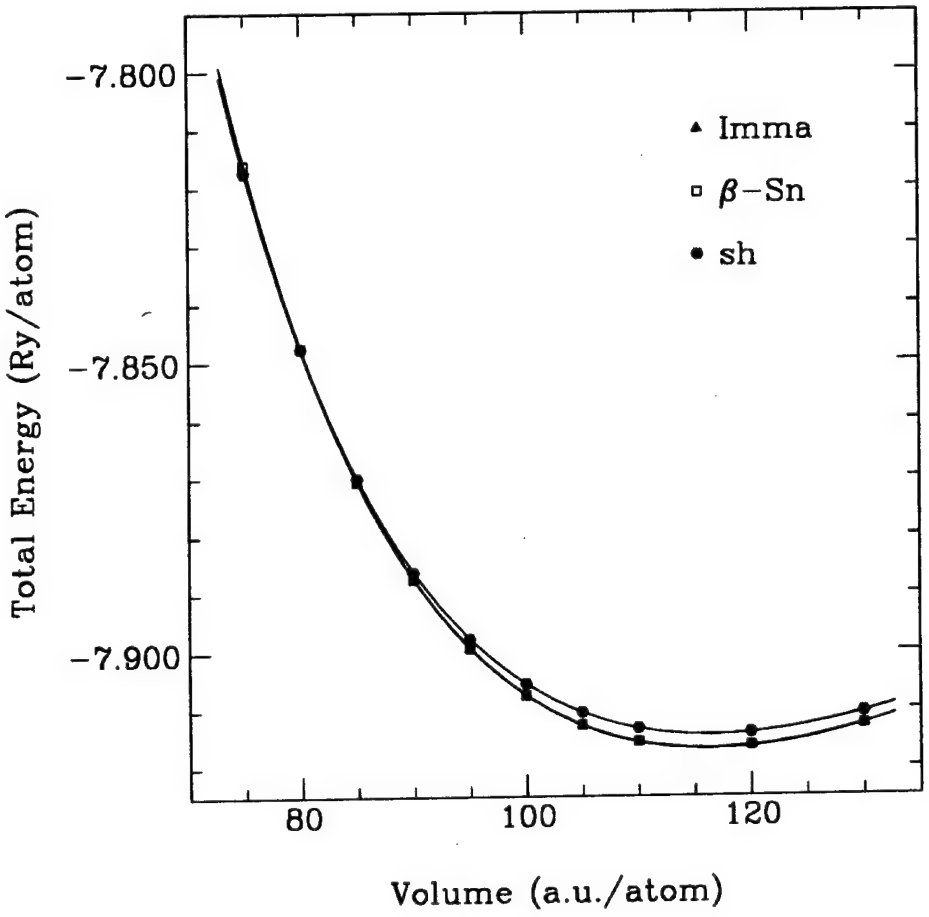

Figure 3.2: Calculated total energy versus volume, fitted to the Birch equation of state [Bir78], for Ge in the Imma, β-Sn, and sh structures. Structural parameters have been optimized at each volume for all three phases.

Structure	V_0 (a.u./atom)	B_0 (GPa)	B_0'
β-Sn	116.3	91.2	4.44
Imma	116.3	93.7	4.21
sh	116.4	86.1	4.54

Table 3.1: Best-fit parameters to the Birch equation of state [Bir78] for Ge in the β-Sn, Imma, and sh structures. The parameters are the equilibrium volume V_0 and the bulk modulus B_0 and its pressure derivative B_0' at this volume.

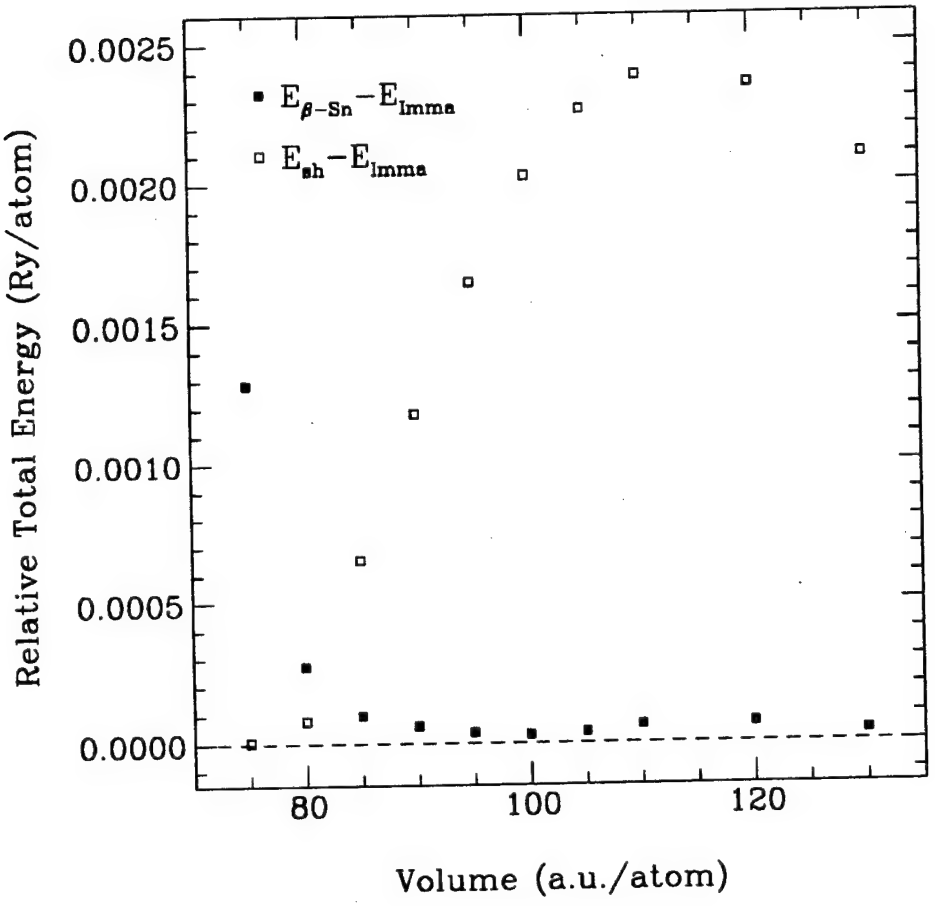

Figure 3.3: Volume-dependence of the total energy of Ge in the β-Sn (filled squares) and sh (open squares) structures relative to the Imma structure. The dashed line through zero corresponds to the energy of the Imma structure.

not of Si was provided by Chang and Cohen [Cha86d].

In the present study of Ge, as in our previous study of Si (Chapter 2), the calculated optimal Imma structure is always at least slightly different from the β-Sn structure even at large volumes. Furthermore, the energy of the β-Sn structure is always at least slightly higher than that of Imma, although at large volumes the energy difference is within the systematic uncertainty of the calculation. In light of these results one would expect that the experiments would at least observe both phases, however only the β-Sn phase has been reported to be observed. One possible explanation of this discrepancy between theory and experiment is that finite temperature effects might be important, especially since the energy differences are so small. The validity of this hypothesis, however, requires further investigation.

NOTES

[1] The c/a ratios for the conventional sh unit cell and the Imma-based sh unit cell are related by $(c/a)_{conv.} \times (c/a)_{Imma} = \frac{1}{2}$.

Part II

Group V Elements Under Pressure

Introduction

The elements in group V of the Periodic Table enjoy a great deal of scientific and technological importance as constituents of molecules and compounds. Both nitrogen and phosphorous are ubiquitous in biology and chemistry. Furthermore, arsenic and antimony play essential roles in condensed matter physics and materials science as components of the widely studied III-V semiconductors. However, in their pure elemental forms, the group V elements have received significantly less attention, especially compared to their neighbors in group IV.

In recent years interest in pure group V solids, and especially their high-pressure properties, has grown largely because of some intriguing observations and predictions. For example, phosphorous and arsenic have been found to undergo interesting displacive structural phase transitions under pressure [Jam63b, Kik83, Kik87]. At low pressure arsenic exists in the semimetallic α-arsenic, or A7, structure. Under pressure, this phase continuously deforms toward the metallic simple cubic (sc) structure which becomes stable at about 30 GPa. Phosphorous exhibits the same structural transition at about 10 GPa. However, it first undergoes a transformation from its low-pressure, semiconducting phase (black phosphorous) to the semimetallic A7 structure at about 5 GPa.

Predictions of molecular-bond dissociation and metallization of solid nitrogen under pressure [McM85, Mar86, Cha86a, Mai92] have also spurred interest in the group V elements. Experimental verification of these transitions could have many important ramifications. For example, the large valence and high Debye temperature of nitrogen both suggest the possibility of high transition-temperature (T_c) superconductivity for a metallic phase. Further motivation for this hypothesis is the discovery of superconductivity at 18 K in compressed phosphorous [Shi90]. This is the highest T_c found among the elements.

The following two chapters and their associated publications [Che92, Lew92] address two aspects of the group V solids under pressure. Chapter 4 contains the theoretical portion of a combined experimental and theoretical investigation of superconductivity in high-pressure arsenic. In Chap. 5 several candidate atomic phases of solid nitrogen are studied to determine their structural-stability and electronic properties.

Chapter 4

Superconductivity in Arsenic at High Pressures

4.1 Introduction

One of the most physically interesting pressure induced structural transformations is the rhombohedral A7 (α-arsenic) to simple cubic (sc) transition in the group V elements phosphorous, arsenic, and antimony. At low pressure the A7 phase is stable [Don74]. X-ray diffraction experiments [Jam63b, Kol69, Kik83, Kik87, Bei90] show that pressure causes the low symmetry rhombohedral unit cell to relax continuously toward the highly symmetric sc phase. The A7 phase [1] is considered to be the result of a Peierls-like distortion of the sc phase at low pressure. This distortion results in a semimetal with a rather low electronic density of states at the Fermi level [$N(E_F)$]. Pressure stabilizes the sc phase and thus increases $N(E_F)$. Various theoretical studies [Nee86, Cha86b, Mat86] have been able to predict the occurrence of such subtle transformations by the onset of phonon softening.

Both the A7 and the sc phases of P, As, and Sb have been shown to be superconducting [Wit68, Wit69, Wit84, Wit85, Ber69]. Because these transitions are nearly continuous (there are slight discontinuities in the lattice constants), it is expected that the superconducting transition temperatures (T_c) will be continuous with pressure as well. Work by Wittig, *et al.* [Wit85] has shown that the T_c of Sb and P exhibit peak values of 5 K and 10 K, respectively, at the transition pressure. These peaks are ascribed to the softening of phonon modes near the transition pressure, which has a positive effect on the electron-phonon coupling. This explanation is supported by *ab initio* total energy calculations performed by Chang and Cohen [Cha86b], which suggest the existence of soft phonons in the sc phase. Wit-

tig [Wit84] also measured T_c of As under pressure. His published data on As did not show a peak in T_c as in the case of P and Sb. However, a later abstract with Kawamura [Kaw85] did mention that T_c in As reached a maximum value of 2.7 K at a pressure of ~24 GPa. Furthermore these authors suggested phonon softening as the probable reason for the peak in T_c.

The vibrational properties of As in the A7 phase were studied as a function of pressure by Beister, *et al.* [Bei90] using Raman scattering. These authors found evidence of softening in the zone-center optical phonon at the A7 → sc transition. The experimental results were found to be qualitatively in good agreement with the theoretical calculation of Needs, *et al.* [Nee86]. Although the experimental and theoretical results so far all suggest that phonon softening plays an important role in determining T_c, the importance of other factors such as $N(E_F)$ is still not clear.

This chapter reports on the theoretical portion of a detailed experimental and theoretical investigation of elemental As which elucidates the roles of phonon softening and $N(E_F)$ in the pressure-dependence of T_c near the A7 → sc transition. The experimental portion of this investigation was conducted by Chen, Su, and Yu [Che92], and includes measurements of the normal state resistance and T_c both as functions of pressure up to 41 GPa. A maximum value of $T_c \sim 2.4$ K at a pressure of 32 GPa is determined. This result is similar to that reported by Kawamura and Wittig [Kaw85], but shifted to higher pressure. First-principles calculations of the pressure-dependences of $N(E_F)$ and relevant phonon modes are performed for both phases. The results on $N(E_F)$ explain qualitatively the pressure-dependence of the normal state resistance and point to the importance of $N(E_F)$ in enhancing T_c. Phonon softening is found to occur as the transition pressure is approached from either side. Thus both an increasing $N(E_F)$ and phonon softening serve to increase T_c rapidly as As is pressurized toward the A7 → sc transition. Above the transition further compression stiffens the phonons while $N(E_F)$ remains relatively constant, so that T_c decreases gradually.

Section 4.2 reviews the experimental results on T_c and normal state resistance of As under pressure. The details and results of the first-principles calculations are then described in Sec. 4.3. Finally, Sec. 4.4 shows that the experimental results can be qualitatively understood by the calculated behavior of $N(E_F)$ and the phonon spectrum under pressure.

4.2 Review of Experimental Results

Figure 4.1(a) displays T_c of As as a function of pressure measured for increasing pressure over several runs. The results show a peak in the pressure-dependence of T_c at approximately 32 GPa. This peak is noticeably asymmetric, with the rate of increase in T_c for pressures below the maximum larger than the rate of decrease in T_c for pressures above the maximum. Similar but more conspicuous behavior is observed in Sb across its A7 $\rightarrow$ sc transition [Wit84]. In the case of Sb, however, there is a discontinuity in the T_c presumably caused by the slight discontinuity in the lattice constants through the transition. The downward arrow on the plot indicates the pressure below which superconductivity was not observed down to the lowest attainable temperatures of the experiment (1.7 K).

The behavior of the normal state electrical resistance as a function of pressure is an indication of the trend in $N(E_F)$, since resistances of semimetals and metals are inversely proportional to $N(E_F)$. Measured pressure-dependence of the resistance of As at 300 K is shown in Fig. 4.1(b). The electrical resistance of As is found to decrease with pressure at an almost constant rate until 32 GPa, above which the resistance becomes roughly independent of pressure. This behavior is qualitatively reproducible upon decreasing the pressure, however, there is a slight difference that is attributable to deformation of the sample. Arrows on the plot indicate which data correspond to increasing and decreasing pressure.

A measure of the A7 $\rightarrow$ sc. transition pressure is given by both the T_c and resistance data. The maximum value of T_c and the kink in the resistance vs pressure

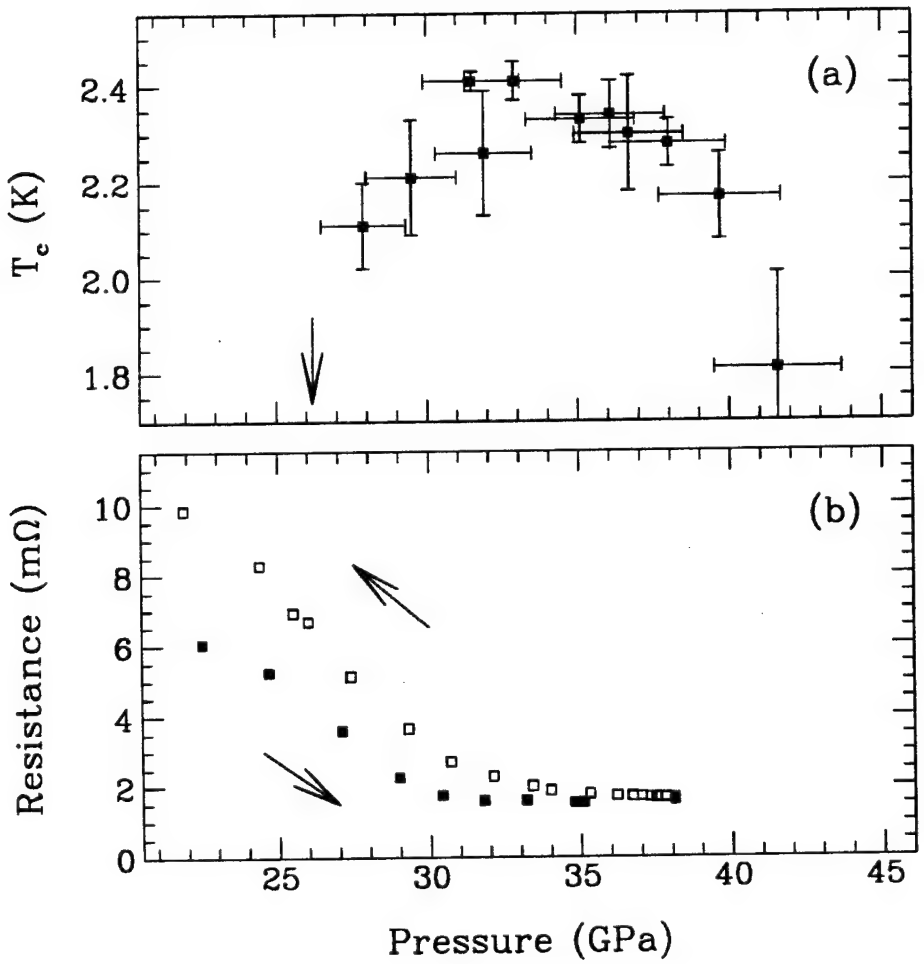

Figure 4.1: Experimental measurements by Chen, Su, and Yu [Che92] of (a) the superconducting transition temperature (T_c) and (b) the normal state resistance (at 300 K) of As as a function of pressure. Horizontal error bars indicate a pressure inhomogeneity of ±5% while vertical error bars represent the transition width. The T_c data were taken for increasing pressure only, while the resistance vs pressure curve was measured for both increasing and decreasing pressures. The downward arrow indicates a pressure at which no superconducting transition was observed above 1.7 K.

both occur at about 32 GPa. Since these features are both related to the structural transition (see below), they both can be interpreted as indicating the transition pressure.

4.3 Calculations

An understanding of the behavior of T_c under pressure requires an analysis of the physical properties that determine superconductivity, namely the electronic density of states at the Fermi level and the electron-phonon coupling . A theoretical investigation of the pressure-dependence of these two properties can provide insight into the pressure-dependence of T_c. In this section results of first-principles calculations of the volume-dependence of $N(E_F)$ and the frequency of the phonon mode corresponding to the sc-A7 distortion are presented. To make contact with the experimental measurements, in which the pressure is the independent variable, a calculation of the equation of state is provided and compared with experimental equations of state.

Total energy calculations are performed within the local-density approximation (LDA) [Lun83] using *ab initio* norm-conserving pseudopotentials [Ham79] and the momentum-space formalism [Ihm79, Coh82, Pic89]. The plane-wave basis is truncated at an energy cutoff of 17 Ry. Aside from the atomic number and mass of As, the only empirical inputs were the structural data for As in the A7 structure [Bei90], which depends, at each volume, on two parameters [1]. The use of these empirical structural data was necessitated by the prohibitive computational cost of relaxing both parameters at each volume.

The calculated equations of state for As in the sc and A7 structures are shown in Fig. 4.2. They were determined from least-squares fits of the calculated total energy vs volume to the Murnaghan equation of state [Mur44]. A Debye model was used to approximate the zero-point motion correction to the total energy. The experimental errors associated with the empirical structural parameters used in the calculation

represent the largest limitation to the accuracy of the calculated equation of state for As in the A7 structure. With that taken into account, the calculated equations of state of As are in reasonably good agreement with the experimental equations of state of As [Bei90, Kik87] (see Fig. 4.2).

According to band theory, As in the sc structure should be a metal with a fairly large $N(E_F)$. At low pressure, the metallic sc phase is unstable with respect to a Peierls-like distortion that doubles the unit cell and produces the lower-symmetry A7 phase. In the A7 structure, As is semimetallic with a small $N(E_F)$. Figure 4.3 shows the calculated $N(E_F)$ vs volume for As in the sc and A7 structures. The error in the calculation is estimated to be 0.1 states/Ry/atom and is attributed to an incomplete sampling of the Brillouin zone. When As in A7 is compressed toward the phase transition, $N(E_F)$ increases rapidly. Since pressure diminishes the Peierls-like distortion from sc, this concomitant increase in $N(E_F)$ is expected. When As in sc is compressed, $N(E_F)$ decreases very gradually. This behavior is consistent with a free-electron-like picture, in which $N(E_F) \sim V^{2/3}$.

If the sc structure is described as two identical, interpenetrating fcc sublattices, then one of the distortions that transforms sc to A7 corresponds to a relative displacement of the fcc sublattices along the [111] direction. The phonon mode corresponding to this displacement can be thought of either as the longitudinal acoustic mode at the corner of the sc Brillouin zone or as the Γ_1-symmetry optic mode at the center of the A7 Brillouin zone. For pressures near the structural transition, this phonon mode is expected to soften to facilitate the necessary displacements.

Since this phonon drives the Peierls-like distortion, it is expected that the overall electron-phonon interaction for this mode is particularly strong. Thus, the superconducting properties of As are likely to depend strongly on the behavior of this mode.

Fig. 4.4 presents the phonon frequency as a function of volume for both the sc and A7 sides of the phase transition. Results of a previous calculation [Nee86] for the

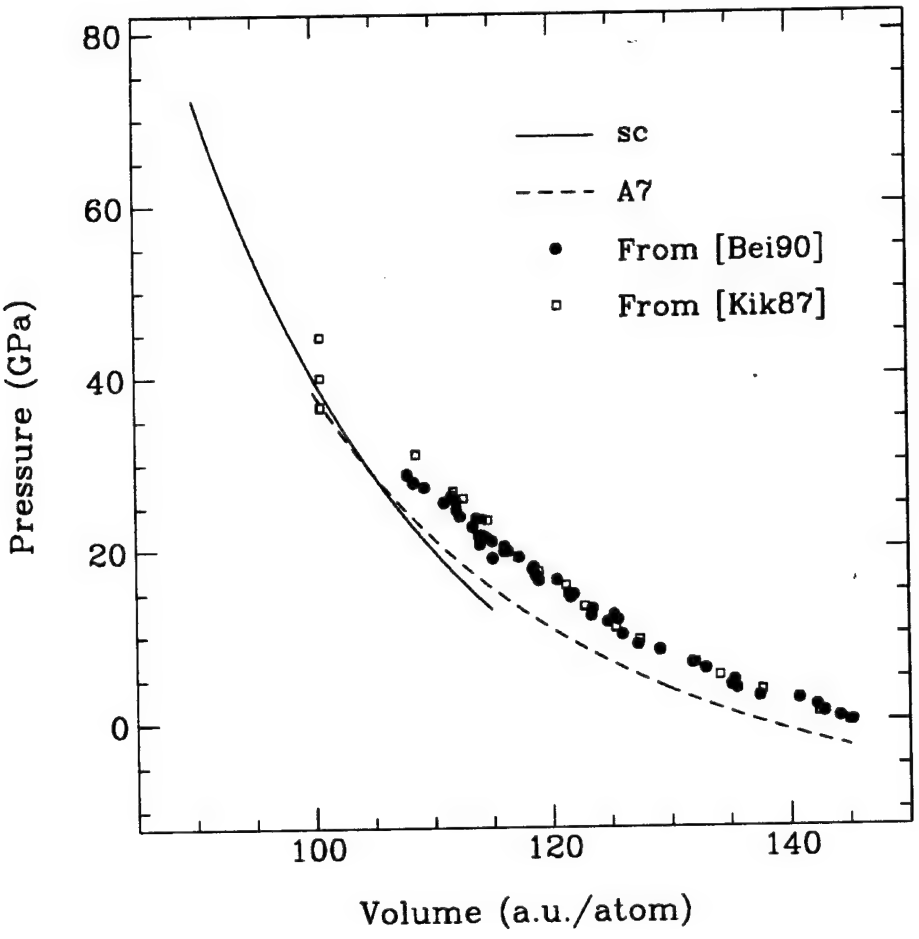

Figure 4.2: Equation of state for arsenic. The solid (dashed) line is the theoretical curve for the sc (A7) phase. Blackened circles denote the experimental measurements of Ref. [Bei90], and open squares denote the experimental measurements of Ref. [Kik87].

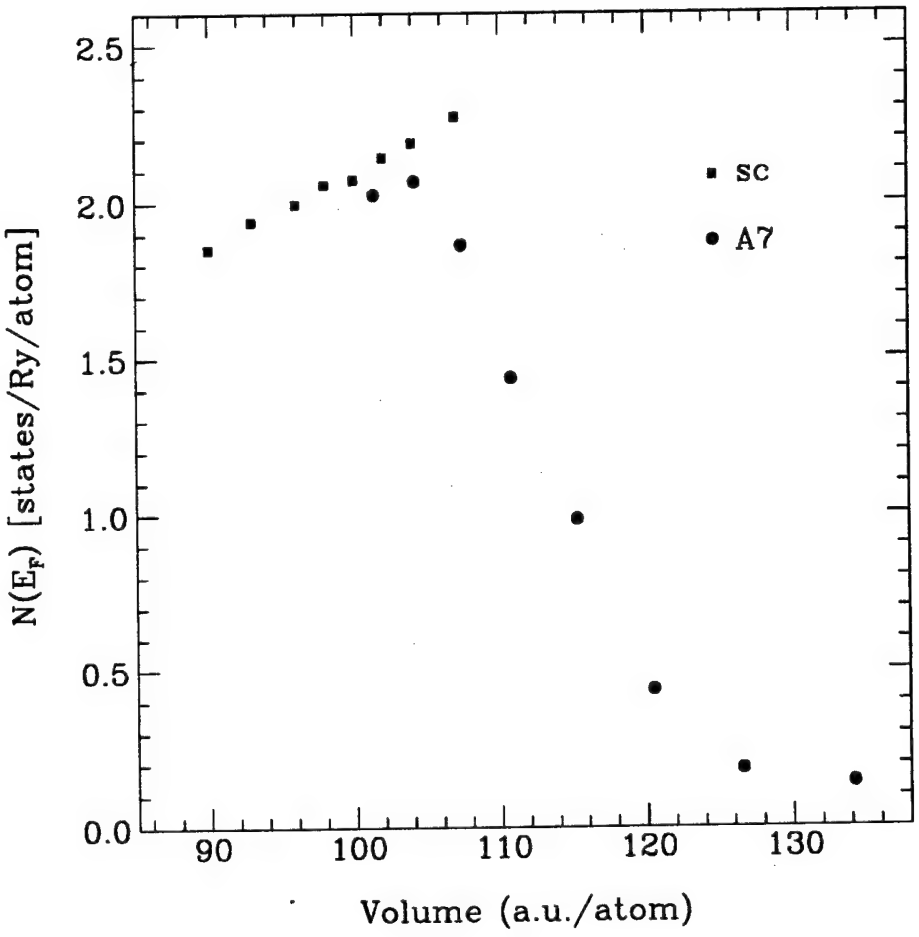

Figure 4.3: Calculated electronic density of states at the Fermi level for arsenic as a function of volume per atom. Circles (squares) correspond to the A7 (sc) phase. The error is approximately 0.1 states/Ry/atom.

A7 phase are also displayed and are found to be in good agreement with the present results. For both structural phases, the phonon frequency was extracted from a fit to an even polynomial of the calculated total energy vs phonon distortion coordinate. This is the frozen-phonon approximation. In the sc case, the polynomials were highly quartic single wells. Since the harmonic definition of phonon frequency fails in this case, the phonon frequency was defined as the energy difference between the ground and first excited states, as calculated by numerically solving the Schrödinger equation. It is reasonable to ignore higher excited states, because the relevant working temperatures ($\leq$ 2.5 K) are much less than the vibrational energy level spacings (typically $\sim 200-300$ K). In the A7 case, the total energy vs displacement was usually well fitted by a sixth order, double-well polynomial. At low pressure the double wells were quite deep. Upon compression toward the phase transition, the position of the well minimum and the depth of the well both decreased. The phonon frequency was calculated by expanding the polynomial to second order around the minimum. This works well at large volumes where the wells are deep, but becomes less reliable at volumes near the transition where the wells become quite shallow.

The general trend of the phonon frequency is that as the structural transition is approached from either side, the mode, as expected, softens considerably. A comparison of the calculated phonon frequency for As with experimental values [Bei90] shows good qualitative agreement overall, with good quantitative agreement at low compression.

4.4 Discussion

Using the results of the theoretical calculation of the pressure-dependence of both $N(E_F)$ and the phonon frequency, we can now understand the measured pressure-dependence of the T_c of As.

We begin by examining the dependence of T_c on the average phonon frequency,

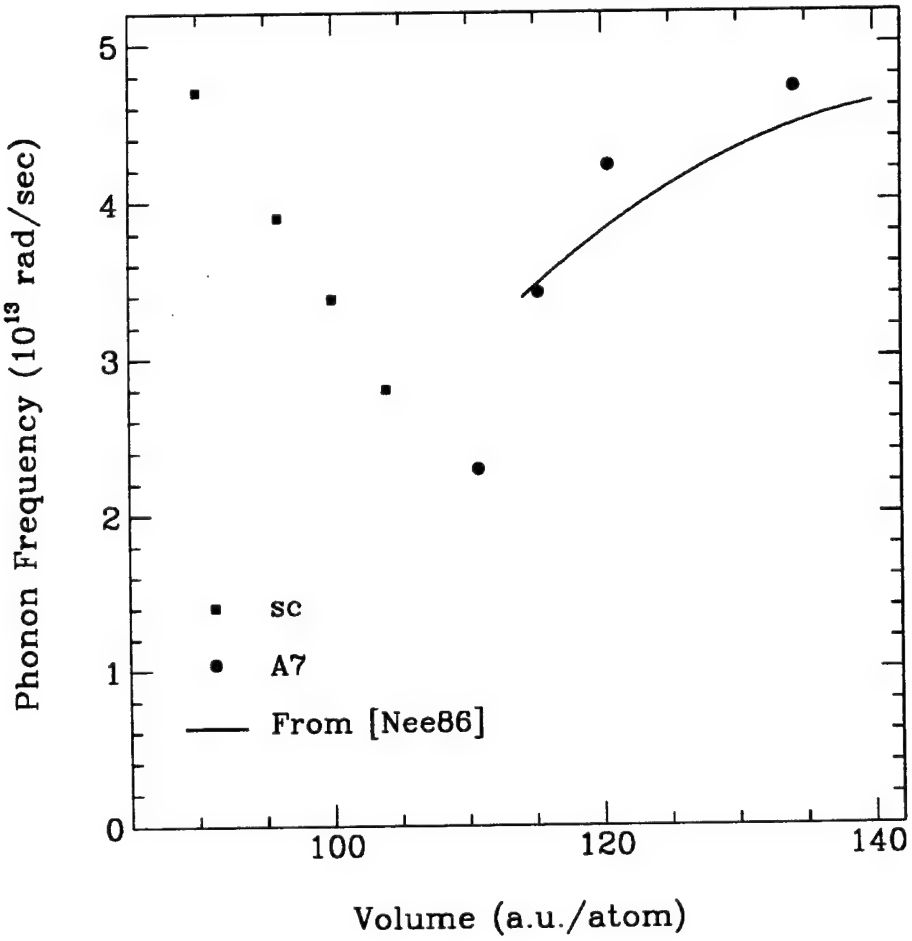

Figure 4.4: Calculated frequency of the phonon mode in arsenic that corresponds to sc-A7 distortion as a function of volume per atom. Circles (squares) correspond to the A7 (sc) phase. The error is largest near the structural transition. Results of a previous calculation [Nee86] are shown for comparison.

$\langle\omega\rangle$, and on $N(E_F)$ through an idealized McMillan equation [McM68]:

$$k_B T_c \simeq \hbar\langle\omega\rangle \exp\left(\frac{-1}{\lambda^* - \mu^*}\right) , \tag{4.1}$$

where

$$\begin{aligned} \lambda^* &= \frac{\lambda}{1+\lambda} , \quad \text{and} \\ \mu^* &= \frac{\mu}{1+z\mu} , \quad z = \ln\left(\frac{E_F}{\hbar\langle\omega\rangle}\right) . \end{aligned} \tag{4.2}$$

The parameter λ is the electron-phonon coupling constant which is proportional to $N(E_F)$ and inversely proportional to $\langle\omega^2\rangle$, and μ is the Coulomb repulsion pseudopotential which is approximately proportional to $N(E_F)$. The logarithmic variation of T_c with respect to $\langle\omega\rangle$ and $N(E_F)$ is given by

$$\begin{aligned} d\log(k_B T_c) &= \left[1 - \frac{2\lambda^{*2}}{(\lambda^* - \mu^*)^2} \cdot \frac{1}{\lambda} - \frac{\mu^{*2}}{(\lambda^* - \mu^*)^2}\right] d\log(\hbar\langle\omega\rangle) \\ &\quad + \left[\frac{\lambda^{*2}}{(\lambda^* - \mu^*)^2} \cdot \frac{1}{\lambda} - \frac{\mu^{*2}}{(\lambda^* - \mu^*)^2} \cdot \frac{1}{\mu}\right] d\log(N(E_F)) . \end{aligned} \tag{4.3}$$

If $\lambda \ll 1$, which is valid in the weak coupling limit, and $\lambda^* > \mu^*$, which is the condition for superconductivity, then Eq. 4.4 implies that an increase in $\langle\omega\rangle$ decreases T_c, while an increase in $N(E_F)$ enhances T_c.

The phonon calculations indicate (Fig. 4.4) that the phonon frequency softens near the structural phase transition, in agreement with previous Raman-scattering results [Bei90]. Because a lower average phonon frequency favors a higher transition temperature, the peak in T_c can then be explained by the minimum in phonon frequency at the phase transition. However, the rate of softening of the phonon frequency is, to the accuracy of our calculations, about the same on both sides of the transition, which cannot explain the slight asymmetry of the peak in T_c. The pressure-dependence of $N(E_F)$ accounts for this asymmetry. Both the calculations (Fig. 4.3) and normal state resistance measurements (Fig. 4.1) show that $N(E_F)$

increases strongly with pressure below the A7 → sc transition and becomes independent of pressure above. Thus the increasing $N(E_F)$ and the decreasing phonon frequencies both contribute to the rapid enhancement of T_c as As is pressurized toward the A7 → sc transition. Above the transition, further compression does not change $N(E_F)$ considerably, but does stiffen the phonon modes, so that T_c decreases more gradually.

The present experimental results of Chen, *et al.*, consistently place the A7 → sc transition at 32 ± 1 GPa, in disagreement with the results of Wittig [Wit84]. Similar disagreements among earlier experimental investigations with regard to the A7 → sc transition in As have been reported. In particular, the x-ray diffraction work of Beister, *et al.*, [Bei90] pinpoint the transition at 24 GPa while x-ray work by Kikegawa and Iwasaki [Kik87] place the transition between 31 and 37 GPa. The cause of this large scatter in the measured transition pressures is not known, although sensitivity of the transition to pressure inhomogeneities is a possible explanation.

Difficulty in establishing the A7 → sc structural transition pressure also extends to the theoretical calculations. It is not possible to predict the transition pressure and volumes using the usual common-tangent technique for the energy vs volume curves. The reason for this is that the A7 → sc transition is nearly continuous, and the energy vs volume curves do not cross but merge.

This difficulty actually suggests another method for determining the transition pressure. Since this transition is nearly continuous, it is expected that the $N(E_F)$ and the phonon frequency are also nearly continuous at the transition. These hypotheses are borne out by Fig. 4.1 of the present work and Fig. 8 of Ref. [Bei90], respectively. Since $N(E_F)$ and the phonon frequencies vary appreciably with volume, the transition pressure can be deduced from the volume where the $N(E_F)$ or phonon frequency curves of the two phases intersect. The calculated $N(E_F)$ for sc and A7 (Fig. 4.3) intersect at a volume of about 102 a.u./atom. According to the equation of state in Fig. 4.2, this corresponds to a pressure of about 36 GPa, which

is in good agreement with the present experimental results. An extrapolation of the calculated phonon frequency (Fig. 4.4) suggests a transition volume that is also consistent with the present experiment, however the large error in this calculation near the transition makes this prediction less reliable.

NOTES

[1] If the sc structure is viewed as two interpenetrating fcc sublattices (*i.e.*, the monatomic analog of the NaCl structure), then the A7 structure is obtained from sc by a relative displacement of the two sublattices along the [111] direction, accompanied by a rhombohedral shear strain of the unit cell. These two distortions are described by two parameters: an internal parameter and the c/a ratio of the rhombohedral unit cell. For a thorough discussion of the A7 structure see, for example, the appendix of Ref. [Nee86].

Chapter 5

High-Pressure Atomic Phases of Solid Nitrogen

5.1 Introduction

Elemental nitrogen exists in nature as a small, very stable diatomic molecule. Its bond length (1.094 Å) is among the smallest of the diatomic molecules, and its bond dissociation energy (9.8 eV/bond) is among the largest [Mah65]. At low pressures, the molecular nature of nitrogen persists in the solid state which forms at low temperatures via weak intermolecular interactions. A variety of stable molecular phases of solid nitrogen, all of which are insulators, are found to exist at low [Don74] and moderate [Rei85] pressures. However, as nitrogen is further compressed and the intermolecular distance becomes comparable to the molecular bond length, these molecular phases are expected to become unstable with respect to more highly coordinated atomic phases. While this molecular–to–nonmolecular transition has not as yet been observed in nitrogen up to 130 GPa [Rei85], it has been predicted theoretically [McM85, Mar86].

Martin and Needs (Ref. [Mar86]) further predict that the stable high-pressure atomic phase is the rhombohedral A7 (α-arsenic) structure. All other elements in group-V exist in this semimetallic, threefold-coordinated structure [Don74, Kik83], which is a slight distortion of the simple cubic (sc) structure [1]. It has been shown [Cha86a, Cha86b, Sas88, Shi90, Bei90, Che92] in P, As, and Sb that pressure diminishes the distortion from sc, and ultimately removes it through a weakly first-order structural phase transition. Because of the odd number of electrons per cell, the group-V elements in the sc structure are metals. These pressure-induced semimetallic-to-metallic phase transitions in P, As, and Sb are accompanied by

peaks in the superconducting transition temperature (T_c) [Che92, Wit84, Wit85], which have been attributed both to an increase in the electronic density of states at the Fermi level ($N(E_F)$) and a softening of phonon modes which are assumed to participate in both the structural transition and in the electron pairing.

This chapter reports on a first-principles investigation of the structural and electronic properties of several candidate atomic phases of solid nitrogen at high pressures. These candidate phases include the sc structure plus three structures which are distortions of sc: the A7 structure and two simple tetragonal (st) structures. The results agree with previous work [Mar86] in that the A7 phase is found to be the lowest energy nonmolecular phase of nitrogen within the manifold of structures considered in the present and previous investigations. A recent theoretical study [Mai92] predicts, however, that a candidate polymeric phase of nitrogen (called cubic gauche) is of even lower energy than the A7 phase and may be the first nonmolecular phase of nitrogen. Since the present study does not investigate the molecular–to–nonmolecular phase transition, the absence of the cubic gauche phase from consideration does not significantly alter the present conclusions.

The present study also agrees with previous authors [Mar86] that the sc structure is unstable with respect to the A7 phase. However, we find that both st structures studied are stable with respect to sc, and therefore possibly metastable with respect to the A7 structure. This is of particular interest because a st form of nitrogen would necessarily be metallic. At extremely high pressures, the distortions from sc in the A7 and st structures are found to diminish to zero, leaving sc as the stable structure.

Following this introduction, Sec. 5.2 deals with computational details and describes the structures studied. Results of the calculations are presented in Sec. 5.3. Section 5.4 contains a discussion of the results, including a brief discussion of the possibility of superconductivity in nitrogen.

5.2 Computations

The calculations for nitrogen were performed using the *ab initio* pseudopotential total energy method [Ihm79, Coh82]. The electron-ion interaction was treated using a nonlocal, norm-conserving pseudopotential [Ham79] [2], the electronic exchange and correlation energies were treated within the local-density approximation (LDA) [Lun83] using a standard form for the exchange–correlation potential [Cep80], and the temperature was assumed to be zero.

Because nitrogen cores lack p states, p-like valence electrons are not effectively excluded from the core region. Hence the $l = 1$ component of the pseudopotential is relatively deep in the core region, and plane-wave expansions of the wavefunctions require a very high kinetic-energy cutoff for good convergence. In the present work, plane waves of up to 60 Ry in energy are used in the expansion. The irreducible part of the Brillouin zone of the various structures studied is sampled at 110–150 special k-points [Mon77], depending on the structure. Using this cutoff energy and this number of k-points, relative total energies of nitrogen between different structures are converged to within ~2 mRy/atom.

This study focuses on two families of structures, A7 and st, both of which are slight distortions of the sc structure. If sc is viewed as two interpenetrating fcc sublattices (*i.e.*, the rocksalt structure with one atomic species), then the A7 structure is obtained from sc by a relative displacement of the two fcc sublattices along the [111] direction, accompanied by a rhombohedral shear strain of the cubic unit cell. These distortions of the metallic sc structure double the unit cell, suggesting a Peierls-like effect. The resulting crystal structure [1] has lattice vectors

$$\begin{aligned} \mathbf{a}_1 &= (a/\sqrt{3}, 0, c/3) \\ \mathbf{a}_2 &= (-a/2\sqrt{3}, -a/2, c/3) \\ \mathbf{a}_3 &= (-a/2\sqrt{3}, a/2, c/3) \end{aligned} \tag{5.1}$$

and basis vectors

$$\tau_{\pm} = \pm(0, 0, uc) = \pm u(\mathbf{a}_1 + \mathbf{a}_2 + \mathbf{a}_3). \tag{5.2}$$

Thus, at each volume, the A7 structure depends on two parameters – the fractional displacement, u, of the fcc sublattices, and the axial ratio, c/a, of the rhombohedral unit cell. For the sc structure, $u = 0.25$ and $c/a = \sqrt{6}$.

The st structure is obtained from sc by either shortening or extending the cubic cell along one of the cubic axes. The lattice vectors of the st structure are $\mathbf{a}_1 = (a, 0, 0)$, $\mathbf{a}_2 = (0, a, 0)$, and $\mathbf{a}_3 = (0, 0, c)$, where $c = a$ for the sc structure.

Structural parameters for both the A7 and st structures were optimized at each unit cell volume. The energy minimization procedure involved a coarse sampling of parameter space followed by a finer sampling near the minimum. This method resulted in a discrepancy with a previous calculation [Mar86] in the relaxed A7 structural parameters at the reference volume 5 Å^3. In the previous work, the calculations were performed using a 50 Ry plane wave energy cutoff and an irreducible Brillouin zone sampling of 10 special points. The optimal parameters ($u = 0.217$ and $c/a = 2.643$) were found by relaxing each parameter one at a time in an alternating fashion for two iterations. In the present work, a broad, deep minimum in the total energy was found at $u = 0.205$ and $c/a = 3.453$ using the more uniform structural-optimization technique described above. No minimum was found at the previously predicted parameters until the k-point sampling and plane wave energy cutoff were reduced to the previous work's values, whereupon a small minimum appeared. This spurious minimum apparently resulted from an inadequate sampling of the Brillouin zone and an insufficient number of plane waves.

Because of nitrogen's small mass, zero-point motion of the ion cores becomes a significant effect. However, the present computational method treats the ion cores as fixed. Therefore, an estimate of the zero-point energy is added to the total energy as a correction using a Debye model

$$E_{ZPM} = \frac{9}{8}\hbar\omega_D = \frac{9}{8}\hbar v_s q_D = \frac{9}{8}\hbar\sqrt{\frac{B}{\rho}}\, q_D \tag{5.3}$$

where ω_D is the Debye frequency, v_s is the speed of sound, B is the bulk modulus, ρ is the mass density, and q_D is the Debye wavevector. The volume dependence of the zero-point energy correction appears in the bulk modulus, the mass density, and the Debye wavevector.

5.3 Results

5.3.1 Structural Stability

Calculations of the relative stability of the various structures studied are presented first. Figure 5.1 shows the relative energy of nitrogen in st as a function of c/a at two volumes; uncompressed (Fig. 5.1(a)) and compressed (Fig. 5.1(b)). In general, three local minima were found – one at $c/a \approx 1$, corresponding to sc; one at $c/a < 1$, referred to as oblate- or o-st; and one at $c/a > 1$, referred to as prolate- or p-st.

At the uncompressed volume, the energetically favored st structure is the o-st structure. It has an activation barrier of about 47 mRy/atom to st structures with a larger c/a ratio. Both the sc and p-st minima are metastable with respect to o-st, and have activation barriers of about 11 and 28 mRy/atom, respectively. The sc structure is the least energetically favored minimum with a barrier to the p-st structure of about 3 mRy/atom. At the compressed volume, the p-st structure becomes energetically favored over the sc and o-st structures by about 30 and 35 mRy/atom, respectively. The other two minima are marginally metastable, with the sc structure slightly more favored than the o-st structure.

Upon compression, the optimum c/a ratio of both the o-st and p-st structures approaches the sc value of unity. Therefore, even though sc is never favored over p-st when both minima exist distinctly, at very high compression the optimal st structure is sc.

In Ref. [Mar86], the sc phase is found to be unstable with respect to variations

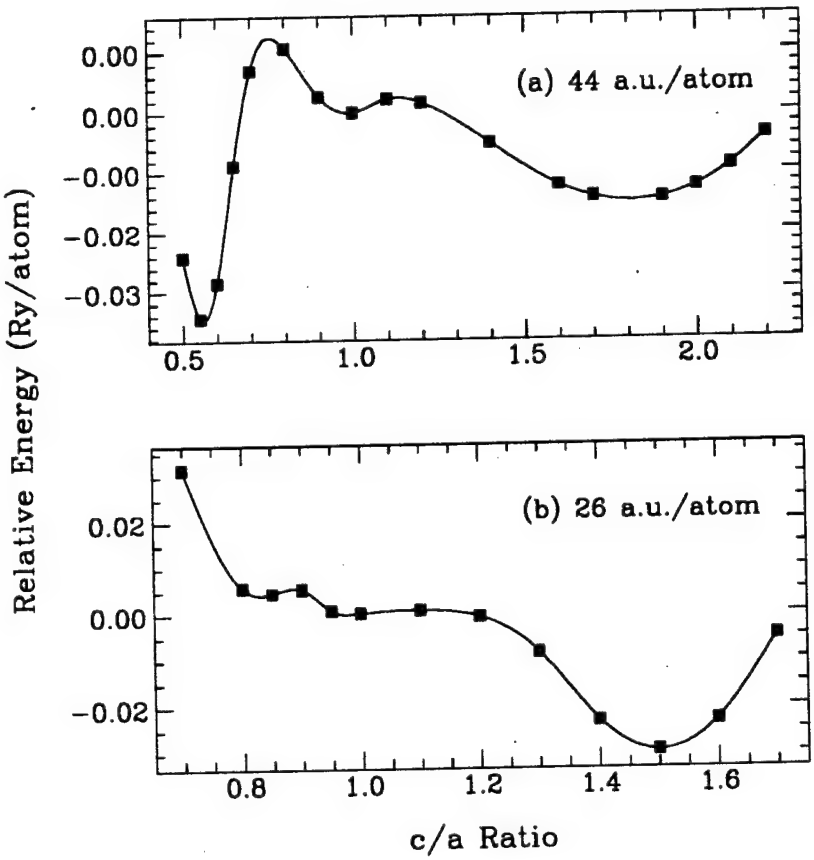

Figure 5.1: Relative energy versus c/a for nitrogen in the simple tetragonal structure at (a) an uncompressed volume (44 a.u./atom) and (b) a compressed volume (26 a.u./atom). At both volumes, three distinct minima are present, one for $c/a < 1$, one for $c/a \approx 1$, and one for $c/a > 1$. The filled squares are calculated data points, which are connected by a solid curve to guide the eye.

of the A7 parameters u and c/a. This instability of sc with respect to A7 distortions is also evident in the present work, however the optimal A7 parameters are found to approach the ideal sc values (see above) continuously upon compression. At a volume of 15 a.u./atom, the optimal A7 structure is indistinguishable from sc to within the accuracy of the calculations. This corresponds to a pressure of about 15 Mbar. Therefore, at very high compression the optimal A7 structure is sc.

The equations of state for the four structures, A7, sc, p-st, and o-st, are shown in Fig. 5.2. The computed data points (dots) are fitted, for each structure, to the Murnaghan equation of state [Mur44] (solid lines). The parameters of the fit (the equilibrium volume, V_0, and the bulk modulus and its pressure derivative both at V_0) are shown in Table 5.1. The correction due to zero-point motion, as described earlier, is included in Fig. 5.2.

The A7 structure is energetically favored within this set of structures, in agreement with Martin and Needs [Mar86]. At low compression, sc is the least energetically favored. At moderate compression, o-st becomes slightly higher in energy. At very high compression, all of the curves merge, because all of the structural parameters tend toward their sc values. This tendency toward sc can be understood in terms of a preference for more highly coordinated compact structures at high pressures where the Madelung (ion-ion interaction) term to the total energy begins to dominate. The sc structure is more highly coordinated (6-fold) than the o-st (2-fold), A7 (3-fold), and p-st (4-fold) structures.

Several other simple structures have been shown not to be viable candidates for high-pressure phases of nitrogen. We have studied nitrogen in a simple hexagonal structure with an optimized c/a ratio. This phase is higher in energy than the A7 phase at all pressures, and higher than the sc phase at all but the lowest pressures. A previous theoretical investigation [McM85] has shown (for atomic volumes down to 20 a.u./atom) that diamond, bcc, hcp, and fcc phases of nitrogen would all be higher in energy than the sc phase.

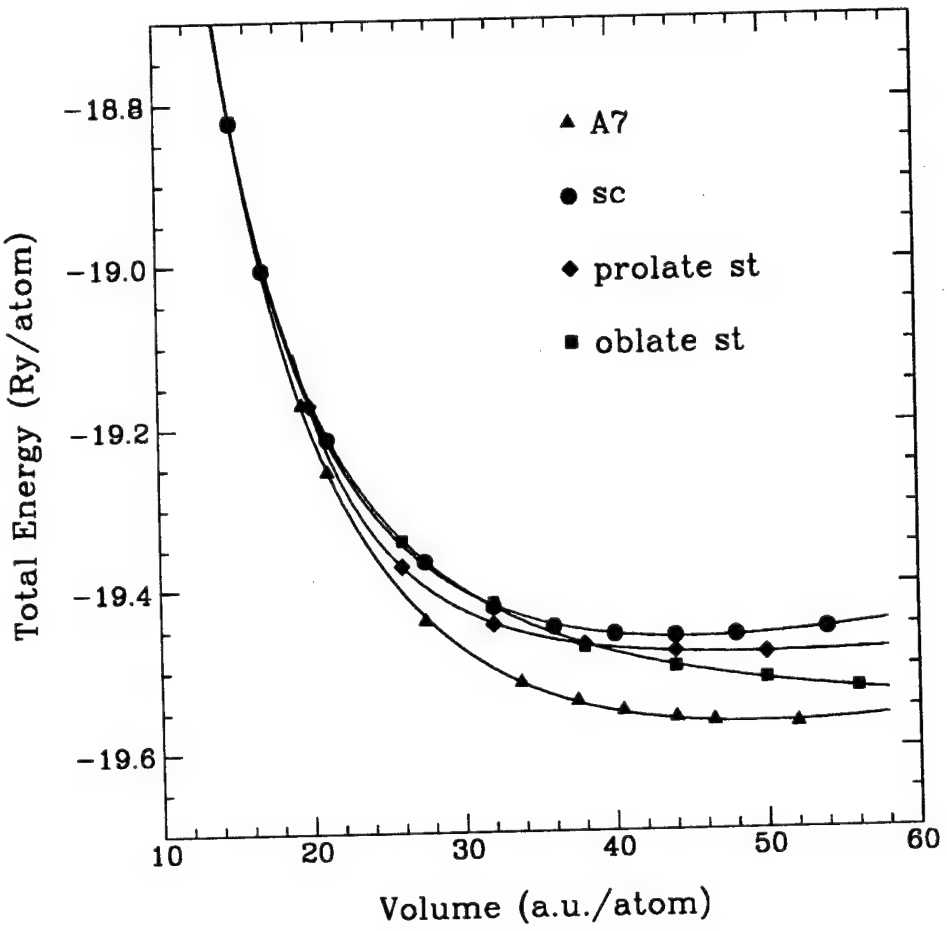

Figure 5.2: Total energy versus volume, fitted to the Murnaghan equation of state [Mur44] (see Table 5.1), for solid nitrogen in the four atomic phases studied. For the A7 and the two st phases, all structural parameters have been optimized at each volume. At very high pressures, these parameters all approach their sc structure limiting values. A zero-point energy correction has been included using the Debye model described in the text.

5.3.2 Electronic States

The nature of the filled electronic states of nitrogen will depend on the cell volume and the crystal structure. Because nitrogen has five valence electrons, it will necessarily be metallic in any structure with one atom per cell, such as sc or either st structure considered earlier. The A7 structure, however, has a two-atom unit cell, and, therefore, nitrogen in A7 can be either insulating, semiconducting, or semimetallic.

The density of states at the Fermi level ($N(E_F)$) of nitrogen in the A7, sc, and p-st structures is tabulated in Table 5.2 for two volumes, 44 and 21 a.u./atom. The former value corresponds approximately to the equilibrium volumes of the three structures; the latter corresponds to a significantly compressed volume. The values of $N(E_F)$ for the o-st structure have not been calculated because it is the less likely of the two st structures to form (see Sec. 5.4 below). As expected, the sc and p-st structures are metallic with fairly large $N(E_F)$, even at low pressures. Upon compression, the $N(E_F)$ of these structures decreases. This behavior is consistent with a free-electron-like picture, in which $N(E_F) \sim V^{2/3}$.

Since the A7 structure is a Peierls-like distortion of sc, a gap at the Fermi level is expected. This is seen in the vanishing of $N(E_F)$ at the uncompressed volume. However, since the A7 structure approaches the sc limit upon compression, the $N(E_F)$ of the A7 phase is expected to become non-zero and approach that of the sc phase. The existence of a finite $N(E_F)$ is indeed found for the compressed A7 phase, however the value is still quite small ($\sim 50\%$ of the sc and p-st values at this volume).

The metallicity of the structures is also exhibited by the nature of the bonding. Charge density contours in planes containing bonds are shown in Fig. 5.3 for the p-st and sc structures and in Fig. 5.4 for the A7 and sc structures. Contours for both uncompressed (44 a.u./atom) and compressed (21 a.u./atom) volumes are included. Bonding in the sc and p-st structures is clearly metallic at both volumes. The

Structure	V_0 (a.u./atom)	B_0 (GPa)	B_0'
A7	48.8	192	2.686
sc	44.4	206	2.833
o-st	111.4	9	3.114
p-st	47.4	92	4.196

Table 5.1: Best-fit parameters to the Murnaghan equation of state [Mur44] for nitrogen in the four phases studied. The parameters are the equilibrium volume V_0 and the bulk modulus B_0 and its pressure derivative B_0' at this volume.

Structure	$N(E_F)$ (states/Ry/atom)	
	V=44 a.u./atom	V=21 a.u./atom
A7	0.00	0.91
sc	4.06	1.82
p-st	3.61	2.06

Table 5.2: Density of states at the Fermi level for nitrogen in three of the phases studied. Values are given for two volumes – one uncompressed (44 a.u./atom) and one compressed (21 a.u./atom). The estimated numerical error is $\sim 10\%$.

difference, $\Delta\rho$, between the maximum and minimum charge density is small (~ 0.45 and ~ 0.57 electrons/a.u. for sc and p-st, respectively), indicating that the electrons are quite delocalized. Furthermore, the bonding in the compressed A7 phase is also metallic, with $\Delta\rho \sim 0.47$ electrons/a.u.

In contrast, the uncompressed A7 phase is covalently bonded, with a comparatively large $\Delta\rho \sim 0.71$ electrons/a.u. The charge density in the bond is quite large compared to the minimum. However, the largest peaks are outside of the bond, positioned on the side of the atom away from the plane formed by its three nearest neighbors. This geometry is reminiscent of the dangling bond in the ammonia molecule, suggesting that the bonding orbitals do not exhaust all of the valence electrons. This is not surprising, since each atom in the A7 structure covalently bonds to three nearest neighbor atoms, while each nitrogen atom has five valence electrons.

5.4 Discussion

As shown above, the A7 structure is the lowest energy atomic form of solid nitrogen of the structures studied. This phase is nonmetallic or semimetallic at all but the very highest pressures (~15 Mbar) where the structure merges with the sc structure. In contrast, the sc phase is a metal with a large $N(E_F)$ at all pressures. However, the sc phase is unstable with respect to distortions that bring about the A7 phase at all pressures for which the two phases are distinct. The ~15 Mbar of pressure required to stabilize the metallic sc phase are, at present, unachievable for static experimental conditions [3].

The question of the existence of a stable metallic form of solid nitrogen is of particular interest because of the possibility of superconductivity at a high transition temperature (T_c) in such a phase. This possibility is suggested both by the small mass and by the large valence of nitrogen. The small mass implies a large Debye temperature, and the large number of valence electrons implies a large carrier density

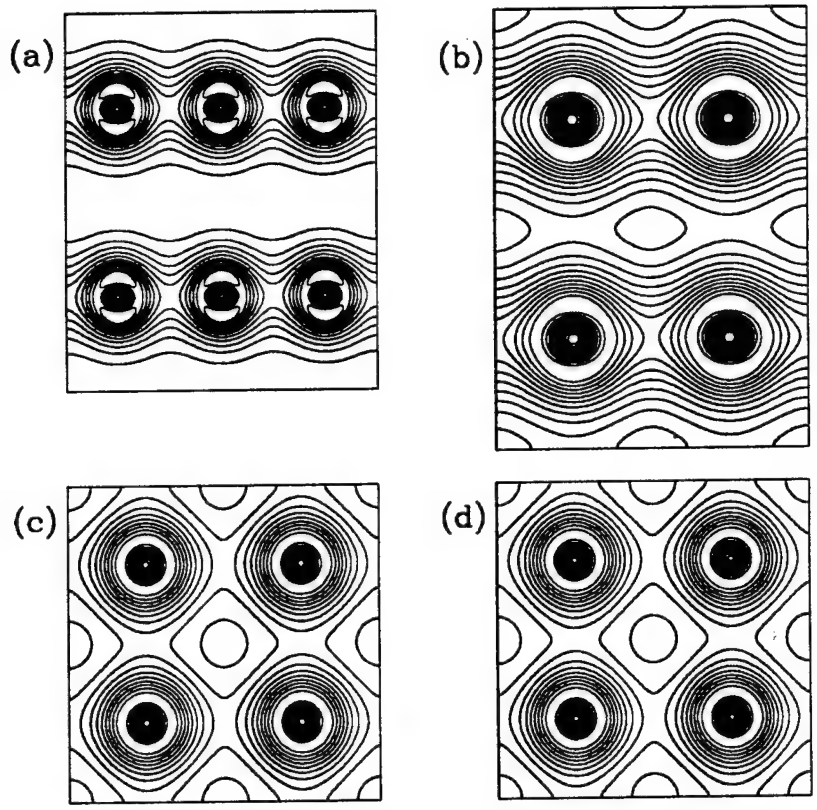

Figure 5.3: Charge density contours for nitrogen in p-st and sc structures at uncompressed and compressed volumes. For all frames, the horizontal axis is parallel to $\mathbf{a}_1$ and the vertical axis is parallel to $\mathbf{a}_3$, where the lattice vectors are those for the st structures. The frames correspond to: (a) the p-st phase at 44 a.u./atom with contours ranging from 2 to 22 electrons/atom; (b) the p-st phase at 21 a.u./atom with contours ranging from 2 to 12 electrons/atom; (c) the sc phase at 44 a.u./atom with contours ranging from 2 to 20 electrons/atom; and (d) the sc phase at 21 a.u./atom with contours ranging from 2 to 20 electrons/atom. All contour levels are evenly spaced.

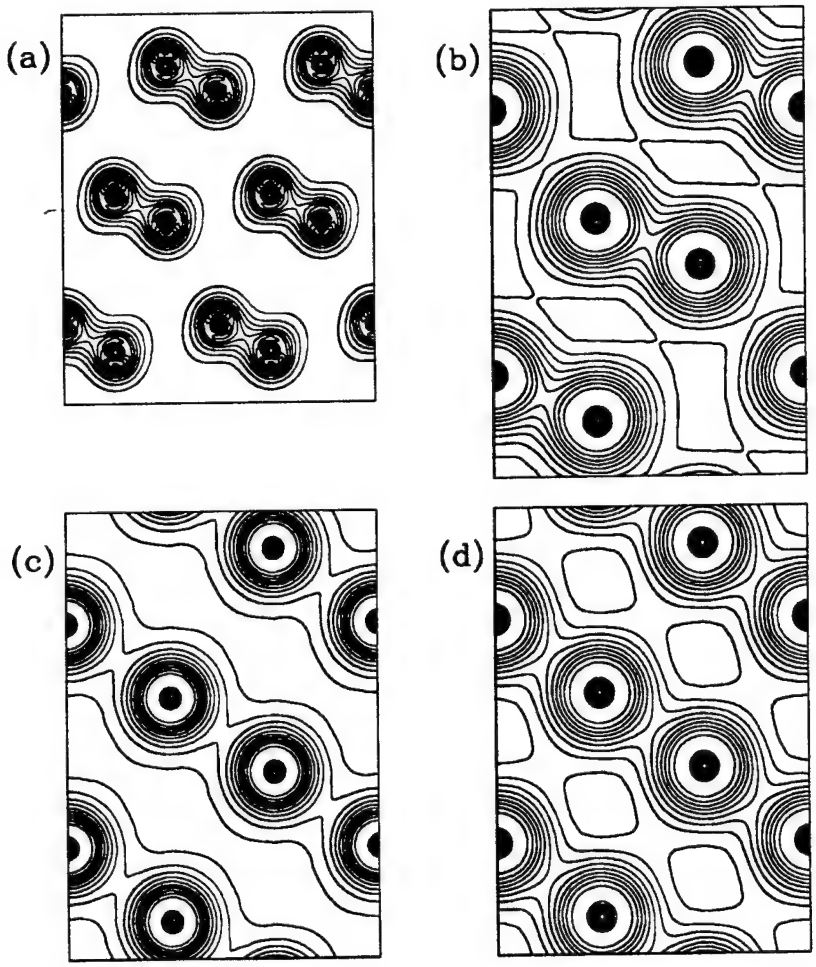

Figure 5.4: Charge density contours for nitrogen in A7 and sc structures at uncompressed and compressed volumes. For all frames, the horizontal axis is parallel to $2\mathbf{a}_1 - \mathbf{a}_2 - \mathbf{a}_3$ and the vertical axis is parallel to $\mathbf{a}_1 + \mathbf{a}_2 + \mathbf{a}_3$, where the lattice vectors are those for the A7-symmetry structures. The frames correspond to: (a) the A7 phase at 44 a.u./atom with contours ranging from 3 to 30 electrons/atom; (b) the A7 phase at 21 a.u./atom with contours ranging from 2.5 to 10.5 electrons/atom; (c) the sc phase at 44 a.u./atom with contours ranging from 2 to 20 electrons/atom; and (d) the sc phase at 21 a.u./atom with contours ranging from 2.5 to 10.5 electrons/atom. All contour levels are evenly spaced.

in a metallic phase. Both of these properties will trend to enhance T_c.

The two st structures studied here, both of which are stable with respect to sc, are candidates for a metastable metallic phase. It is important to point out, however, that the metastability of a st phase of nitrogen with respect to the A7 phase has not been proven here. Indeed, the only path connecting the two structures that has been considered is st $\rightarrow$ sc $\rightarrow$ A7. The st structure might be unstable with respect to distortions analogous to the A7 distortions of sc. However, such considerations have not been explored here.

Assuming the st structures are metastable, one possible mechanism for achieving such a phase would be to compress the A7 sample to sc, and then quench it into a st phase on releasing the pressure. Such a procedure, if possible, is likely to favor the p-st structure, even though the o-st structure has a lower energy at low pressures. This can be seen by examining Fig. 5.1. A sample prepared in the sc structure is more apt to "find" the p-st minimum than the o-st minimum as pressure is released. The sample is then likely to remain in the p-st minimum due to the large activation barrier to the o-st minimum.

As was stated earlier, the zero-point energy of the ion cores is an important correction in systems of light atoms, such as nitrogen. This large effect of zero-point motion might be important in explaining the discrepancy between theory and experiment on the pressure of the molecular-to-atomic transition in solid nitrogen. Martin and Needs [Mar86] predicted that the structural transition from a molecular phase to the A7 phase would occur at $\sim$0.7 Mbar, in disagreement with experiments [Rei85], which indicate no atomic phase up to $\sim$1.3 Mbar. In the molecular solid, only the intermolecular zero-point motion is likely to be relevant to the total energy. Since the molecule is twice as massive as the atom, the zero-point correction in the molecular solid is smaller than in the atomic solid. Thus, including a correction for zero-point motion produces a relative shift in the total energies of the two phases. Since structural transition pressures are very sensitive functions of the

relative energy between two phases, this effect could result in a significant increase in the predicted molecular-to-nonmolecular transition pressure. A rigorous test of this hypothesis and its analogy for finite temperatures, however, is beyond the scope of the present work.

NOTES

[1] For a thorough discussion of the A7 structure see, for example, the appendix of Ref. [Nee86].

[2] The nitrogen pseudopotential chosen for the present work is the one suggested in Ref. [Bac82].

[3] For a discussion of high pressure technology and the regime of pressures achievable, see, for example, Ref. [Jay83].

Part III

Stoichiometric Effects in Compounds

Chapter 6

Electronic Structure of Non-Stoichiometric Ga-As Compounds

6.1 Introduction

Modern high-precision sample-growth techniques, such as Molecular Beam Epitaxy (MBE), provide a great deal of control in preparing new materials. By manipulating parameters such as temperature, substrate, and so forth, it is possible to grow substances which do not occur naturally, but which have interesting and useful properties [Her89]. The ability to control the growth process suggests that quantities previously considered to be fixed, such as stoichiometry, can now become experimental variables. Here we use theoretical computations to explore the Ga-As system with the goal of motivating experimental studies. This study of the effect of stoichiometry is focused on GaAs because it is one of the most thoroughly investigated compounds and because of its technological importance. In addition GaAs often serves as the prototypical III-V material, and has been one of the main "testing grounds" for new theoretical and experimental techniques.

The purpose of the present study is to provide model calculations of the effect of varying stoichiometry on the electronic properties of Ga-As crystalline compounds. The model chosen consists of five systems with an underlying diamond structure, all of which can be described by the same four-atom unit cell. These systems can be characterized as $Ga_{4-n}As_n$, $n = 0, \ldots, 4$, and range from pure Ga in the diamond structure ($n = 0$) through GaAs ($n = 2$) to pure diamond-structure As ($n = 4$). It should be pointed out that the diamond structure is not the naturally occurring stable configuration for either pure Ga or pure As [Don74].

Only two intermediate compounds ($n = 1$ and $n = 3$) are contained in this model, and they can be viewed, respectively, as Ga-As/Ga-Ga and Ga-As/As-As superlattice structures along the cubic [111] axis. Other related intermediate compounds (*i.e.*, superlattices with longer repeat distances) would have larger unit cells and, therefore, would be more computationally intensive. The electronic properties of the systems studied here, however, should be indicative of the electronic behavior of these more complicated systems. This supposition is reinforced by the result (discussed below) that the electronic charge density of a given type of superlattice layer (Ga-As, Ga-Ga, or As-As) is relatively insensitive to the type of layers surrounding it. Thus, while the present model treats only five systems directly, it has useful implications for more complicated Ga-As systems.

Because this study is designed only as a basis for future explorations and as a guide for experimental studies, no structural relaxation or stability analysis has been performed. Structural relaxation calculations involve computing quantum mechanical forces on each atom and then moving the atoms repeatedly until the forces vanish. These calculations tend to be costly and time-consuming and would be warranted only if experimental investigations give some confirmation for the models chosen. Since structural relaxations find local (not necessarily global) minima of the energy, a rigorous stability analysis would be even more computationally intensive and thus beyond the scope of this study.

Analyses of the respective electronic band structures show that the four systems which are off-stoichiometric with respect to GaAs are metallic with fairly large densities of states at the Fermi level. Furthermore, an analysis of the valence charge density of the Ga_3As_1 and Ga_1As_3 compounds suggests that the Ga-As layers would be semiconducting (as in bulk GaAs) and that the Ga-Ga and As-As layers, respectively, would be metallic. Such a metal-semiconductor superlattice should have ideal Schottky barriers.

This chapter is organized as follows: the following section discusses the compu-

tational method and describes in detail the systems under investigation. Section 6.3 presents and discusses the calculated electronic energy levels and charge densities of the five systems, including a brief discussion of the possibility of superconductivity. Finally, the study is summarized in Sec. 6.4.

6.2 Computations

Calculations are performed using the *ab initio* pseudopotential total energy method [Ihm79, Coh82, Pic89]. Electron-ion interactions are evaluated in this method using nonlocal, norm-conserving pseudopotentials [Ham79]. The Ga (As) pseudopotential used here has reference configuration $4s^{1.875}4p^{0.875}4d^{0.25}$ ($4s^{1.875}4p^{2.875}4d^{0.25}$) and cutoff radii (in a.u.) for the s, p, and d potentials equal to 2.21, 2.21, and 2.50 (2.18, 2.18, and 2.18), respectively. Effects stemming from slight core-valence overlap are treated using the scheme of Ref. [Lou82]. Electronic exchange and correlation energies are calculated within the local-density approximation (LDA) [Lun83] using a standard form for the exchange-correlation potential [Cep80]. The only external inputs to the calculation are the atomic numbers of the constituent atoms and their positions in the unit cell.

Wavefunctions and pseudopotentials are expanded in a plane-wave basis up to an energy cutoff of 20 Ry, and the irreducible part of the Brillouin zone (IBZ) is sampled at 60 special points [Cha73, Mon77]. These values produce a well-converged self-consistent potential. Electronic densities of states (DOS's) are generated from energy levels calculated at 580 points in the IBZ. The tetrahedron method [Leh72] is used to interpolate between these sampled points.

The family of compounds studied here is designated by $Ga_{4-n}As_n$, where $n = 0, 1, \ldots, 4$ is the stoichiometric parameter. An underlying diamond lattice is chosen for all five systems with the lattice constant fixed at the experimental value for GaAs, $a = 5.654$ Å[Coh88]. The four-atom unit cell describing the family of compounds is rhombohedral with trigonal axis pointing along the cubic [111] direction and lattice

vectors

$$\mathbf{a}_1 = \frac{a}{2}[112],\ \mathbf{a}_2 = \frac{a}{2}[211],\ \text{and}\ \mathbf{a}_3 = \frac{a}{2}[121] \qquad (6.1)$$

Cartesian coordinates used here correspond to the edges of the diamond structure cubic cell. Basis vectors for the four atoms in the unit cell are given by

$$\tau_i = \alpha_i\,(\mathbf{a}_1 + \mathbf{a}_2 + \mathbf{a}_3) \qquad (6.2)$$

where $\alpha_i = 0, \frac{1}{8}, \frac{1}{2}, \frac{5}{8}$ for $i = 1,2,3,4$, respectively. We denote this quasi-cubic, rhombohedral structure by qcr4.

Given the qcr4 unit cell, the stoichiometric parameter n uniquely defines the crystal structure for all values except $n = 2$. That is, for any value of $n \neq 2$, all arrangements of the four atoms in the unit cell are equivalent by symmetry. For $n = 2$, there are two non-equivalent qcr4 crystal structures, however the one studied here consists of alternating Ga and As atoms in the unit cell and is equivalent to ordinary GaAs in the zincblende structure. The $n = 0$ and $n = 4$ systems correspond to pure Ga and pure As, respectively, in the diamond structure. The resulting crystal structure for $n = 1$ ($n = 3$) is shown in Fig. 6.1, where the larger circles represent Ga (As) atoms, and the smaller circles represent As (Ga) atoms. This can be viewed as a superlattice of alternating Ga-As and Ga-Ga (As-As) corrugated layers in the [111] direction.

6.3 Results

6.3.1 Energy Levels

The calculated energy levels for the $Ga_{4-n}As_n$ family are presented in two series: the As-rich series ($Ga_2As_2 \rightarrow Ga_0As_4$) and the Ga-rich series ($Ga_2As_2 \rightarrow Ga_4As_0$). All energy levels are referred to the top of the Ga_2As_2 valence band as the zero of energy. Electronic DOS's for the As-rich series are exhibited in Fig. 6.2. The two As-enriched compounds (Ga_1As_3 and Ga_0As_4) are found to be metallic with fairly

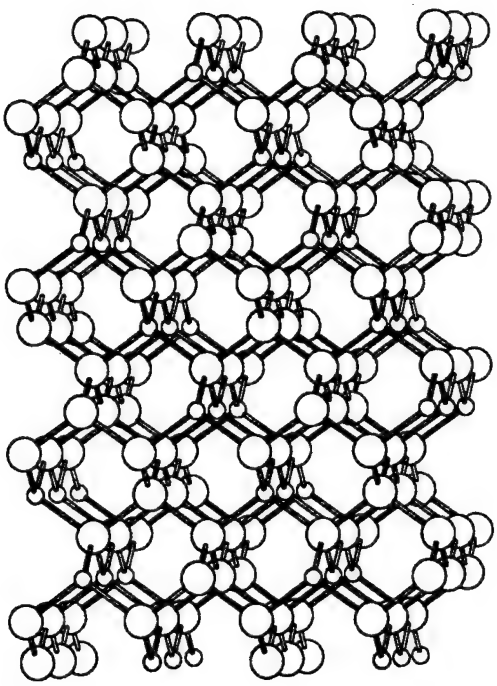

Figure 6.1: The qcr4 structure for the Ga_3As_1 and Ga_1As_3 systems. Large (small) circles correspond to Ga (As) in the former system and to As (Ga) in the latter system. This structure can be thought of as a stacking of corrugated layers in the cubic [111] direction that alternate between Ga-As layers and either Ga-Ga or As-As layers, depending on the stoichiometry.

large DOS's at the Fermi level. This is not surprising since each atom in these compounds has, on average, more than the four electrons required to satisfy the tetrahedral bonds. The excess electrons are thus available for itinerancy.

As expected, the DOS for the $n = 2$ compound agrees well with previously published DOS's for GaAs [Coh88]. Furthermore, the DOS for Ga_0As_4 is in good qualitative agreement with that of Si [Coh88] in its zero pressure diamond structure, however there are important differences. In particular, there is no band gap in diamond As between the fourth and fifth bands. Also, there is a relative separation between peaks b and c (see Fig. 6.2 for labels) compared to Si. The small gap in the DOS between peaks a and b, which is forbidden by symmetry for the diamond structure, is an artifact associated with sparse counting of the states in the DOS calculation near the zone boundary.

Detailed structure of the DOS's can be understood by examining the corresponding band structures, which are shown in Fig. 6.3. To facilitate comparisons, band structures for all of the systems considered are plotted in the qcr4 Brilloiun zone, even though this structure is not primitive for the $n = 0, 2$, and 4 systems. In these cases the band structures shown are folded with respect to their "primitive" band structures. Symmetry points for the rhombohedral Brillouin zone are labeled as in Ref. [Wan86].

It is natural to compare the electronic structure of Ga_1As_3 to that of its stoichiometric "neighbors" Ga_0As_4 and Ga_2As_2. Since Ga_1As_3 corresponds to a reduction in symmetry along [111] with respect to either of its neighbors, a comparison of electronic structures along the $\Gamma \rightarrow T$ direction (*i.e.*, along [111]) is particularly illustrative. For Ga_0As_4 and Ga_2As_2, bands come together in pairs at the T-point due to the zone folding. The reduction in symmetry in going to Ga_1As_3 splits this degeneracy, and similar splittings occur at other high symmetry points of the qcr4 Brillouin zone. However, the intrinsic degeneracies of the bands in the $n = 2$ and 4 systems are maintained for $n = 3$ which is attributed to the underlying diamond

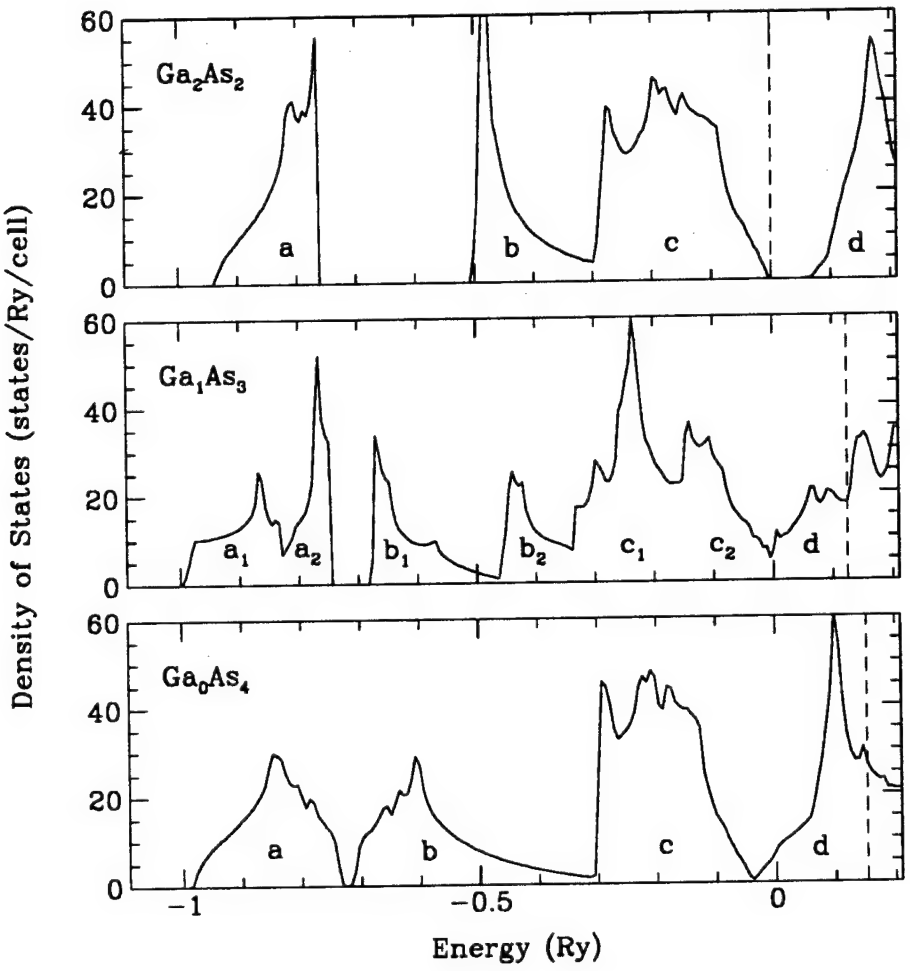

Figure 6.2: Electronic density of states for the As-rich series of materials, including Ga_2As_2, Ga_1As_3, and Ga_0As_4. The zero of energy is taken to be the top of the valence band in Ga_2As_2. A dashed line marks the Fermi energy, and letters denote specific regions or peaks of the density of states which are discussed in the text.

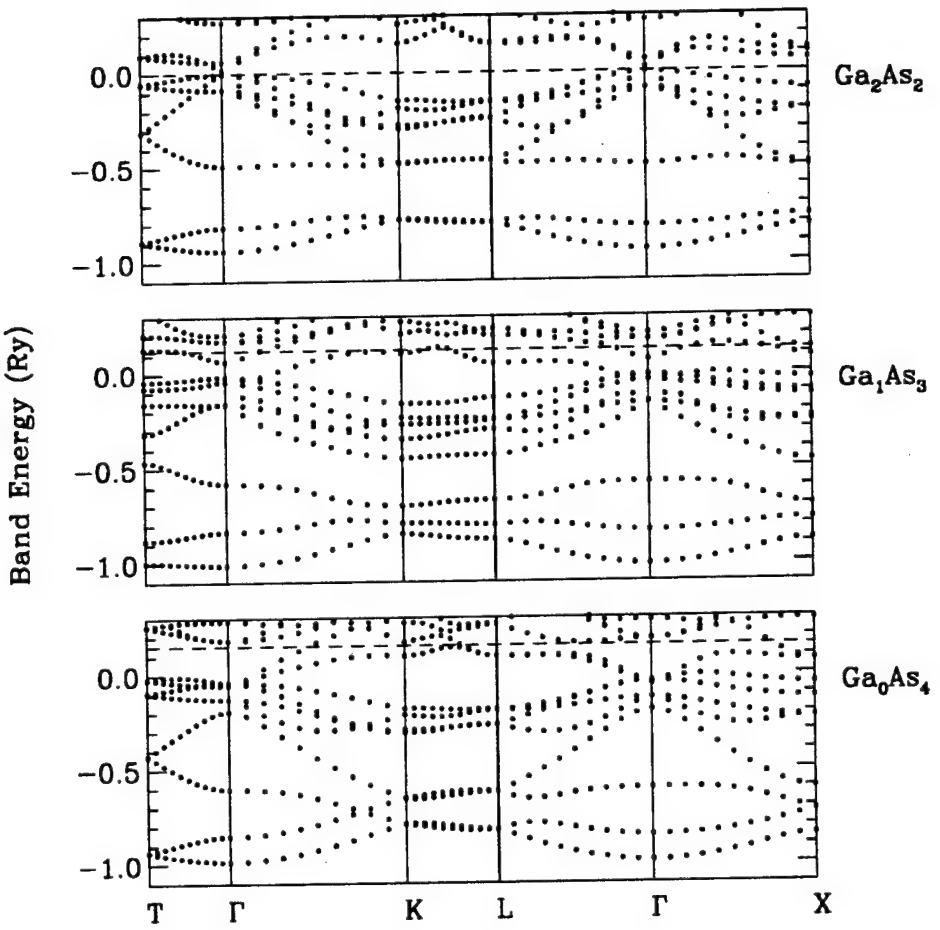

Figure 6.3: Electronic band structure for the As-rich series of materials, including Ga_2As_2, Ga_1As_3, and Ga_0As_4. High-symmetry points of the rhombohedral Brillouin zone are labeled in the manner of Ref. [Wan86]. The top of the valence band of Ga_2As_2 defines the zero of energy. A dashed line marks the Fermi energy.

symmetry.

The splitting of the a, b, and c peaks of the DOS's of Ga_0As_4 and Ga_2As_2 into two peaks each in Ga_1As_3 is a direct result of the band splitting. This is particularly evident for the splitting of the b-complex into b_1 and b_2. For Ga_2As_2, the large b-peak occurs at about -0.5 Ry and is due to the flatness of the bands just above the well-known antisymmetric gap. This peak diminishes as energy increases until the onset of the c-complex at about -0.3 Ry, where the bands flatten out near the K- and L-points.

Because there is no antisymmetric potential for Ga_0As_4, the degeneracy at X and near K is not lifted, and the a- and b-complexes touch. The onset of the b-complex is, therefore, more gradual than for Ga_2As_2 and the peak is smaller and occurs at about -0.6 Ry, where the bands are flat near the Γ- and X-points and between the K- and L-points. The onset of the c-complex in Ga_0As_4 is similar to that of Ga_2As_2.

A small antisymmetric-like gap is seen for Ga_1As_3 between the a- and b-complexes. Its presence causes the bands to flatten at the onset of the b-complex, producing a sharp peak, b_1, in the DOS analogous to that of Ga_2As_2, but smaller in magnitude. This peak diminishes up to about -0.45 Ry where peak b_2 abruptly appears due to flat bands at the X-point and between the K- and L-points. The features of the band structure which produce the separate b_1 and b_2 peaks in Ga_1As_3 are merged for the two neighboring systems and thus contribute to only a single peak. A similar analysis can be used to explain the splitting of the a and c-complexes in Ga_1As_3.

Electronic DOS's for the Ga-rich series are shown in Fig. 6.4, with the corresponding band structures in Fig. 6.5. Regions of the DOS plots have been labeled in the same fashion as Fig. 6.2. The two Ga-enriched compounds (Ga_3As_1 and Ga_4As_0) are both found to be metallic with large DOS's at the Fermi level. The smaller number of valence electrons in these two systems with respect to the average

of four electrons per atom required to satisfy tetrahedral bonds suggests that they would be hole-like metals.

The DOS of Ga_4As_0 is qualitatively very similar to that of both Ga_0As_4 (Fig. 6.2) and the Group IV semiconductors (Ref. [Coh88]). As with diamond As, there is no band gap in diamond Ga between the fourth and fifth bands as there is for the Group IV materials. Detailed structure of the DOS of Ga_3As_1 can be understood from the band structure in a manner similar to Ga_1As_3 (see above). Certain significant differences do exist, however. Most strikingly, the split in the two lowest bands is much larger in Ga_3As_1 than in Ga_1As_3. In fact, the a-complex completely separates into two disjoint peaks, a_1 and a_2. This is reflected in the band structure by a large splitting of the lowest valence bands in going from either Ga_2As_2 or Ga_4As_0 to Ga_3As_1. Another difference is that the band splitting which produced the distinct b_1 and b_2 peaks in Ga_1As_3 is much smaller for Ga_3As_1, leaving a single b-complex. Compared to Ga_2As_2, the b-complex of Ga_3As_1 is more spread out and, thus, has a smaller peak.

In light of the large DOS's at the Fermi level calculated for the off-stoichiometric systems ($\sim 20 - 30$ states/Ry/cell), it is interesting to consider the possibility of superconductivity in these materials. Superconductivity has been observed in similar systems. In particular, a high pressure metallic phase of GaAs, denoted GaAs II, is superconducting with $T_c \approx 4.5$ K and a calculated DOS at the Fermi level ~ 16 states/Ry/four-atom cell [Zha89]. Furthermore, at high pressure, elemental As is also a superconductor at around 2.5 K with a calculated DOS of ~ 8 states/Ry/four-atom cell [Che92]. Assuming the vibrational and electron-phonon coupling properties of the present model systems are similar to those of the observed superconductors, the off-stoichiometric materials are expected to be superconductors with T_c's in the range 5–10 K due to the large calculated DOS's at the Fermi level. Detailed theoretical calculations to explore this suggestion are possible, but are beyond the scope of the present study.

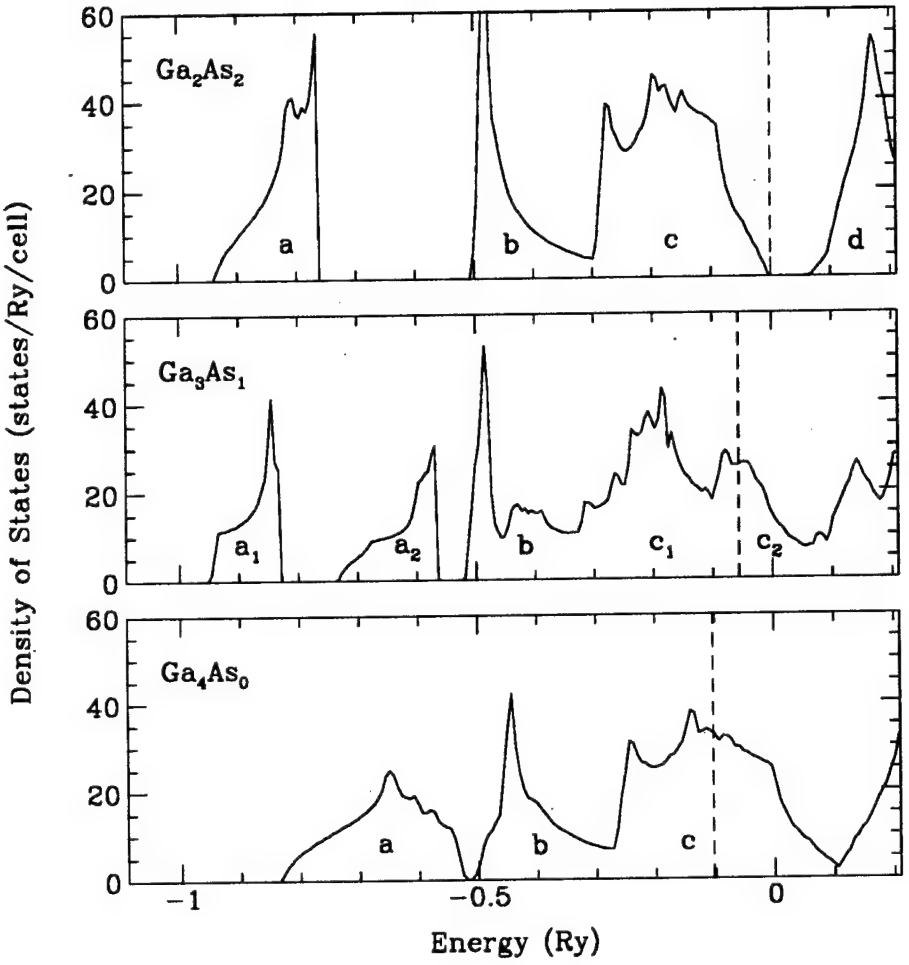

Figure 6.4: Electronic density of states for the Ga-rich series of materials, including Ga_2As_2, Ga_3As_1, and Ga_4As_0. The zero of energy is taken to be the top of the valence band in Ga_2As_2. A dashed line marks the Fermi energy, and letters denote specific regions or peaks of the density of states which are discussed in the text.

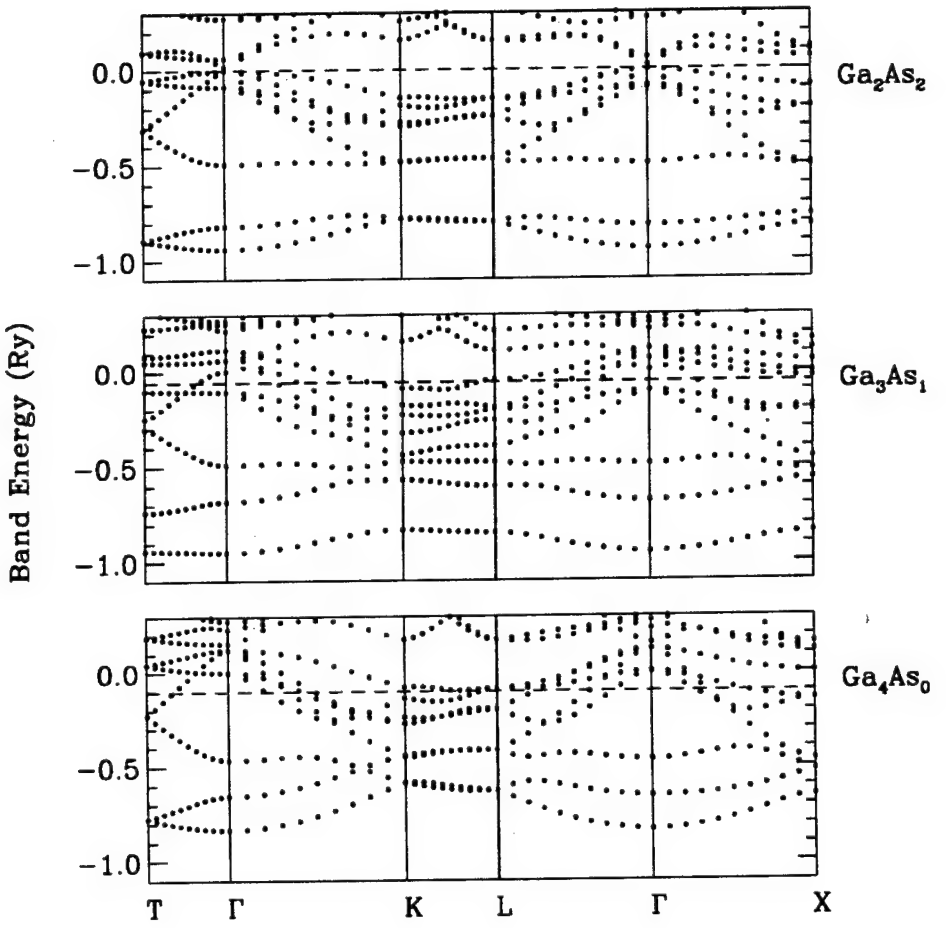

Figure 6.5: Electronic band structure for the Ga-rich series of materials, including Ga_2As_2, Ga_3As_1, and Ga_4As_0. High-symmetry points of the rhombohedral Brillouin zone are labeled in the manner of Ref. [Wan86]. The top of the valence band of Ga_2As_2 defines the zero of energy. A dashed line marks the Fermi energy.

6.3.2 Electronic Charge Density

Electronic charge density contours in the cubic (110) plane are shown in Fig. 6.6 for the $Ga_{4-n}As_n$ systems. Contours are separated by 5 electrons/cell and range from 5 to 55 electrons/cell with the lowest (highest) contour in each panel denoted by a dashed (bold) line. Triangles (pentagons) are used to mark the positions of the Ga (As) atoms.

If the qcr4 structure is thought of as corrugated planes stacked along the cubic [111] direction, then each panel in Fig. 6.6 shows bonds lying within two neighboring planes. A comparison of consecutive panels of Fig. 6.6, then, shows that the charge density within a given plane is insensitive to the makeup of its neighboring planes. For example, a Ga-As plane has essentially the same charge density profile regardless of whether its neighboring planes are also Ga-As or are Ga-Ga or As-As. Thus, the additional electron (hole) introduced in going from Ga_2As_2 to Ga_1As_3 (Ga_3As_1) remains localized in the As-As (Ga-Ga) plane. The As-As (Ga-Ga) plane may, therefore, be thought of as being metallic, while the Ga-As plane remains semiconducting. Such a metal-semiconductor superlattice should have ideal Schottky barriers.

The charge density between the corrugated planes is examined in Fig. 6.7 which shows contours in the cubic $(0\bar{1}1)$ plane for Ga_3As_1 and Ga_1As_3. Bonds pointing to the upper right corner connect adjacent planes, whereas bonds pointing to the upper left corner lie within a plane. Similar contour plots for the other three systems are not necessary due to the higher symmetry of those systems.

The charge densities of the interplanar bonds are very similar, in general, to their intraplanar counterparts. In particular, the interplanar and intraplanar Ga-As bonds look essentially the same. There are, however, slight differences between the charge density of the interplanar and intraplanar As-As and Ga-Ga bonds. In Ga_1As_3, for example, the interplanar As-As bond is slightly lopsided compared to its in-plane counterpart and favors the atom in the As-As plane. This is further

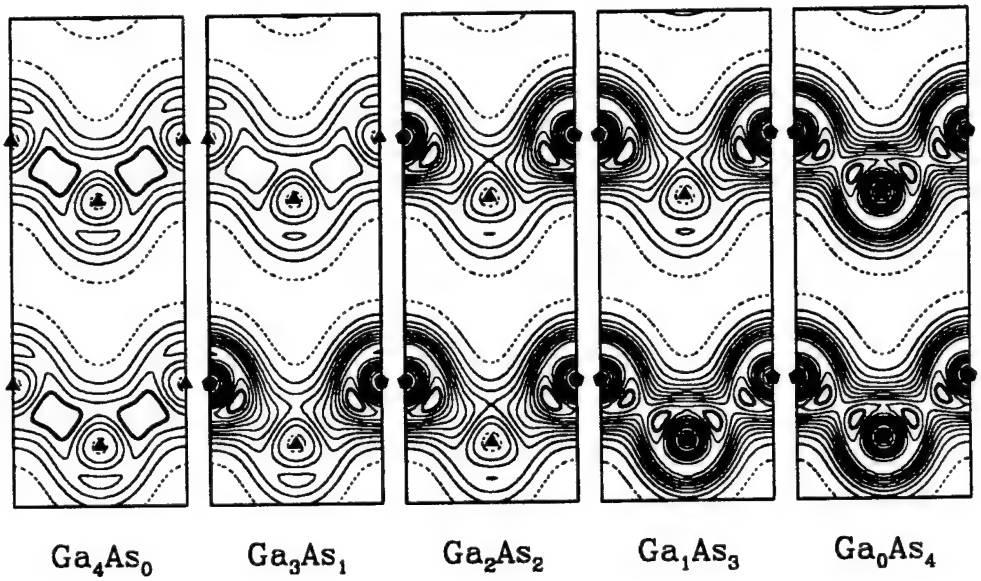

Figure 6.6: Valence charge density contours in the cubic (110) plane for the five systems $Ga_{4-n}As_n$, $n = 0,\ldots,4$. Intraplanar bonds for two adjacent corrugated layers are shown in each panel. Contours are separated by 5 electrons/cell and range from 5 to 55 electrons/cell with the lowest (highest) contour in each panel denoted by a dashed (bold) line. Triangles (pentagons) mark the positions of the Ga (As) atoms.

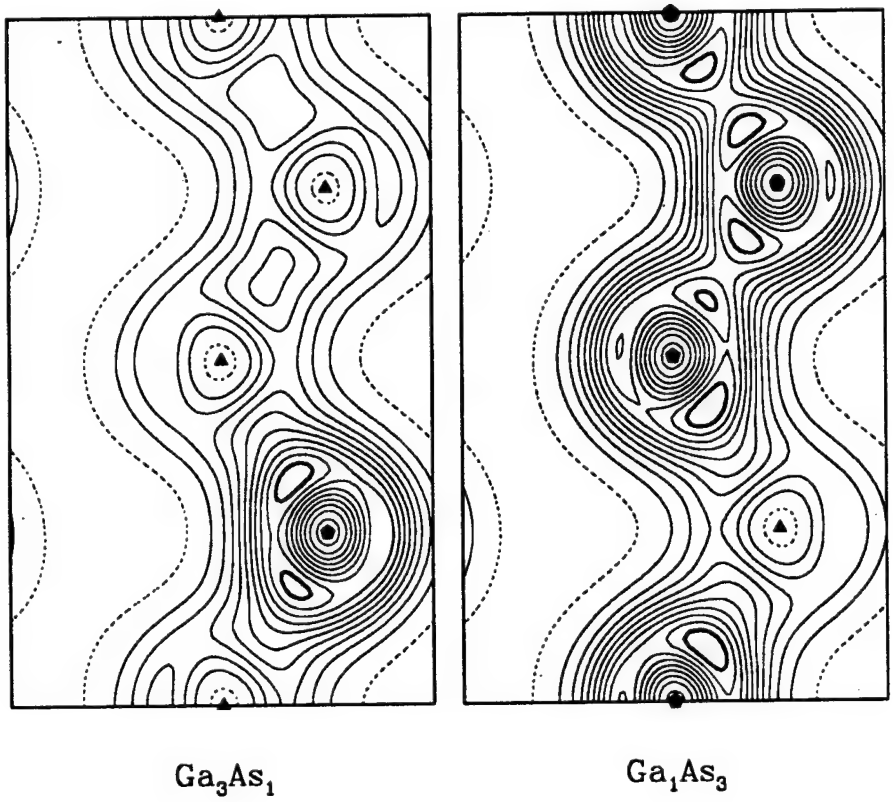

Figure 6.7: Valence charge density contours in the cubic $(0\bar{1}1)$ plane for Ga_3As_1 and Ga_1As_3. In each panel, interplanar bonds point to the upper right corner, and intraplanar bonds point to the upper left corner. Contours are separated by 5 electrons/cell and range from 5 to 55 electrons/cell with the lowest (highest) contour in each panel denoted by a dashed (bold) line. Triangles (pentagons) mark the positions of the Ga (As) atoms.

indication that the extra electron tends to be localized in the As-As plane. Analogously, the interplanar Ga-Ga bond in Ga_3As_1 has a higher electronic charge density than the in-plane Ga-Ga bond which suggests that the extra hole per atom in the Ga-Ga plane is confined, for the most part, in the plane.

Contour plots in Figs. 6.6 and 6.7 also provide insight into the nature and strength of the bonding in these systems. For the Ga-As bond, the figures show that the bonding is partially covalent and partially ionic. However, for the As-As and Ga-Ga bonds, no ionic bonding is possible. For the As-As bond, charge between the atoms is seen to segregate into two humps, indicating that the additional electron is filling an anti-bonding orbital. Such a double-hump structure is usually indicative of weakening, or even breaking, of bonds (although for diamond, a strongly-bound covalent material, similar structure is seen in the charge density [Yin81b]). For the Ga-Ga bond, the charge density between the atoms is not very large compared to the surrounding charge density. In particular, there are peaks in the charge density near but not between the Ga atoms that are comparable to the charge density peak between the Ga atoms. This suggests that the covalent bond between the Ga atoms is not particularly strong.

6.4 Summary

This study has investigated the dependence of the electronic properties of hypothetical Ga-As compounds on stoichiometry. In particular, systems designated by $Ga_{4-n}As_n$ for $n = 0, \ldots, 4$, which include GaAs and four other hypothetical materials on an underlying diamond lattice, have been studied. We have not relaxed structural parameters since this is a model calculation designed to motivate further experimental and theoretical studies of these systems.

The four systems which are off-stoichiometric with respect to GaAs are all found to be metallic with fairly large DOS's at the Fermi level. A comparison to the electronic properties of similar materials which exhibit superconductivity below ~ 5

K suggests that these model systems are good candidates for superconductors with T_c's in the range of 5–10 K. For the Ga_3As_1 (Ga_1As_3) system, the charge density of the Ga-As layer is essentially the same as in pure GaAs, and the charge density of the Ga-Ga (As-As) layer is essentially the same as in diamond Ga (As). This suggests that the Ga-As layers would be semiconducting similar to pure GaAs and that the Ga-Ga (As-As) layers would be metallic.

An analysis of the charge density indicates that the off-stoichiometric materials might be weakly bound and thus might be unstable with respect to cleavage or structural distortions. A simple bond-counting argument reinforces this conclusion [Cha93]. Similar Ga-As systems that are less "off-stoichiometric" (*i.e.*, superlattices with longer repeat distances) should be less unstable, but the large unit cells implied preclude their inclusion in an exploratory study such as this at this time. However, the calculated electronic properties of the systems studied here are expected to be indicative of the properties of these larger-celled systems.

Bibliography

[Asa78] K. Asaumi and S. Minomura, J. Phys. Soc. Japan **45**, 1061 (1978).

[Bac82] G. B. Bachelet, D. R. Hamann, and M. Schlüter, Phys. Rev. B **26**, 4199 (1982).

[Bar66] J. D. Barnett, V. E. Dean, and H. T. Hall, J. Appl. Phys. **37**, 875 (1966).

[Bat65] C. H. Bates, F. Dachille, and R. Roy, Science **147**, 860 (1965).

[Bei90] H. J. Beister, K. Strössner, and K. Syassen, Phys. Rev. B **41**, 5535 (1990).

[Ber69] I. V. Berman and N. B. Brandt, Soviet Phys. JETP Lett. **7**, 323 (1968); **10**, 55 (1969).

[Bir78] F. Birch, J. Geophys. Res. **83**, 1257 (1978).

[Bun63] F. P. Bundy and J. S. Kasper, Science **139**, 340 (1963).

[Cep80] D. M. Ceperley and B. J. Alder, Phys. Rev. Lett. **45**, 566 (1980); J. Perdew and A. Zunger, Phys. Rev. B **23**, 5048 (1981).

[Cha73] D. J. Chadi and M. L. Cohen, Phys. Rev. B **8**, 5747 (1973).

[Cha93] J. Chadi, private communication.

[Cha84] K. J. Chang and M. L. Cohen, Phys. Rev. B **30**, 5376 (1984).

[Cha85a] K. J. Chang and M. L. Cohen, Phys. Rev. B **31**, 7819 (1985).

[Cha85b] K. J. Chang, M. M. Dacorogna, M. L. Cohen, J. M. Mignot, G. Chouteau, and G. Martinez, Phys. Rev. Lett. **54**, 2375 (1985).

[Cha86a] K. J. Chang and M. L. Cohen, Phys. Rev. B **33**, 6177 (1986).

[Cha86b] K. J. Chang and M. L. Cohen, Phys. Rev. B **33**, 7371 (1986).

[Cha86c] K. J. Chang and M. L. Cohen, Phys. Rev. B **34**, 4552 (1986).

[Cha86d] K. J. Chang and M. L. Cohen, Phys. Rev. B **34**, 8581 (1986).

[Che91] B. H. Cheong and K. J. Chang, Phys. Rev. B **44**, 4103 (1991).

[Che92] A. L. Chen, S. P. Lewis, Z. Su, P. Y. Yu, and M. L. Cohen, Phys. Rev. B **46**, 5523 (1992).

[Coh70] M. L. Cohen and V. Heine, in *Solid State Physics*, edited by H. Ehrenreich, F. Seitz, and D. Turnbull (Academic, New York, 1970), Vol. 24, p. 37.

[Coh82] M. L. Cohen, Phys. Scr. **T1**, 5 (1982).

[Coh85] M. L. Cohen, K. J. Chang, and M. M. Dacorogna, Physica **135B**, 229 (1985).

[Coh86] M. L. Cohen, Science **234**, 549 (1986).

[Coh88] M. L. Cohen and J. R. Chelikowsky, *Electronic Structure and Optical Properties of Semiconductors*, (Springer, Berlin, 1988).

[Coh89] M. L. Cohen, Nature **338**, 291 (1989).

[Cor91] J. L. Corkill, A. García, and M. L. Cohen, Phys. Rev. B **43**, 9251 (1991).

[Dac85] M. M. Dacorogna, K. J. Chang, and M. L. Cohen, Phys. Rev. B **32**, 1853 (1985).

[Des89] S. Desgreniers, Y. K. Vohra, and A. L. Ruoff, Phys. Rev. B **39**, 10359 (1989).

[Don74] J. Donohue, *The Structures of the Elements* (Wiley, New York, 1974).

[Duc87] S. J. Duclos, Y. K. Vohra, and A. L. Ruoff, Phys. Rev. Lett. **58**, 775 (1987).

[Duc90] S. J. Duclos, Y. K. Vohra, and A. L. Ruoff, Phys. Rev. B **41**, 12021 (1990).

[Ers86] D. Erskine, P. Y. Yu, K. J. Chang, and M. L. Cohen, Phys. Rev. Lett. **57**, 2741 (1986).

[Fah87] S. Fahy and S. G. Louie, Phys. Rev. B **36**, 3373 (1987).

[Gup80] M. C. Gupta and A. L. Ruoff, J. Appl. Phys. **51**, 1072 (1980).

[Ham79] D. R. Hamann, M. Schlüter, and C. Chiang, Phys. Rev. Lett. **43**, 1494 (1979).

[Hem88] R. J. Hemley and H. K. Mao, Phys. Rev. Lett. **61**, 857 (1988).

[Her89] M. A. Herman and H. Sitter, *Molecular Beam Epitaxy: Fundamentals and Current Status* (Springer-Verlag, Berlin, 1989), and references therein.

[Hoh64] P. Hohenberg and W. Kohn, Phys. Rev. **136**, B864 (1964).

[Hu84] J. Z. Hu and I. L. Spain, Solid State Commun. **51**, 263 (1984).

[Hu86] J. Z. Hu, L. D. Merkle, C. S. Menoni, and I. L. Spain, Phys. Rev. B **34**, 4679 (1986).

[Ihm79] J. Ihm, A. Zunger, and M. L. Cohen, J. Phys. C **12**, 4401 (1979).

[Jam63a] J. Jamieson, Science **139**, 762 (1963); **139**, 845 (1963).

[Jam63b] J. Jamieson, Science **139**, 1291 (1963).

[Jam65] J. C. Jamieson, in *Metallurgy at High Pressures and High Temperatures*, edited by K. A. Gschneidner, M. T. Hepworth, and N. D. A. Parlee (Gordon and Breach, New York, 1965).

[Jay63] A. Jayaraman, W. Klement, Jr., and G. C. Kennedy, Phys. Rev. **130**, 540 (1963).

[Jay83] A. Jayaraman, Rev. Mod. Phys. **55**, 65 (1983).

[Kas64] J. S. Kasper and S. M. Richards, Acta Crystallogr. **17**, 752 (1964).

[Kaw85] H. Kawamura and J. Wittig, Physica **135**B, 239 (1985).

[Kik83] T. Kikegawa and H. Iwasaki, Acta Crystallogr. B **39**, 158 (1983).

[Kik87] T. Kikegawa and H. Iwasaki, J. Phys. Soc. Japan **56**, 3417 (1987).

[Kni91] E. Knittle and R. Jeanloz, Science **251**, 1438 (1991).

[Koh65] W. Kohn and L. J. Sham, Phys. Rev. **140**, A1133 (1965).

[Kol69] T. N. Kolobyanina, S. S. Kabalkina, L. F. Vereshchagin, and L. V. Fedina, Sov. Phys. JETP **28**, 88 (1969).

[Kru92] J. A. Krumhansl, Solid State Commun. **84**, 251 (1992).

[Leh72] G. Lehmann and M. Taut, Phys. Stat. Sol. B **54**, 469 (1972).

[Lew92] S. P. Lewis and M. L. Cohen, Phys. Rev. B **46**, 11117 (1992).

[Lew93a] S. P. Lewis and M. L. Cohen, Phys. Rev. B **48**, 3646 (1993).

[Lew93b] S. P. Lewis and M. L. Cohen, Mat. Sci. and Engr. B, in press.

[Lew93c] S. P. Lewis and M. L. Cohen, submitted to Phys. Rev. B.

[Lew93d] S. P. Lewis and M. L. Cohen, submitted to Solid State Commun.

[Liu86] M. Liu and L. Liu, High Temp.-High Pressure **18**, 79 (1986).

[Liu88] A. Y. Liu, K. J. Chang, and M. L. Cohen, Phys. Rev. B **37**, 6344 (1988).

[Liu91] A. Y. Liu, A. García, M. L. Cohen, B. K. Godwal, and R. Jeanloz, Phys. Rev. B **43**, 1795 (1991).

[Lou82] S. G. Louie, S. Froyen, and M. L. Cohen, Phys. Rev. B **26**, 1738 (1982).

[Lun83] *Theory of the Inhomogeneous Electron Gas*, edited by S. Lundqvist and N. H. March (Plenum, New York, 1983), and references therein.

[Mad78] O. Madelung, *Introduction to Solid-State Theory* (Springer, Berlin, 1978).

[Mah65] B. H. Mahan, *University Chemistry* (Addison-Wesley, Reading, 1965), pp. 392-5.

[Mai92] C. Mailhiot, L. H. Yang, A. K. McMahan, Phys. Rev. B **46**, 14419 (1992).

[Mar86] R. M. Martin and R. J. Needs, Phys. Rev. B **34**, 5082 (1986).

[Mar88] J. L. Martins and M. L. Cohen, Phys. Rev. B **37**, 3304 (1988).

[Mat86] L. F. Mattheiss, D. R. Hamann, and W. Weber, Phys. Rev. B **34**, 2190 (1986).

[McM68] W. L. McMillan, Phys. Rev. **167**, 331 (1968).

[McM83] A. K. McMahan and J. A. Moriarity, Phys. Rev. B **27**, 3235 (1983).

[McM85] A. K. McMahan and R. LeSar, Phys. Rev. Lett. **54**, 1929 (1985).

[McM93] M. I. McMahon and R. J. Nelmes, Phys. Rev. B **47**, 8337 (1993).

[Mig86] J. M. Mignot, G. Chouteau, and G. Martinez, Phys. Rev. B **34**, 3150 (1986), and references therein.

[Min62] S. Minomura and H. G. Drickamer, J. Phys. Chem. Solids **23**, 451 (1962).

[Mon77] H. J. Monkhorst and J. D. Pack, Phys. Rev. B **16**, 1748 (1977).

[Mur44] F. D. Murnaghan, Proc. Natl. Acad. Sci. U.S.A. **30**, 244 (1944).

[Nie85] O. H. Nielsen and R. M. Martin, Phys. Rev. B **32**, 3780 (1985).

[Nee84] R. J. Needs and R. M. Martin, Phys. Rev. B **30**, 5390 (1984).

[Nee86] R. J. Needs, R. M. Martin, and O. H. Nielsen, Phys. Rev. B **33**, 3778 (1986).

[Nee91] A. Neethiulagarajan and S. Balasubramanian, Phys. Rev. B **43**, 13525 (1991).

[Nee93] A. Neethiulagarajan and V. Vijayakumar, Phys. Rev. B **47**, 487 (1993).

[Nel93] R. J. Nelmes, M. I. McMahon, P. D. Hatton, J. Crain, and R. O. Piltz, Phys. Rev. B **47**, 35 (1993).

[Oli84a] H. Olijnyk and W. B. Holzapfel, J. Phys. (Paris) Colloq. **45**, Suppl. 11, C8-153 (1984).

[Oli84b] H. Olijnyk, S. K. Sikka, and W. B. Holzapfel, Phys. Lett. **103A**, 137 (1984).

[Oli92] H. Olijnyk, Phys. Rev. Lett. **68**, 2232 (1992); and Phys. Rev. B **46**, 6589 (1992).

[Phi59] J. C. Phillips and L. Kleinman, Phys. Rev. **116**, 287 (1950).

[Pic89] W. E. Pickett, Comp. Phys. Rep. **9**, 115 (1989).

[Pie75] G. J. Piermarini and S. Block, Rev. Sci. Instrum. **46**, 973 (1975).

[Rei85] R. Reichlin, D. Schiferl, S. Martin, C. Vanderborgh, and R. L. Mills, Phys. Rev. Lett. **55**, 1464 (1985).

[Ruo90] A. L. Ruoff, H. Xia, H. Luo, and Y. K. Vohra, Rev. Sci. Instrum. **61**, 3830 (1990).

[Sas88] T. Sasaki, K. Shindo, and K. Niizeki, Solid State Commun. **67**, 569 (1988).

[Shi90] I. Shirotani, K. Tsuji, M. Imai, H. Kawamura, O. Shimomura, T. Kikegawa, and T. Nakijima, Phys. Lett. A **144**, 102 (1990).

[Van71] J. A. Van Vechten, Phys. Status Solidi **47**, 261 (1971).

[Van72] J. A. Van Vechten, Phys. Rev. B **7**, 1479 (1972).

[Van89] C. A. Vanderborgh and D. Schiferl, Phys. Rev. B **40**, 9595 (1989).

[Voh86] Y. K. Vohra, K. E. Brister, S. Desgreniers, A. L. Ruoff, K. J. Chang, and M. L. Cohen, Phys. Rev. Lett. **56**, 1944 (1986).

[Wan86] Y. R. Wang and A. W. Overhauser, Phys. Rev. B **34**, 8401 (1986).

[Wei75] B. A. Weinstein and G. J. Piermarini, Phys. Rev. B **12**, 1172 (1975).

[Wei89] S. T. Weir, Y. K. Vohra, C. A. Vanderborgh, and A. L. Ruoff, Phys. Rev. B **39**, 1280 (1989).

[Wen63] R. H. Wentorf and J. S. Kasper, Science **139**, 338 (1963).

[Wit66] J. Wittig, Z. Phys. **195**, 215 (1966).

[Wit68] J. Wittig and B. T. Matthias, Science **160**, 994 (1968).

[Wit69] J. Wittig, J. Phys. Chem. Solids **30**, 1407 (1969).

[Wit84] J. Wittig, in *High Pressure Science and Technology*, edited by C. Homan, R. K. MacCrone, E. Whalley (North-Holland, New York, 1984), Pt. I, p. 17.

[Wit85] J. Wittig, B. Bireckoven, and T. Weidlich, in *Solid State Physics Under Pressure*, edited by S. Minomura (Terra Scientific, Dordrecht, 1985), p. 217.

[Yin80] M. T. Yin and M. L. Cohen, Phys. Rev. Lett. **45**, 1004 (1980).

[Yin81a] M. T. Yin and M. L. Cohen, Solid State Commun. **38**, 625 (1981).

[Yin81b] M. T. Yin and M. L. Cohen, Phys. Rev. B **24**, 6121 (1981).

[Yin82] M. T. Yin and M. L. Cohen, Phys. Rev. B **26**, 5668 (1982).

[Zan90] F. Zandiehnadem and W. Y. Ching, Phys. Rev. B **41**, 12162 (1990).

[Zha89] S. B. Zhang, D. Erskine, M. L. Cohen, and P. Y. Yu, Solid State Commun. **71**, 369 (1989).